

**IDAHO DEPARTMENT OF FISH AND GAME**

**Ed Schriever, Director**

**Project F19AF00856**

**Final Performance Report  
Wildlife Restoration and Basic Hunter Education**



**Statewide Wildlife Research**

July 1, 2019 to June 30, 2020

Prepared by:

Mark Hurley  
Wildlife Research and Data Manager  
&  
Shane Roberts  
Wildlife Research Coordinator

September 2020  
Boise, Idaho

Idaho Department of Fish and Game (IDFG) adheres to all applicable state and federal laws and regulations related to discrimination on the basis of race, color, national origin, age, gender, disability or veteran's status. If you feel you have been discriminated against in any program, activity, or facility of IDFG, or if you desire further information, please write to: Idaho Department of Fish and Game, PO Box 25, Boise, ID 83707 or US Fish and Wildlife Service, Division of Wildlife and Sport Fish Restoration Program, 5275 Leesburg Pike, MS: WSFR, Falls Church, VA 22041-3803, Telephone: (703) 358-2156. This publication will be made available in alternative formats upon request. Please contact IDFG for assistance.

Please note that IDFG databases containing this information are dynamic. Records are added, deleted, and/or edited on a frequent basis. This information was current as of the date of this report. Raw data do not have the benefit of interpretation or synthesis by IDFG.

IDFG requests that you direct any requests for this information to us rather than forwarding this information to third parties.

## Table of Contents

|  |    |
|--|----|
| F19AF00856 Statewide Wildlife Research Final Report .....  | 3  |
| Strategy .....   | 3  |
| Standard Objective.....  | 3  |
| Activity Tag(s).....   | 3  |
| Species and/or Habitat Types .....   | 3  |
| Investigation 1 – Conduct 1 Mule Deer study by 30 June, 2020.....  | 3  |
| Results.....   | 3  |
| Investigation 2 – Conduct 1 White-tailed Deer study by 30 June, 2020 .....   | 10 |
| Results.....   | 10 |
| Investigation 3 – Conduct 1 Elk study by 30 June, 2020 .....   | 11 |
| Results.....   | 11 |
| Investigation 4 – Conduct 1 Bighorn Sheep study by 30 June, 2020 .....   | 27 |
| Results.....   | 27 |
| Investigation 5 – Conduct 1 Moose study by 30 June, 2020 .....   | 34 |
| Results.....   | 34 |
| Investigation 6 – Conduct 1 Mountain Goat study by 30 June, 2020.....  | 35 |
| Results.....   | 35 |
| Investigation 7 – Conduct 1 Gray Wolf study by 30 June, 2020.....  | 37 |
| Results.....   | 37 |
| Investigation 8 – Conduct 1 Mountain Lion study by 30 June, 2020.....  | 40 |
| Results.....   | 40 |
| Investigation 9 – Conduct 1 Black Bear study by 30 June, 2020 .....  | 42 |
| Results.....   | 42 |
| Investigation 10 – Conduct 1 Greater Sage-grouse study by 30 June, 2020 .....  | 43 |
| Results.....   | 43 |
| Investigation 11 – Conduct 1 Study of the Effects of Agriculture Landscape Change on Wildlife Populations by 30 June, 2020 ..... | 58 |
| Results.....   | 58 |
| Literature Cited .....   | 60 |

## Figures

|   |    |
|---|----|
| Figure 1. A demonstration of the effect of sparse data on corridor area estimation using a Brownian Bridge Movement Model.....  | 6  |
| Figure 2. a) Proportion of each component .....   | 7  |
| Figure 3. Comparison of mule deer stopover locations .....  | 8  |
| Figure 4. Twelve mule deer seasonal migration routes in Southern Idaho. ....  | 9  |
| Figure 5. Probability of local extinction due to varying environmental stochasticity as a function of intrinsic rate of growth ( $r_{max}$ ) and nonlinear density dependence ( $\theta$ ).....                                 | 12 |
| Figure 6. Population growth under predation stochasticity with high ( $K = 20$ ) and low carrying capacity ( $K = 5$ ). a) .....  | 14 |
| Figure 7. Effect size of predator removal experiments by ungulate response variable measured.....   | 15 |
| Figure 8. Bias (dotted lines) and precision (thin solid line) of the estimated neonate survival curve under five scenarios of prior information .....   | 20 |
| Figure 9. Location of the a) study area (black outline) in Idaho and b) 70 motion-triggered cameras used to estimate survival of neonatal elk.....  | 21 |
| Figure 10. Elk seasonal migration stopover comparison between BBMM and Rate and Duration Methods in the South Fork of the Payette River.....  | 23 |
| Figure 11. Seven seasonal elk migrations occurring in southern Idaho. ....  | 24 |
| Figure 12. Age of last canopy disturbance in forested habitats in Idaho.....  | 26 |
| Figure 13. Lamb survival and pneumonia induced mortality.....   | 29 |
| Figure 14. Estimates of summer lamb survival for bighorn sheep in the Lost River Range.....   | 31 |
| Figure 15. Probability of bighorn sheep lamb survival as a function of ewe condition.....   | 31 |
| Figure 16. Boxplots comparing variation in ewe condition .....  | 32 |
| Figure 17. Relationship of fall ewe body condition to a) pregnancy.....   | 33 |
| Figure 18. Mountain goat population estimation project study area, Snake River Range, Idaho .....   | 36 |
| Figure 19. Relative number of wolf pictures captured from statewide camera grid, 2019 .....   | 38 |
| (blue circle means wolf pictures were taken, size of blue circle reflects relative number of pictures taken, gray circle means no pictures of wolves).....  | 38 |
| Figure 20. Map of camera grid, and primary and alternate random camera location points.....   | 41 |
| Figure 21. A) Survival estimates ( $\pm 95\%$ C.I.) of female sage-grouse during the breeding season monitoring period (Mar – Jul) and B) annual probability of nest survival ( $\pm 95\%$ C.I.) .....                          | 43 |
| Figure 22. Monitoring and treatment schedule used to evaluate effects of cattle grazing on sage-grouse demographic traits and habitat features within 4 treatment pastures at each southern Idaho project study area. ....      | 44 |
| Figure 23. Map of estimated livestock utilization at Browns Bench study area, Idaho, 2015-2019 .....  | 45 |
| Figure 24. Mean values ( $\pm 1$ SE for droop height only) of 3 height measurements of the 5 most common species of perennial grasses collected at post-growing season (Jul-Aug) random plots at Browns Bench, Idaho, 2019..... | 46 |
| Figure 25. Shrub canopy cover of all brush species combined within each of 4 treatment pastures at Browns Bench, Idaho, 2015-2019. ....   | 47 |
| Figure 26. Sage-grouse nests of marked females monitored in the Upper Snake Region, Idaho, 2015-2020. ....  | 48 |
| Figure 27. Apparent nest success from marked female sage-grouse monitored in the Upper Snake Region, Idaho, 2015-2020. ....   | 49 |
| Figure 28. Partial effects plots of shrub, perennial grass, and forb cover from best preliminary model describing vegetation nest site selection by sage-grouse in the Upper Snake Region, Idaho, 2015-2020. ....               | 50 |

|  |    |
|--|----|
| Figure 29. Locations of monitored sage-grouse nests, before (2015-2018 = green dots) and after (2019-2020 = red dots) the Grassy Ridge fire (cross-hatched area = burn boundary), on the Sand Creek desert, Idaho.....   | 51 |
| Figure 30. Previously-documented sage-grouse leks that we aerially surveyed on April 15-17, 2017 in the Greater Curlew Valley Area, Idaho. ....  | 52 |
| Figure 31. Plot of the modeled effect of remotely-sensed shrub canopy cover on the relative probability of an area being selected by a nesting sage-grouse (top model in Table 14), Greater Curlew Valley Area, Idaho, 2017-2018. ....   | 54 |
| Figure 32. Plot of the modeled effects of field-measured forb canopy cover (%) and sagebrush height (cm) from the top two univariate models (Table 3) describing the probability of sage-grouse nest success, Greater Curlew Valley Area, Idaho, 2017-2018.....                  | 55 |
| Figure 33. Parameter estimates ( $\pm$ 95% C.I.) from resource selection function models—each containing xeric grass, xeric shrub, and agriculture land cover variables—from season-specific location datasets of sage-grouse, Greater Curlew Valley Area, Idaho, 2017-2018..... | 58 |
| Figure 34. Area map and time series of measured normalized difference vegetation index (NDVI) values from three agriculture fields in Arbon Valley, Idaho. ....  | 59 |

## Tables

|   |    |
|---|----|
| Table 1. White-tailed deer collared during February-March 2020 in north Idaho. ....   | 11 |
| Table 2. Performance of neonate survival model based on remote camera trap data. ....   | 19 |
| Table 3. Bighorn sheep captured in Hells Canyon, July 2019 – June 2020. ....  | 27 |
| Table 4. Summary of <i>Mycoplasma ovipneumoniae</i> (Movi) testing in the Lostine Oregon bighorn sheep population November 2019 – April 2020. ....  | 28 |
| Table 5. Survival of radio-collared adult bighorn sheep in 13 Hells Canyon populations, 1 May 2019 to 30 April 2020. ....   | 28 |
| Table 6. Observed productivity of radio-collared ewes and survival of lambs born in 2019 in 12 Hells Canyon bighorn sheep populations, Idaho. ....  | 29 |
| Table 7. Mark-resight survey results from 4 Hells Canyon bighorn sheep populations, 2019-2020. ....   | 30 |
| Table 8. Game management unit (GMU) of capture locations for female moose collared during winter of 2020 ( $n = 113$ ), Idaho. ....   | 34 |
| Table 9. Abundance estimates ( $\hat{N}$ ), standard errors (SE) and 95% confidence intervals (LCL-UCL) for wolves in Idaho in 2019 across three strata from camera data. Area represents the entire area of each stratum, not predicted high use wolf rendezvous site habitat only. .... | 39 |
| Table 10. Regional summary of cameras deployed, photos taken, and species detected during 2019 statewide wolf estimation efforts, Idaho. ....   | 39 |
| Table 11. Black bears collared, slipped collars, and currently active collars for Idaho research. ....  | 42 |
| Table 12. Adult and yearling female greater sage-grouse captured by year across 6 study sites in southern Idaho for the grazing project. ....   | 43 |
| Table 13. Summary of arthropod sampling efforts at 6 study sites across southern Idaho, 2015-2019.  | 47 |
| Table 14. Model selection results and parameter estimates for resource selection function models describing sage-grouse nest site selection of remotely-sensed habitat variables in the Greater Curlew Valley Area, Idaho, 2017-2018. ....  | 54 |
| Table 15. Additive model selection results describing seasonal habitat selection of sage-grouse, Greater Curlew Valley Area, Idaho, 2017-2018. ....   | 55 |
| Table 16. Summary of 30-day brood flush count data, Greater Curlew Valley Area, Idaho, 2017-2018. ....  | 56 |
| Table 17. Summary of monitoring and survival statistics from sage-grouse marked with PTTs in the Greater Curlew Valley Area, Idaho, 2017-2018. ....   | 56 |
| Table 18. Additive model selection results (top 3 models only) describing seasonal habitat selection of sage-grouse, Greater Curlew Valley Area, Idaho, 2017-2018. ....   | 57 |

# FEDERAL AID IN WILDLIFE RESTORATION

## ANNUAL PERFORMANCE REPORT

**State:** Idaho

**Grant number:** F19AF00856

**Grant name:** Statewide Wildlife Research

**Report Period:** July 1, 2019 through June 30, 2020

**Report due date:** September 28, 2020

**Geographic Location** Statewide

**If the work in this grant was part of a larger undertaking with other components and funding, present a brief overview of the larger activity and the role of this project.**

N/A

**Describe how objectives were met:**

See individual project reports contained herein.

**Discuss differences between work anticipated in grant proposal and grant agreement, and that actually carried out with WSFR grant funds; include differences between expected and actual costs**

N/A

**List any publications or in-house reports resulting from this work.**

Aikens, E. O., A. Mysterud, J. A. Merkle, F. Cagnacci, I. M. Rivrud, M. Hebblewhite, M. A. Hurley, W. Peters, S. Bergen, J. De Groeve, S. P. H. Dwinnell, B. Gehr, M. Heurich, A. J. M. Hewison, A. Jarnemo, P. Kjellander, M. Kroschel, A. Licoppe, J. D. C. Linnell, E. H. Merrill, A. D. Middleton, N. Morellet, L. Neufeld, A. C. Ortega, K. L. Parker, L. Pedrotti, K. M. Proffitt, S. Said, H. Sawyer, B. M. Scurlock, J. Signer, P. Stent, P. Sustr, T. Szkorupa, K. L. Monteith, and M. J. Kauffman. 2020. Wave-like patterns of plant phenology determine ungulate movement tactics. *Current Biology* 30:1–6.

Atwood, M. P., J. G. Kie, J. J. Millspaugh, M. D. Matocq, and R. T. Bowyer. 2020. Condition of mule deer during winter: stress and spatial overlap with North American elk. *Mammal Research* 65:349–358. <https://doi.org/10.1007/s13364-019-00474-x>

Garwood, T., C. P. Lehman, D. P. Walsh, E. F. Cassirer, T. E. Besser, and J. A. Jenks. 2020. Removal of chronic *Mycoplasma ovipneumoniae* carrier ewes eliminates pneumonia in a bighorn sheep population. *Ecology and Evolution* 10:3491–3502.  
<https://doi.org/10.1002/ece3.6146>

Hurley, M. A., M. Hebblewhite, and J.-M. Gaillard. 2020. Competition for safe real estate, not food, drive density-dependent juvenile survival in a large herbivore. *Ecology and Evolution* 00:1–12. <https://doi.org/10.1002/ece3.6289>

Kamath, P. L., K. Manlove, E. F. Cassirer, P. C. Cross, and T. E. Besser. 2019. Genetic structure of *Mycoplasma ovipneumoniae* informs pathogen spillover dynamics between domestic and

wild Caprinae in the western United States. *Scientific Reports* 9, 15318.

<https://doi.org/10.1038/s41598-019-51444-x>

Loonam, K. E., D. E. Ausband, P. M. Lukacs, M. S. Mitchell, and H. S. Robinson. 2020.

Estimating abundance of an unmarked, low-density species using cameras. *Journal of Wildlife Management* 1-10. <https://doi.org/10.1002/jwmg.21950>

# F19AF00856 Statewide Wildlife Research Final Report

## Strategy

Research, Survey, Data Collection, and Analysis

## Standard Objective

Conduct 11 investigations by 30 June 2020

## Activity Tag(s)

Fish and wildlife species data acquisition and analysis, habitat data acquisition and analysis, and utilization data acquisition and analysis. Number of investigations.

## Species and/or Habitat Types

*Species* - mule deer, white-tailed deer, moose, elk, greater sage-grouse, Columbian sharp-tailed grouse, bighorn sheep, mountain goat, black bear, gray wolf, mountain lion.

*Habitat types* – work will be conducted in almost every major habitat type in the State of Idaho, including: agriculture, sage-steppe, aspen, coniferous forest, alpine, riparian, grasslands

## Investigation 1 – Conduct 1 Mule Deer study by 30 June, 2020.

### Results

*Estimating Habitat Quality* - Our focus this year has been on validation of our statewide fine-scale vegetation model. We created a data collection application to assist biologists in collecting consistent ground-truthing data across the state. The protocol includes assessment of overstory vegetation structure and species with a quick plot and a more detailed plot to validate the understory modeling. We developed a ground-truthing sampling scheme for all of Idaho, focusing our initial efforts on locations and overstory types that had the most uncertainty during overstory modeling, habitat types that were underrepresented in initial modeling efforts (e.g., alpine meadows), and areas that have been disturbed (e.g., fire, logging) since the NAIP imagery used to develop the initial overstory model was taken (2014). We'll use the ground-truthing data collected during this reporting period to measure error in our modeling, inform the need for future ground-truthing efforts, and develop methods to make the map/modeling "live" to accommodate landscape-scale vegetation disturbances. We completed 416 ground-truthing plots during the summer of 2020.

*Estimating Phenological Variation in Nutrition* - We are also updating the spatiotemporal covariate databases used in statistical analyses for estimating mule deer winter and summer range quality. Idaho Department of Fish & Game (IDFG) worked with TerraPulse to create a normalized vegetation difference index (NDVI) that fuses smaller 30m resolution Thematic Mapper data with daily images from MODIS satellite imagery to produce 30m resolution daily NDVI estimates (unpublished data, TerraPulse, <http://www.terrapulse.com>). This 2002-2019 dataset can be used as a proxy for vegetation growth across the state of Idaho and provides several other informative spatial databases that add valuable information for estimating temporal forage quality within a daily time increment.

With data of this spatial and temporal resolution, we can compare pixel values across the 18 year history, allowing us to quantify vegetation growth within a specific location, area, or region. This allows for a much more precise and accurate evaluation of vegetation performance and

correlation to mule deer productivity across the state. The temporal detail also allows for investigations of intra-seasonality of vegetation growth and production, which can be key to understanding how annual phenology affects mule deer populations and individual mule deer movements. For example, the southeast portion of the Idaho can receive monsoon rain systems as early as August, which can promote additional vegetation growth and increased forage quality as deer physiologically prepare for winter. This nutrition increase can be a critical factor in determining overwinter survival, especially during more severe winters. The temporal nature of these monsoonal rains is highly variable and this database provides a proxy that will help us better understand vegetation factors affecting summer range selection.

*Survival and Demographics Modeling with Integrated Population Models* - We assisted management staff with the capture, collaring, and survival monitoring of 254 mule deer (196 6-month old fawns, 4 yearling females, 56 adult females, and 2 adult males) during winter 2019-2020 for statewide modeling efforts. We used field necropsy techniques to document causes of mortality when possible. We are developing automation techniques and an interface application that will allow managers to estimate survival and examine cause-specific mortality across the state.

Snowfall and snow condition are known to have a large influence on mule deer location within their winter range. Research collaborators from Colorado State University have produced snow condition estimates across the state of Idaho from 1995 to 2019 (unpublished data, Cooperative Institute for Research in the Atmosphere, Colorado State University). This database is at a 90m resolution and at a daily time increment. It increases the spatial accuracy by nearly two orders of magnitude relative to previous SNODAS snow data, which is initially provided at a 1km resolution. Snow can now be utilized as a primary component of the survival models incorporated in our population modeling software, PopR. Similar to the TerraPulse NDVI data, the snow model data will allow us to move beyond qualitative measures of winter snow conditions that influence winter mule deer location. The current hierarchical survival models will be reparametrized with these new data sources, providing a finer spatial resolution and increased accuracy of the winter survival estimates of fawns.

Recent location data from mule deer fitted with GPS radio collars provided a more informed understanding of how populations are distributed on summer, winter, and migratory habitats across Idaho. In light of this new information, we revised the geographical boundaries of the data analysis units that are used for mule deer population monitoring and management and incorporated these changes into the integrated population model. We continued the development of our suite of online tools designed to help managers estimate and monitor mule deer populations and continued our evaluation of several methods of obtaining the vital rate data needed to populate the integrated population model to estimate annual mule deer abundance throughout Idaho. Increasing the accuracy of survival models, along with refining population boundaries, will increase the accuracy of the population estimates generated with integrated population models in PopR. In addition, we added tools to the integrated population model for investigating relationships between population abundance, population growth rate, juvenile to adult ratio, and juvenile survival.

*Alternative Monitoring Methods* – We continued to develop the camera-based abundance and survival estimation methods for multiple species, including mule deer. During spring-summer of 2020, we deployed 250 remote cameras in each of 2 GMUs (6 and 10A) to seasonally estimate density and abundance of all large mammals, including mule deer, with the methods described

by Moeller et al. (2018). We generated random points throughout the study areas and deployed 2 cameras within 1 km of the generated points. One of the cameras at each point was restricted to being placed within 30m of the point, while the other could be placed on the best road/trail within 1 km of the point. This paired camera design will allow us to investigate the effect of random and non-random camera placement on detection of the various species, estimate the density of all large mammals in the system (even those that occur in low density), and attempt to estimate neonatal ungulate survival with cameras. These camera grids will remain deployed year-round, with visits by field staff for picture retrieval and battery replacement, allowing us to also examine seasonal changes in spatial distribution/density and interactions between the species over time and space.

We're actively developing methods for estimating neonatal ungulate survival solely from camera data, see Elk research section for a more detailed explanation, and the feasibility of estimating December fawn:doe ratios from cameras. We've evaluated several sets of photos collected from camera arrays across the state so far. Potential issues for fawn:doe ratio estimation from cameras that we've identified to date, and need to be resolved, include incorrect sex/age classification of deer in photos and understanding and mitigating for the effect of multiple photos of the same animal.

*Seasonal Range and Migration Modeling* - Brownian bridge movement modeling (BBMM) techniques are less precise with less frequent locations because greater time increments increase the motion variance to estimate the utilization distribution from known GPS locations (Horne et al. 2007). As a technical guide, BBMM requires a location interval of at least 1 location/7.5 hours to construct utilized distribution probability surfaces that are precise enough to inform management. Therefore, we focused on exploring and developing new techniques that would allow for more precise estimation of movement corridors from GPS locations that were collected >7.5 hours apart. We investigated the use of continuous time movement models (CTMM; Fleming et al. 2015, Fleming et al. 2016) and forced motion variance (FMV). We found that CTMM provided a more accurate estimation of mule deer movement corridors than FMV, but FMV techniques were more precise and accurate in determining stopover locations.

In continued collaboration with the University of Wyoming's Migration Initiative, we have experimented with the CTMM and FMV methods by artificially manipulating the spatial variance of a subset of 12-hr location frequency data and then comparing those estimates to estimates generated from the original 2-hr location frequency data using BBMM (Figures 1 and 2). In this framework, FMV variances were incrementally adjusted between 200 and 3,000 m. In this incremental process, we are able to identify the most accurate spatial variance to use ( $1,100 \pm 360$  m for mule deer). We also were able to calibrate how topographic complexity affected the spatial variance (Aikens et al. 2020). In less complex seasonal migrations, it is likely that a variance of less than 1,100m can be used, but the spatial variance will increase in regions with complex topography (e.g., when multiple mountain valley systems are traversed in a single seasonal migration). Also during this investigation, we found that when scheduled location data is missed for periods of longer than 30 hours, the accuracy of any of the techniques is challenged. Therefore, during these intermittent lapses in locations for >30 hours, no estimate should be drawn.

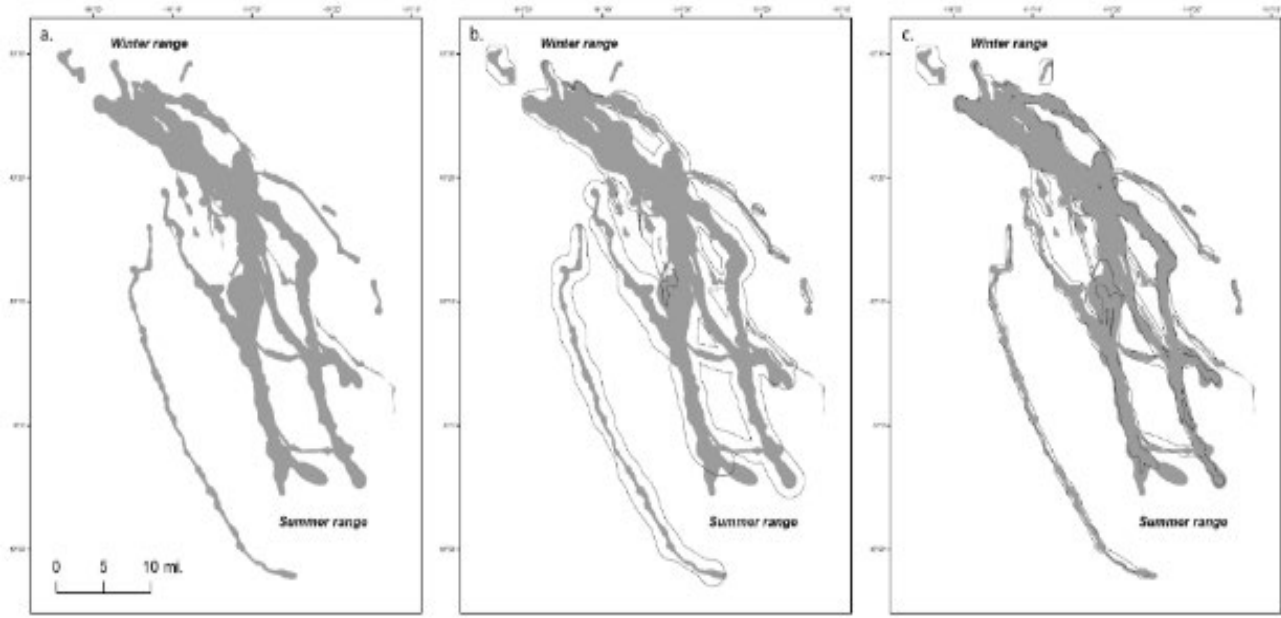


Figure 1. A demonstration of the effect of sparse data on corridor area estimation using a Brownian Bridge Movement Model (BBMM) and the application of fixed motion variance (FMV) to constrain the corridor width of the Tex Creek mule deer dataset, Idaho. a) baseline corridor is delineated using a BBMM fitted to 2-hour fix rate migration data (light grey polygon), b) a BBMM fit to a dataset rarefied to a 12-hour fix rate overestimates the corridor area (black outline), c) a BBMM fit with fixed motion variance to the rarefied 12-hour dataset constrains the width of the corridor so that it overlaps with most of the baseline corridor, without overestimating its surface area.

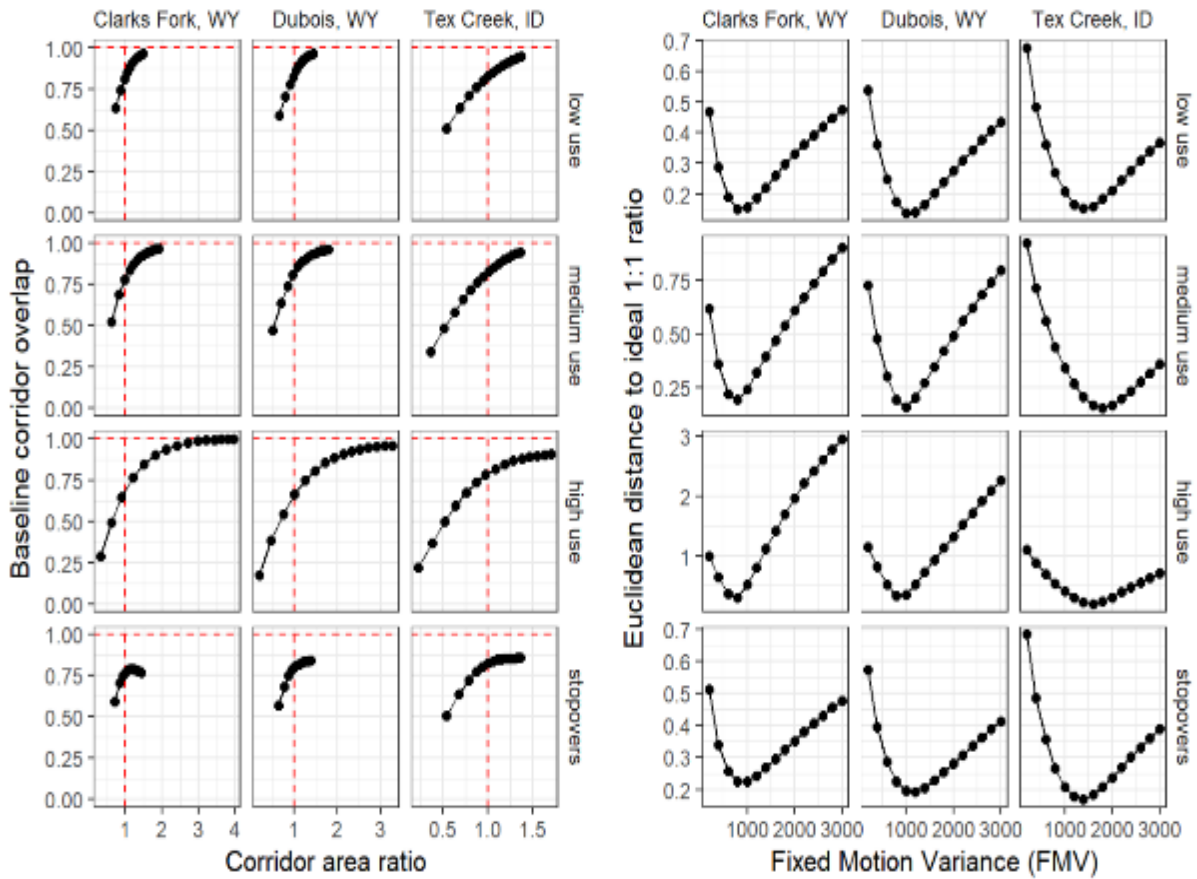


Figure 2. a) Proportion of each component (low use, medium use, high use, stopover) of the 2-hour baseline corridor (Figure 1a) overlapped by corridors produced by BBMMs fitted to 12-hour data with fixed motion variance values ranging between 200-3,000 and b) plots of the Euclidean distance from an ideal 1:1 ratio for each fixed motion variance value for three mule deer populations in Wyoming and Idaho, USA, 2007 – 2018. Red dashed lines in a) mark the ratio of 1 for each metric, corresponding to a theoretical perfect match between the 12-hour corridors and the 2-hour baseline corridors. In b), the optimal FMV was identified as the value that minimized the Euclidean distance to the ideal 1:1 ratio intersection.

Mule Deer migrations are composed of two types of movement, high rate of movement areas punctuated by stopover forage and rest locations (Sawyer and Kauffman 2011). Stopovers are often identified as the top 25% of a percent volume contour of an entire migration path but could also be identified by using an individual's rate of movement and duration of slower movement (i.e., identify when the individual is moving slowly for extended periods of time). To do so, we used our mule deer GPS location dataset to first estimate the slowest 10% of movement rates within a 12 hr time period as a baseline for what a “slow” rate of movement is for Idaho mule deer (~ 144m/hr following Calenge 2006, Calenge et al. 2009, and Calenge 2019). We measured sequential distances between the stopover locations identified, using rate and duration of stay to estimate the ‘bandwidth’ (i.e., distance to draw an ellipse from the identified stopover locations). Using the identified stopover locations and the bandwidth, we estimated the area of stopovers using kernel density estimates with a quartic estimation procedure (KDE). This new method of identifying individual mule deer stopovers is capable of estimating stopover areas with

confidence intervals. Initial comparisons to traditional BBMM techniques show that the two techniques agree on about one third of stopover locations and the rate and duration technique identifies many more stopover locations used within a seasonal migration. Learning from earlier experiences, we are now in the process of expanding this analysis to other areas of the state where deer migratory behavior may differ from those used in initial analyses.

When we organize the location data into population level analyses (i.e., population = winter herd), there are additional differences between the two methods (Figure 3). For this comparison, we added together all of the stopover locations, dissolved any boundaries between them, and compared those polygons to those generated from established BBMM methods for population level stopover assessments. The BBMM and rate and duration methods shared 34% of the stopover areas they identified. Twenty-four percent of stopover areas produced with BBMM were unique and seemed to be strongly associated with individual mule deer migrations that were of a shorter length relative to the rest of collared deer. In addition, BBMM derived stopovers appeared to be centered on prevalent migrations routes. Rate and duration stopover locations not shared with BBMM methods comprised 41% of all stopovers. Further, the rate and duration method also generated stopovers in the distal portions of the seasonal migration routes.

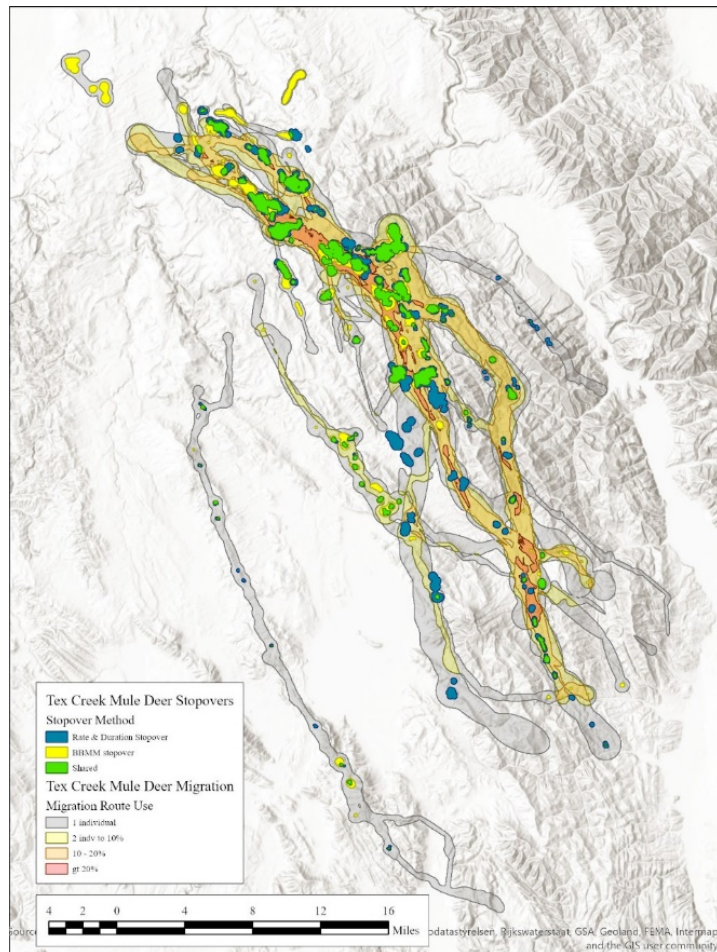


Figure 3. Comparison of mule deer stopover locations as identified by rate and duration and BBMM methods on Tex Creek seasonal mule deer migration routes, Idaho.

In collaboration with Department of Interior Secretarial Order 3362, we have produced migration routes for 12 winter herds in southern Idaho (Figure 4). The mule deer seasonal migration routes are derived from individuals that are using common winter ranges and are wearing GPS collars. Strength of use within each migration route is broken in to three categories: 2 individuals to 10%, 10 to 20%, and greater than 20% use by the winter herd. Stopovers were delineated using the BBMM stopover method but we manually removed stopover locations and migration routes that were only used by one individual deer.

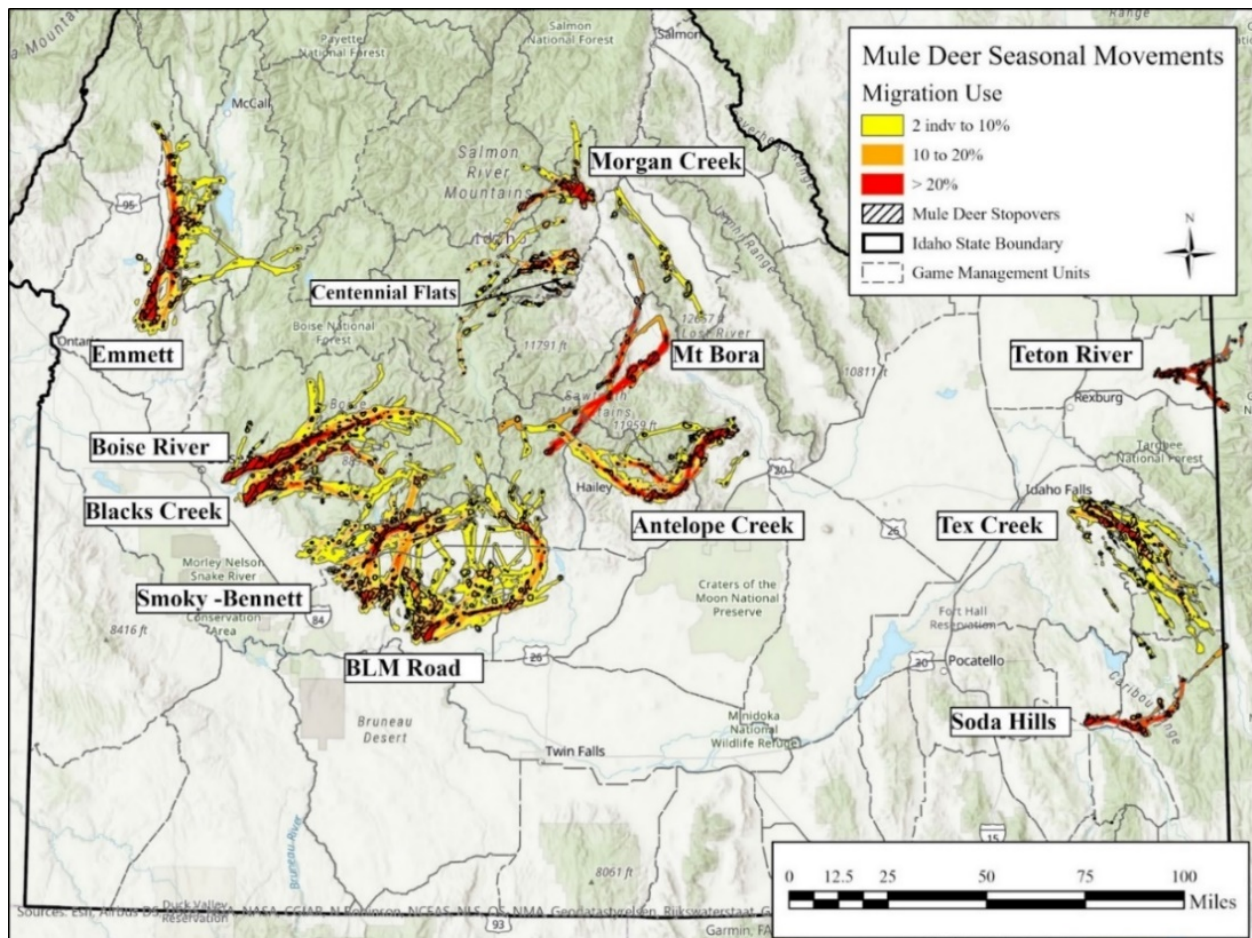


Figure 4. Twelve mule deer seasonal migration routes in Southern Idaho.

IDFG's work on mule deer seasonal ranges focused on updating mule deer location databases, collected since September 2016, where we perform net-squared displacement techniques to delineate a mule deer's annual movement into winter range, spring migration, summer range, and fall migration. The NSD analysis is complete for all mule deer locations collected through December of 2019.

*Habitat Change and Connectivity Modeling* – We're also using the mule deer locations, movements, seasonal range, and migration work described above to evaluate connectivity and the potential effects of habitat change. Some studies have found that partial migration is spatially associated with large agricultural developments or when irrigated agriculture is prevalent at a landscape scale (Middleton et al. 2013, Berg et al. 2019). We are using net squared displacement to quantify the portion of each wintering mule deer population that exhibits partial migratory behavior. The degree of partial migration will be a strong indicator of when large-

scale agricultural practices impact or change the spatial life histories of these seasonally migratory species. The TerraPulse NDVI database has the capacity to distinguish land tenure and land tenure changes throughout the history of IDFG's GPS collar deployments on mule deer. This database will be invaluable for the purposes of characterizing regional land tenure histories and comparing them with the spatial life histories of mule deer populations.

In coordination with Department of Interior Secretarial Order 3362, we successfully deployed GPS collars on a winter herd of mule deer in southeastern Idaho as part of a project to evaluate where mule deer are crossing state highway 30. Their location data suggests that 96% of the herd crosses the state highway within a ‘pinch-point’ that has one of the highest wildlife collision rates in Idaho. IDFG is coordinating with Idaho Department of Transportation in the design of mitigation efforts to lower wildlife vehicle collisions in this area.

*Buck Vulnerability* - We captured and GPS-collared male mule deer in an effort to predict the effects of hunting season structure and habitat security on male deer survival. Because one season type or structure will not produce the same mortality results in GMUs with different hunter access and security cover, we are alternating through tests of season type and habitat security, while maintaining adequate control GMUs. This project is utilizing the ongoing statewide vegetation modeling efforts to provide vegetation security cover estimates. We deployed 3 expandable GPS collars on mule deer bucks ( $\geq 1.5$  years of age) in GMUs 39, 40, and 6. Blood samples and body measurements were collected on captured deer. We will monitor these, and additional collared male deer in future years, for survival and movements related to habitat and human activity until death or collar failure. This research will provide managers with objective estimates of the effects of changing hunting season structure or habitat security, with the goal of maintaining hunter opportunity. To date, we have documented 13 mortalities of collared adult male mule deer.

## **Investigation 2 – Conduct 1 White-tailed Deer study by 30 June, 2020**

### **Results**

In winter 2018-2019, we used box/clover traps to capture adult and 6-month old fawn white-tailed deer in GMUs 1, 6, and 10A (Table 1). We successfully collared 140 deer in all three GMUs combined. In GMUs 6 and 10A, 60 of the collared females were pregnant adults that received a vaginal implant transmitter (VIT) to aid in the capture and collaring of neonatal fawns. We did not attempt to use VITs on pregnant females in GMU 1 during 2020, but plan to in future years. In May-June of 2020, we used VIT signals combined with grid searches around does suspected of giving birth to capture and collar 39 neonatal white-tailed deer fawns (20 in GMU 6, 19 in GMU 10A) and 2 mule deer fawns (both in GMU 6). Fawns were fitted with expandable collars that communicated with their doe’s GPS collar to transmit their status. Neonatal fawn survival monitoring continued past this reporting period, but black bear predation was the primary cause of early mortality in GMU 6 while predation by mountain lions or bobcats was the primary cause of early mortalities in GMU 10A. We will continue to monitor these deer year-round to document annual survival, seasonal movements, and habitat selection and utilize those results to help inform and refine camera-based population and survival estimation efforts.

Table 1. White-tailed deer collared during February-March 2020 in north Idaho.

| Sex/Age Class                 | GMU |    |     |
|-------------------------------|-----|----|-----|
|                               | 1   | 6  | 10A |
| Adult Male                    | 2   | 7  | 12  |
| Adult Female                  | 15  | 33 | 35  |
| 6-month old Fawn (both sexes) | 4   | 22 | 10  |
| Total                         | 21  | 62 | 57  |

During spring-summer of 2020, we also deployed 500 remote cameras in GMUs 6 and 10A (250 per GMU) to seasonally estimate density and abundance of all large mammals, including deer, in these study areas with the methods described by Moeller et al. (2018). We generated random points throughout the study areas and deployed 2 cameras within 1 km of the generated points. One of the cameras at each point was restricted to being placed within 30m of the point, while the other could be placed on the best road/trail within 1 km of the point. This paired camera design will allow us to investigate the effect of random and non-random camera placement on detection of the various species, estimate the density of all large mammals in the system (even those that occur in low density), and attempt to estimate neonatal ungulate survival with cameras. These camera grids will remain deployed year-round, with visits by field staff for picture retrieval and battery replacement, allowing us to also examine seasonal changes in spatial distribution/density and interactions between the species over time and space.

The male white-tailed deer captured and GPS-collared during this project will also be used to evaluate the effects of hunting season structure and habitat security on male white-tailed deer survival. We're utilizing the ongoing statewide vegetation modeling efforts to provide vegetation security cover estimates. We will monitor these, and additional collared male deer in future years, for survival and movements related to habitat and human activity until death or collar failure. This research will provide managers with objective estimates of the effects of changing hunting season structure or habitat security, with the goal of maintaining hunter opportunity. To date, we have documented 2 mortalities on collared adult male white-tailed deer.

### Investigation 3 – Conduct 1 Elk study by 30 June, 2020

#### Results

*Modeled Effects of Predator Harvest on Ungulate Survival* - We collaborated with the University of Montana to bring on a Ph.D. student in fall of 2017 to work on this project. The student completed an approved dissertation proposal in November 2018. The overall objective is to build multi-predator, multi-prey population models (MPPMs) for IDFG to explore various management strategies and optimize management across the large mammal predator-prey community. The Ph.D. project is split into 6 chapters.

Chapters 1 and 2 address internal ecological processes (e.g., density dependence) that drive ungulate and carnivore population dynamics. This is essential to determine so that population dynamics in MPPMs are built sufficiently. The goal of Chapter 1 is to determine if animal population dynamics, including ungulates and carnivores, are capable of complex, nonlinear dynamics, and has been published in *Nature Ecology & Evolution* (see code at [https://github.com/teejclark/Ubiquitous\\_Nonlinearity](https://github.com/teejclark/Ubiquitous_Nonlinearity) and paper at

[https://teejclark.netlify.app/pdf/ClarkLuis\\_2019\\_NatureEE.pdf](https://teejclark.netlify.app/pdf/ClarkLuis_2019_NatureEE.pdf)). By analyzing >700 time-series of animal population dynamics, we determined that most animals, including 60% of ungulates and 40% of carnivores, were capable of nonlinear dynamics. This indicates the need to build nonlinear, phase-space reconstructions to model these animal dynamics. The aim of Chapter 2 is to explore how environmental stochasticity and density-dependence affect ungulate population dynamics. We've found that fast life-history species (i.e., r-selected) are more resistant to low densities and extinction due to environmental stochasticity. In contrast, slow life-history species like ungulates are prone to extinction due to environmental stochasticity (Figure 5). However, ungulate species like white-tailed deer may be able to buffer the effects of environmental stochasticity due to their demography, such as reproductive potential (high likelihood of twinning) and relatively linear density-dependence. Currently, we are building alternative nonlinear density-dependent population models that account for a realistic relationship between density and population growth rate.

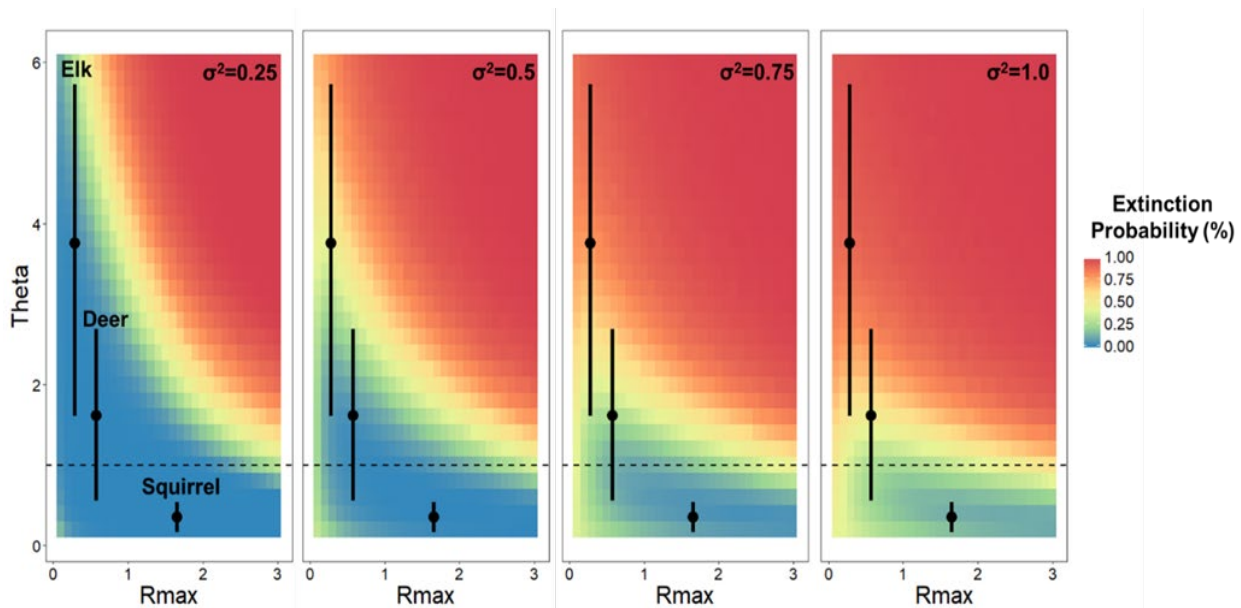


Figure 5. Probability of local extinction due to varying environmental stochasticity as a function of intrinsic rate of growth ( $r_{max}$ ) and nonlinear density dependence ( $\theta$ ). This was carried out with 5,000 simulations of the theta-logistic model at a constant carrying capacity of 5. The dashed line indicates the parameter space in which life-history strategies switch between r-selected ( $\theta < 1$ ) and K-selected ( $\theta > 1$ ). Vertical lines for elk, white-tailed deer (“deer”), and arctic ground squirrels (“squirrel”) represent the mean (black dot) and 95% CI for  $\theta$ .

Chapters 3 and 4 address single-predator, single-prey population models to determine broadly if large carnivores affect their ungulate prey. Chapter 3 addresses whether stochastic predation can cause predator-pit dynamics, where two alternative stable states exist and prey are held at a low density equilibrium by predation and cannot pass the threshold needed to attain a high density equilibrium. We found that stochastic predation can generate predator pits (Figure 6), but in poor habitat quality environments (i.e., low carrying capacity), predator pits do not occur and only low-density equilibria or extinction happens. This suggests two potential management scenarios of prey populations under stochastic predation given our simulations. If habitat is poor, then only one low-density stable state is possible. In this scenario, one cannot use predator control to increase prey populations, then let the predator populations regrow and expect prey to stay at high densities, as a predator pit is not occurring and there are no alternative stable states. To have

both high densities of predators and prey, improving the habitat is essential to move the population to a predator pit scenario. If habitat is productive or is improved from the previous scenario (i.e., high carrying capacity), then a predator pit could occur and prey populations might be held at a low density equilibrium. In this scenario, predator control might allow prey to grow to a high density equilibrium, then letting predator populations regrow should achieve both predator and prey populations at high densities. Chapter 3 has been submitted for publication in the journal *Oikos*. The aim of Chapter 4 is to conduct a meta-analysis of predator control experiments to determine if they are effective in increasing ungulate populations for managers. We found that predator removal did improve ungulate demographic responses by 13%, however prediction intervals overlapped with 0 (95% PI = -34 – 93%), indicating that future predator removal experiments will have uncertain effects (Figure 7). We found that this uncertainty was mainly driven by major flaws in experimental design, replication, and publication bias in predator control experiments we reviewed.

Lastly, the aims of Chapters 5 and 6 are to build MPPMs to investigate how predation and competition regulate large mammal assemblages, and how IDFG should optimize ungulate management given these assemblages. Chapter 5 focuses on building a framework and developing MPPMs as Bayesian integrated community models, and testing their ability to estimate demographic parameters and community-level interactions across patchy agency-collected data with observation and process error. We then tested MPPMs using an example of wolf-black bear-mountain lion (predator) and mule deer-elk (prey) management in the Sawtooth Elk Management Zone (GMUs 33, 34, 35, and 36). Broadly, we have found that MPPMs are able to estimate demographic and interaction parameters by using species with a lot of data (e.g., elk) to inform parameters of species with scant data (e.g., black bears). Chapter 5's analysis is finished and is being written for publication in the journal *Methods in Ecology & Evolution*. Finally, Chapter 6 is the MPPM to determine how harvest of predators/prey in large mammal assemblages across Idaho affects population management. In this chapter, we will be expanding the MPPM for the Sawtooths to incorporate functional responses, predation rates, etc. We will also build MPPMs for different regions across Idaho, as an extension of Chapter 5, to do the following: a) determine the relevant predator-prey community; b) determine the influence of functional/numerical responses; c) determine the coexistence of these species sans human harvest; and d) determine how harvest of one species affects the other species in the system, and if harvest strategies of multiple species should be considered together. Preliminarily, this research is intended for publication in *Ecological Monographs* or *Wildlife Monographs*.

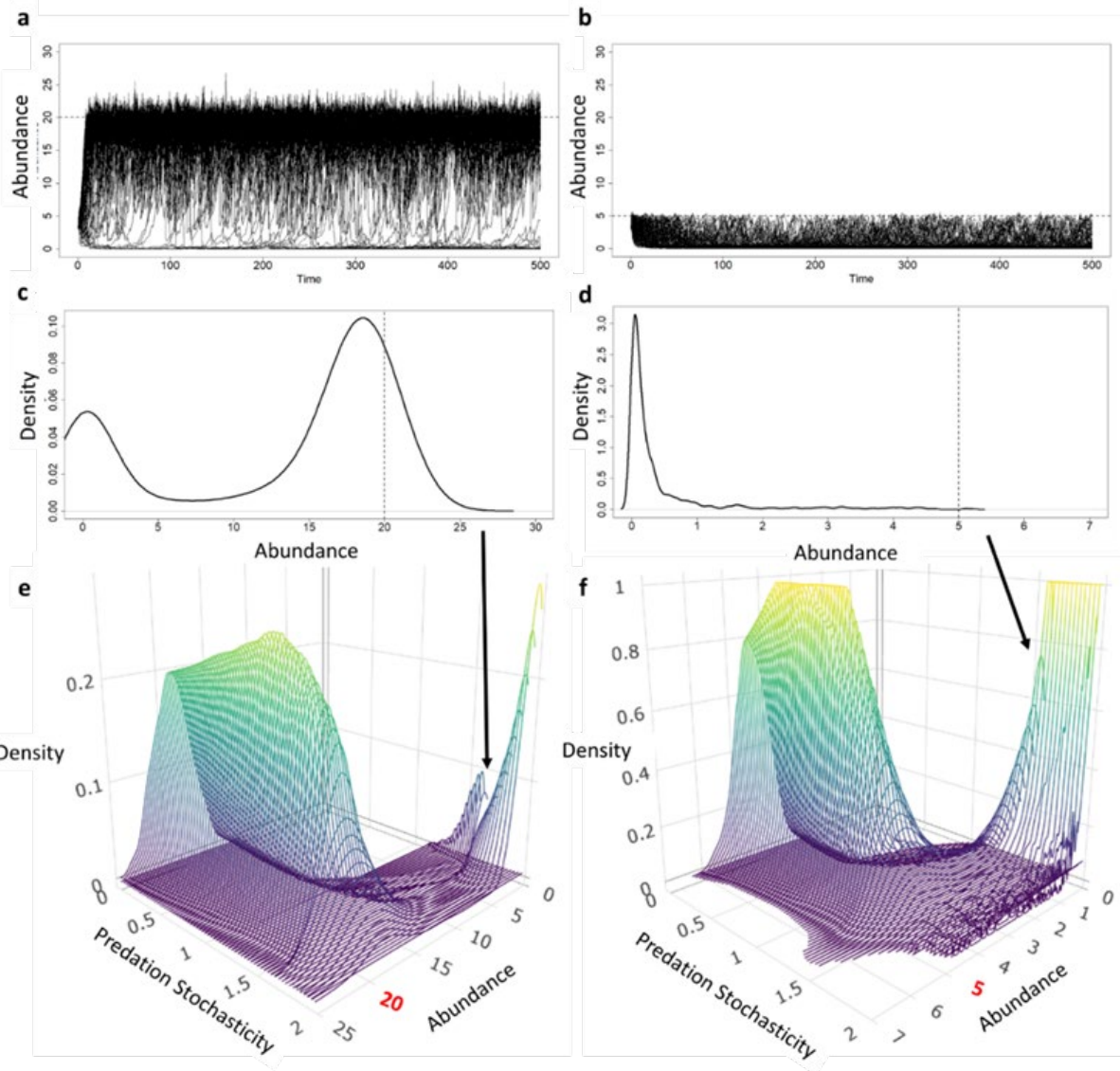


Figure 6. Population growth under predation stochasticity with high ( $K = 20$ ) and low carrying capacity ( $K = 5$ ). a) and b) represent 1,000 simulations of population growth with high predation stochasticity ( $\tau^2 = 1.75$ ) under high (a) and low (b) carrying capacity. c) and d) are density plots of the stationary distribution of abundances a) and b) at  $t = 500$ . Dashed lines represent carrying capacity. e) and f) show the change in the distribution of abundances at  $t = 500$  across varying levels of predation stochasticity ( $\tau^2$ ). Bold arrows indicate the relative position of the distribution in c) and d) in the density plots e) and f). Red numbers in the “abundance” axis indicate carrying capacity.

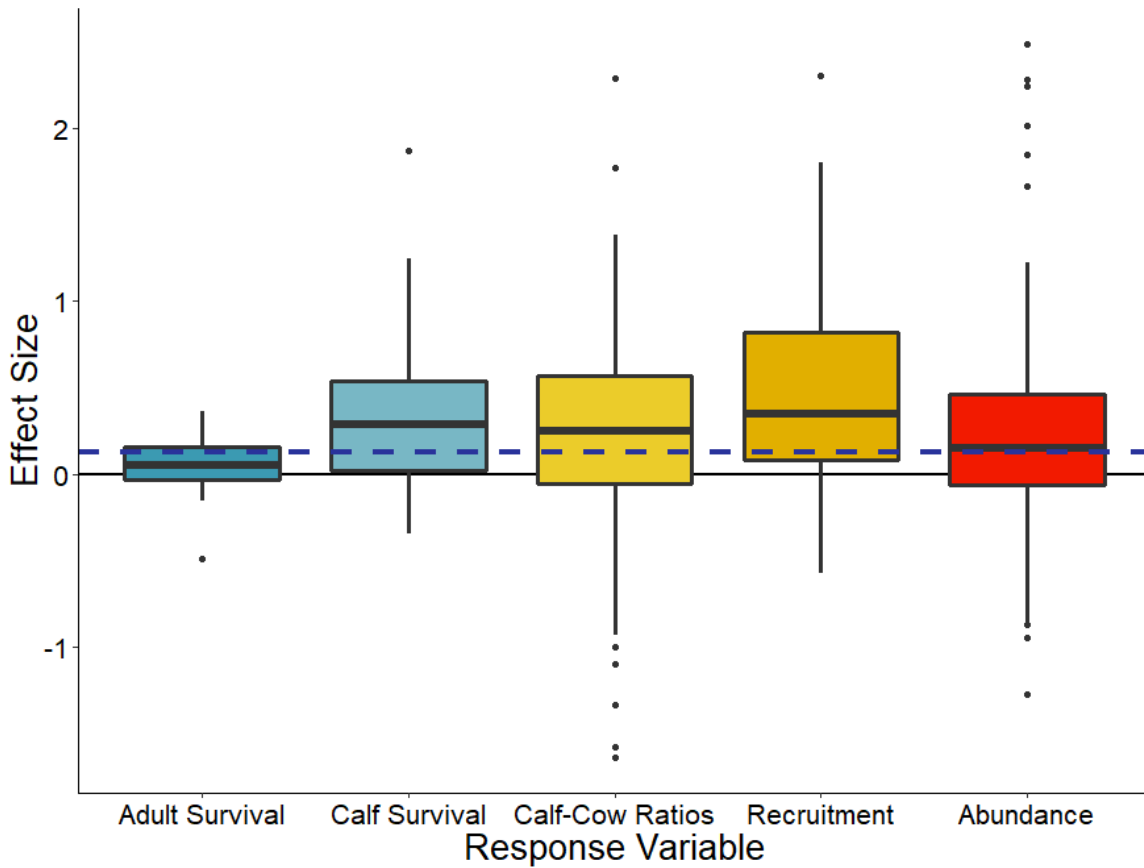


Figure 7. Effect size of predator removal experiments by ungulate response variable measured. Effect size was calculated as the log-response ratio of the experimental over control group. Effect size  $> 0$  indicates that predator removal has a positive effect on ungulate prey,  $< 0$  indicates a negative effect, and  $\approx 0$  indicates a negligible effect. “Abundance” represents experiments which measured abundance, density, or population growth rate. Dashed blue line represents the overall mean of the effect size of predator removal experiments in our meta-analysis.

*Elk Population Modeling* – We continued the development of our suite of online tools designed to help managers estimate and monitor elk populations and continued our evaluation of several methods of obtaining the vital rate data needed to populate an integrated population model to estimate annual elk abundance throughout Idaho (i.e., periodic population estimates, survival of young, survival of adults, fecundity, harvest rate).

SpeedGoat ([www.speedgoat.io](http://www.speedgoat.io)) has developed the integrated population model structure and incorporated it into the online modeling and reporting software PopR. The online platform was updated throughout the year with many of those updates focused on improving reliability and ease of use. We dramatically refactored the population model, which altered the process model to make it easier for users to predict not only future population growth but also evaluate the effects of potential management decisions on population growth. We also included our aerial survey models (program Aerial Survey) in the PopR software and developed a new data entry application. We are collectively writing an online book that will be made available to the entire agency for educational and reference purposes. Overall, our ability to serve decision makers with

online tools has been markedly improved through a major migration to a new server facility and upgrades to underlying software.

Our recent research and modeling software upgrades make it possible to use the lower cost, camera-based abundance estimates described in other sections of this report in integrated population models. Through this process of rewriting and organizing the code related to elk in PopR, we were able to generalize many of the routines and build capacity that will translate to management and analysis of other species' data. We deployed 500 cameras to estimate abundance of multiple species, including elk, in two GMUs in early summer. The data from these cameras will be collected in autumn 2020 and used to estimate deer and elk abundance in the summer for use in integrated population models.

We're examining how recently completed research on estimating pregnancy rates from remote sensed variables translates to other areas of Idaho where the models were not developed. Pregnancy rate is variable across habitat types in Idaho and is the most important component in the fecundity equation for elk. Estimating pregnancy and evaluating the model predictions will continue through the coming year.

Survival and recruitment of offspring is an important driver of elk population dynamics. We used GPS collars in seven areas of the state, which represent the primary ecotypes of the state with replication, to estimate survival of 6-month old calves through the winter and ensuing spring. We are then using these survival rates to represent the survival of neighboring elk zones with similar ecotype and predator density in the integrated population model. We monitored the survival of adult elk in each ecotype for many years to determine average survival and variation in survival. We use these adult survival averages in the integrated population model.

Estimating survival of neonatal ungulates, from parturition to six months of age, is logically challenging and oftentimes cost-prohibitive. As a result, our ecological understanding of neonate survival is limited for many species and management decisions are often made without an adequate understanding of their implications. For this reason, we have devoted a significant part of our research effort toward developing a method for estimating neonate survival of ungulates using remote camera data. We developed a model to estimate the overall survival rate of neonates, as well as the timing of mortality (i.e., shape of the survival curve), based on changes in the ratio of neonates to adult females observed in camera trap photographs. We evaluated the model with simulations and applied the model to camera data we collected on elk in northern Idaho.

The model is based on the number of adult females ( $y_{f,T}$ , females hereafter) and neonates ( $y_{n,T}$ ) in a picture, or set of pictures, taken at time  $T$  (e.g., day) from an array of motion-triggered CTs deployed on the landscape. We modeled the number of neonates photographed as a binomial variate,

$$y_{n,T} \sim \text{Binomial}(\phi_{n,T}, y_T), \quad (1)$$

where  $\phi_{n,T}$  is the probability that a photographed individual is a neonate and  $y_T$  is the total number of photographed individuals ( $y_{n,T} + y_{f,T}$ ). We defined  $\phi_{n,T}$  based on the ratio of the

abundance of neonates ( $N_{n,T}$ ) to females ( $N_{f,T}$ ) in the study area and their respective detection probabilities ( $d_{n,T}, d_{f,T}$ ),

$$\phi_{n,T} = 1 - \left[ 1 + \frac{N_{n,T} \times d_{n,T}}{N_{f,T} \times d_{f,T}} \right]^{-1}. \quad (2)$$

Next, we expanded equation 2 to accommodate the biological processes that determine the abundance of females and neonates. The expected number of females at time  $T$  is the number at the beginning of the observation period ( $T = 0$ ) multiplied by the probability of surviving to  $T$

$$N_{f,T} = N_{f,0} \times S_f(T). \quad (3)$$

Because our observation period starts before neonates are born, the expected number of neonates at time  $T$  is a function of (1) the number of females, (2) the birth rate (expected number of young born to each female), (3) the distribution of birth dates, and (4) the neonate survival function

$$N_{n,T} = \int_{t=0}^T [N_{f,t} \times B \times b(t)] \times [S_n(T-t)], \quad (4)$$

where  $B$  is the birth rate (offspring per female),  $b(t)$  is a function describing the probability density that a neonate is born at time  $t$ , and  $S_n(T-t)$  is a function describing the probability that a neonate will survive to age  $z = T - t$ . The first bracketed term in equation 4 is the expected number of neonates born at time  $t$  and the second bracketed term is the expected proportion of neonates born at time  $t$  that survive to  $T$ . Combining equations 2, 3, and 4 we have

$$\phi_{n,T} = 1 - \left[ 1 + \frac{\int_{t=0}^T N_{f,0} \times S_f(t) \times B \times b(t) \times S_n(z) \times d_{n,T}}{N_{f,0} \times S_f(T) \times d_{f,T}} \right]^{-1}. \quad (5)$$

The probabilities that an individual neonate ( $d_n$ ) and female ( $d_f$ ) is photographed at time  $T$  are the last components that connect our CT data to the neonate survival process. For the neonate detection probability, we recognize that for most ungulates there is a hiding phase where the mobility of the newborn is restricted compared to females, but as the neonate ages and becomes more mobile, it will eventually acquire mobility similar to that of the maternal adult. Thus, we modeled  $d_{n,T}$  as a combination of two probabilities: the probability that a neonate of age  $z$  is available (e.g., mobile enough) to have a picture taken, and given that it is available, the probability that a photo is taken ( $p_T$ ). Thus,  $d_{n,T} = a(z) \times p_T$ , where  $a(z)$  is a function describing the cumulative probability over time that a neonate of age  $z$  is available to be photographed. For females, we assume that they have the same probability of being photographed at time  $T$  as neonates when  $a(z)=1$ .

Thus, our ratio-based model for the probability of obtaining a neonate picture, after moving appropriate terms outside of the integral, is

$$\phi_{n,T} = 1 - \left[ 1 + \frac{B \times p_T \times N_{f,0} \int_{t=0}^T S_f(t) \times b(t) \times S_n(z) \times a(z)}{p_T \times N_{f,0} \times S_f(T)} \right]^{-1}, \quad (6)$$

and after cancelling terms,

$$\phi_{n,T} = 1 - \left[ 1 + \frac{B \int_{t=0}^T S_f(t) \times b(t) \times S_n(z) \times a(z)}{S_f(T)} \right]^{-1}. \quad (7)$$

Our simulations suggested that estimates of the overall neonate survival rate and the shape of the survival curve are accurate when researchers provide unbiased estimates of adult female survival, birth rate (offspring per adult female), and the distribution of birth dates (Table 2, Figure 8a and 8b). When researchers can provide *a priori* values for just adult female survival and birth rate, estimates of the overall survival rate were accurate but early neonate mortality was underestimated. Estimates were also precise with 90% occurring within 0.1 of the true survival rate (Figure 8a and 8b). When parameters associated with the distribution of birth dates were estimated in addition to neonate survival and time-to-availability, the overall survival rate ( $S_E$ ) remained unbiased whereas the shape parameter ( $\alpha$ ) was biased high, which caused estimates of survival during the middle of the period to be biased high by approximately 5 to 10% (Table 2, Figure 8c). Estimates of neonate survival were unreliable when we attempted to estimate the female survival rate or the birth rate with CT data (Table 2, Figure 8d and 8e).

As an example application, we estimated survival of neonate elk using CT data collected in northern Idaho, USA, during 20 May 2019 to 30 September 2019. We divided our 1078 km<sup>2</sup> study area into 226 grid cells and selected 70 cells based on a spatially balanced random sample (R package spsurvey; Kincaid and Olsen, 2019) to deploy motion-triggered cameras (Reconyx XR6 Ultrafire; Holmen, WI, USA; Figure 9). Our estimate of neonate elk survival in Idaho was consistent with values generated by capture-based studies.

Table 2. Performance of neonate survival model based on remote camera trap data. We investigated which parameters could be reliably estimated with CT data by progressively adding unknown processes to the estimation procedure and monitoring potential bias in the estimated neonate survival function.

| Biological processes estimated with CT data                           | Parameters estimated                       | Bias                       |                                |
|---|--|----------------------------|--------------------------------|
|   |  | Overall survival ( $S_E$ ) | Shape of survival ( $\alpha$ ) |
| Neonate survival  | $S_E, \alpha$                              | Unbiased                   | Unbiased                       |
| Neonate survival + time-to-availability                               | $S_E, \alpha, \delta, \gamma$              | Unbiased                   | Unbiased                       |
| Neonate survival + time-to-availability + distribution of birth dates | $S_E, \alpha, \delta, \gamma, \mu, \sigma$ | Unbiased                   | Biased                         |
| Neonate survival + time-to-availability + birth rate                  | $S_E, \alpha, \delta, \gamma, B$           | Biased                     | Biased                         |
| Neonate survival + time-to-availability + adult female survival       | $S_E, \alpha, \delta, \gamma, \lambda$     | Biased                     | Biased                         |

Our ratio-based model provides an accurate alternative to traditional methods for estimating neonate survival and does not rely on invasive or expensive capture and monitoring techniques. We believe this method could apply to a wide variety of species due to the ease of data collection and the relatively small number of critical model assumptions. A major benefit of our model is the ability to simultaneously monitor other species in the community, which will facilitate a better understanding of drivers of variation in neonate survival.

Bias was calculated as the difference between the mean of the estimated survival functions (across 300 replications) and the survival function used to generate the simulated data.

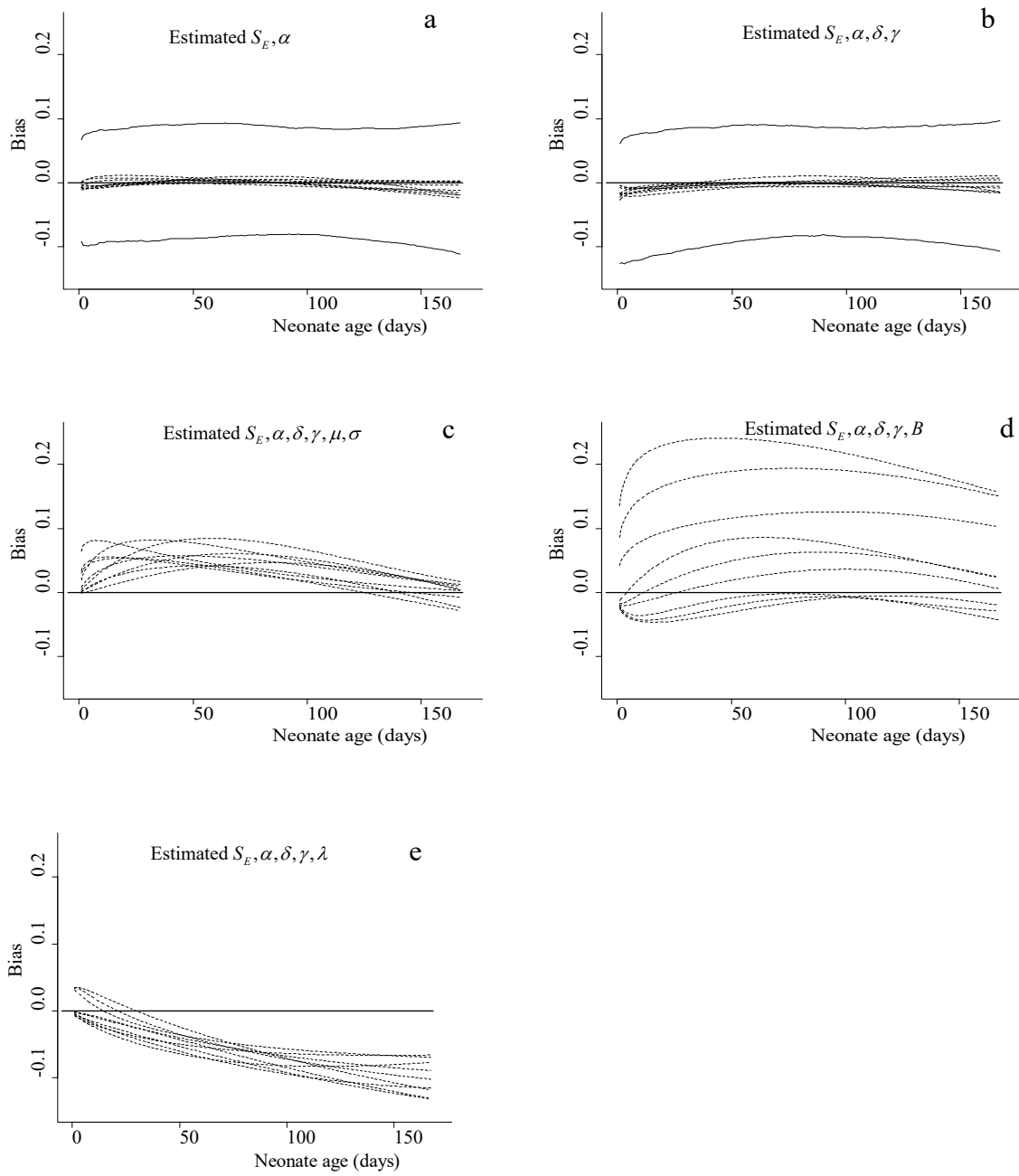


Figure 8. Bias (dotted lines) and precision (thin solid line) of the estimated neonate survival curve under five scenarios of prior information (a through e). Dotted lines are the mean (across 300 replications) estimated survival function minus the true survival function for each of nine alternatives. Precision was measured as the 90% quantiles of the estimated survival functions minus the true survival function across nine alternative survival functions.

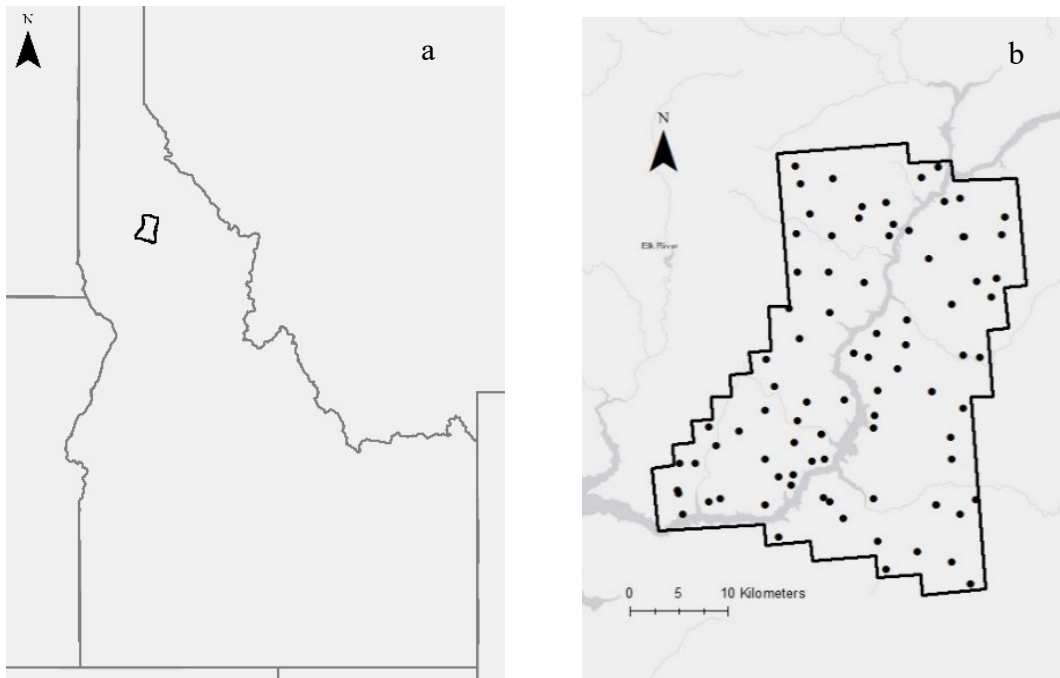


Figure 9. Location of the a) study area (black outline) in Idaho and b) 70 motion-triggered cameras used to estimate survival of neonatal elk.

*Seasonal Range and Migration Modeling* - Brownian bridge movement modeling (BBMM) techniques are less precise with less frequent locations because greater time increments increase the motion variance to estimate the utilization distribution from known GPS locations (Horne et al. 2007). Generally, BBMM require a location interval of more than 1 location/7.5 hours to construct utilization distribution probability surfaces that are useful for management purposes. Therefore, we focused on exploring and developing new techniques that would allow for more precise estimation of movement corridors from GPS locations that were collected >7.5 hours apart. We examined continuous time movement models (CTMM; Fleming et al. 2015, Fleming et al. 2016) and forced motion variance (FMV), and found that CTMM provided a more accurate estimation of elk movement corridors than FMV. However, FMV techniques were more precise and accurate in determining stopover locations.

In continued collaboration with the University of Wyoming Migration Initiative, we have continued to investigate CTMM and FMV methods and techniques by manipulating the spatial variance of data subset to a 12-hr location interval and comparing those estimates to estimates generated from the original 2-hr location interval data and traditional BBMM methods. In this framework, FMV variances were incrementally adjusted between 200 and 3,000m, then compared to the BBMM model using 2-hr location data. This process allowed us to identify the most accurate spatial variance to use for elk ( $1,200 \pm 460$ m). We also were able to calibrate how topographic complexity will affect the spatial variance. In less complex seasonal migrations, it is likely that a variance of less than 1,200m can be used. However, spatial variance will increase in regions with complex topography (e.g., when multiple mountain valley systems are traversed in a single seasonal migration). We also found that when scheduled location data is missed for periods of longer than 30hours, the accuracy of any of the techniques is depleted to the point where estimates should not be used.

Elk migrations are composed of two types of movement, high rate of movement travel areas punctuated by stopover forage and rest locations. Stopovers are typically identified as the top 25% of a percent volume contour for an entire migration route (similar to Sawyer and Kauffman 2011 with mule deer). However, they could also be identified by using an individual's rate of movement and duration of slower movement (i.e., identify when the individual is moving slowly for extended periods of time). To do so, we used our elk GPS location data to identify the slowest 10% of individual elk movement rates over a 12 hr period to establish a baseline for what a "slow" rate of movement is for elk in Idaho (~ 144m/hr following Calenge 2006, Calenge et al. 2009, and Calenge 2019). We then measured the sequential distances between stopover locations identified using this rate and duration of stay method to estimate the 'bandwidth' (i.e., distance to draw an ellipse from the identified stopover locations). Using the identified stopover locations and the bandwidth, we then estimated the area of stopovers with kernel density estimates with a quartic estimation procedure (KDE). This new method of identifying individual mule deer stopovers is capable of estimating stopover areas with confidence intervals. Initial comparisons to traditional BBMM techniques show that the techniques agree on one third of stopover locations and the rate and duration technique identifies many more stopover locations within a seasonal migration. Learning from earlier experiences, we are now in the process of expanding this analysis to other regions of Idaho where elk migratory behavior may differ from the animals used in this initial analysis. When individual elk migrations were compared between the rate and duration and BBMM methods, we see a close agreement between the techniques; with 86% of the identified stopover areas being shared, 6% unique to BBMM, and 9% unique to the rate and duration method.

When we organize the location data into population level analysis (i.e., population = winter herd), there are further differences between the two methods (Figure 10). At this level, we added together all of the stopover locations, dissolved any boundaries between them, and compared them to established BBMM methods for population level stopover assessment. The BBMM and rate and duration methods shared 42% of the stopover areas identified. Six percent of stopovers identified by BBMM methods were unique and most appeared to be centered on prevalent migrations routes. Rate and duration stopover locations not shared with BBMM methods comprised 52% of all stopovers. Further, rate and duration stopovers were more apparent in the distal portions of the seasonal migration routes. We saw similar results with our investigation of mule deer seasonal migration stopover estimates.

In collaboration with Department of Interior Secretarial Order 3362, we have produced migration routes for seven winter elk herds in southern Idaho (Figure 11). The elk seasonal migration routes were derived from individuals that are using a common winter range and are wearing GPS collars. Elk often exhibit lower winter range fidelity than other ungulates species in Idaho. We categorized intensity of use of each site in to three classes: 2 individuals to 10%, 10 to 20%, and greater than 20% use by the wintering herd. Stopovers and migration routes that were only used by one individual were manually removed.

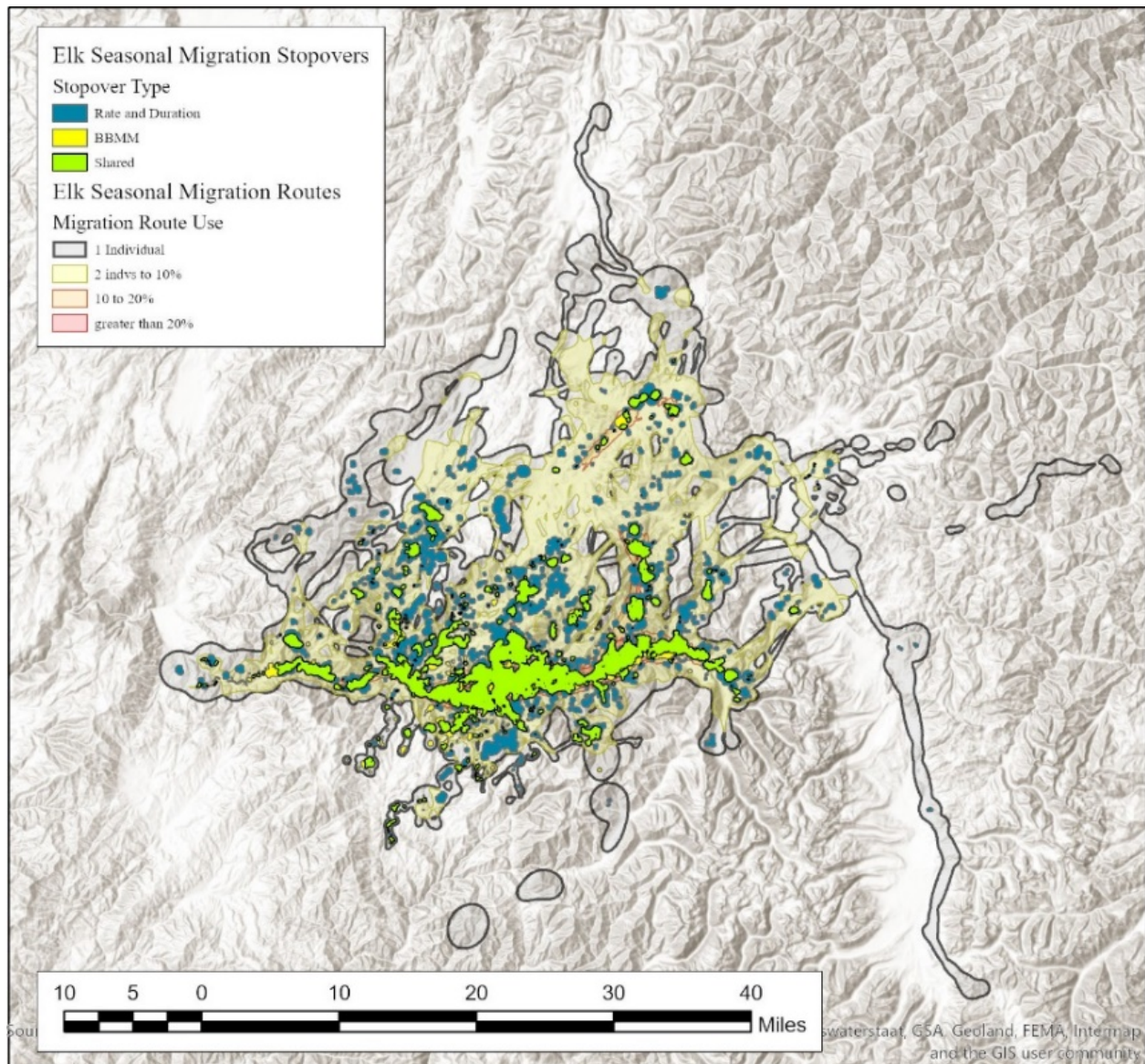


Figure 10. Elk seasonal migration stopover comparison between BBMM and Rate and Duration Methods in the South Fork of the Payette River.

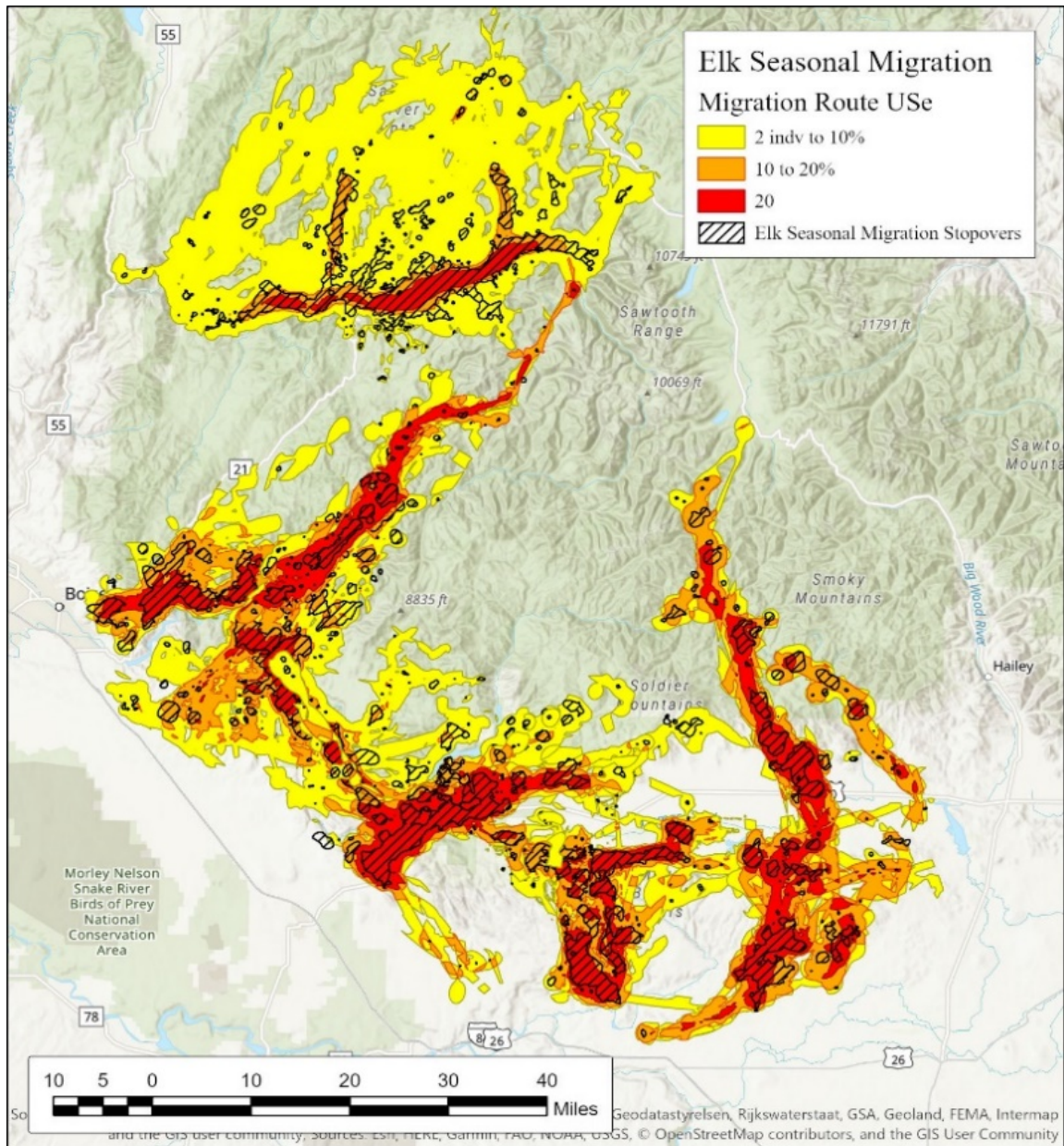


Figure 11. Seven seasonal elk migrations occurring in southern Idaho.

Our work on elk seasonal ranges focused on updating elk location databases collected since September 2016 and updating net-squared displacement techniques to delineate annual movement into winter range, spring migration, summer range, and fall migration. The NSD analysis is not yet complete for all elk locations collected. We are also updating the spatiotemporal covariate databases used for statistical analyses for estimating elk winter and summer ranges.

IDFG worked with TerraPulse to create a normalized vegetation difference index (NDVI) that fuses smaller 30m resolution Thematic Mapper data with daily images from MODIS satellite imagery to produce 30m resolution daily NDVI estimates (unpublished data, TerraPulse, <http://www.terrapulse.com>). This 2002-2019 dataset can be used as a proxy for vegetation growth across the state of Idaho and provides several other informative spatial databases that add

valuable information on estimating elk seasonal ranges. With data of this level of spatial and temporal detail, pixels within this dataset can be compared to the 18 year history, allowing for a temporal quantification of vegetation growth. This allows for a much more precise and accurate evaluation of vegetation performance and correlation to elk productivity across the state. Data of temporal nature allows us to construct phenological metrics at local and regional scales. The temporally-explicit nature of the NDVI information allows for inter- and intra-annual examinations of how vegetation effects elk habitat selection, especially in summer range. One of the accessory covariates that is provided in the TerraPulse data is time since forest disturbance (Figure 12). This data is at an annual increment but tracks the spatial heterogeneity of fire disturbances. Fire disturbances have changed forest structure and composition greatly in some regions in Idaho. Typically, in regions where fire has been prevalent transforming landscapes, we have also seen similar shifts in elk abundance and distributions. Having vegetation data that is capable of depicting inter-annual changes will help inform managers of how elk might shift in response to vegetation.

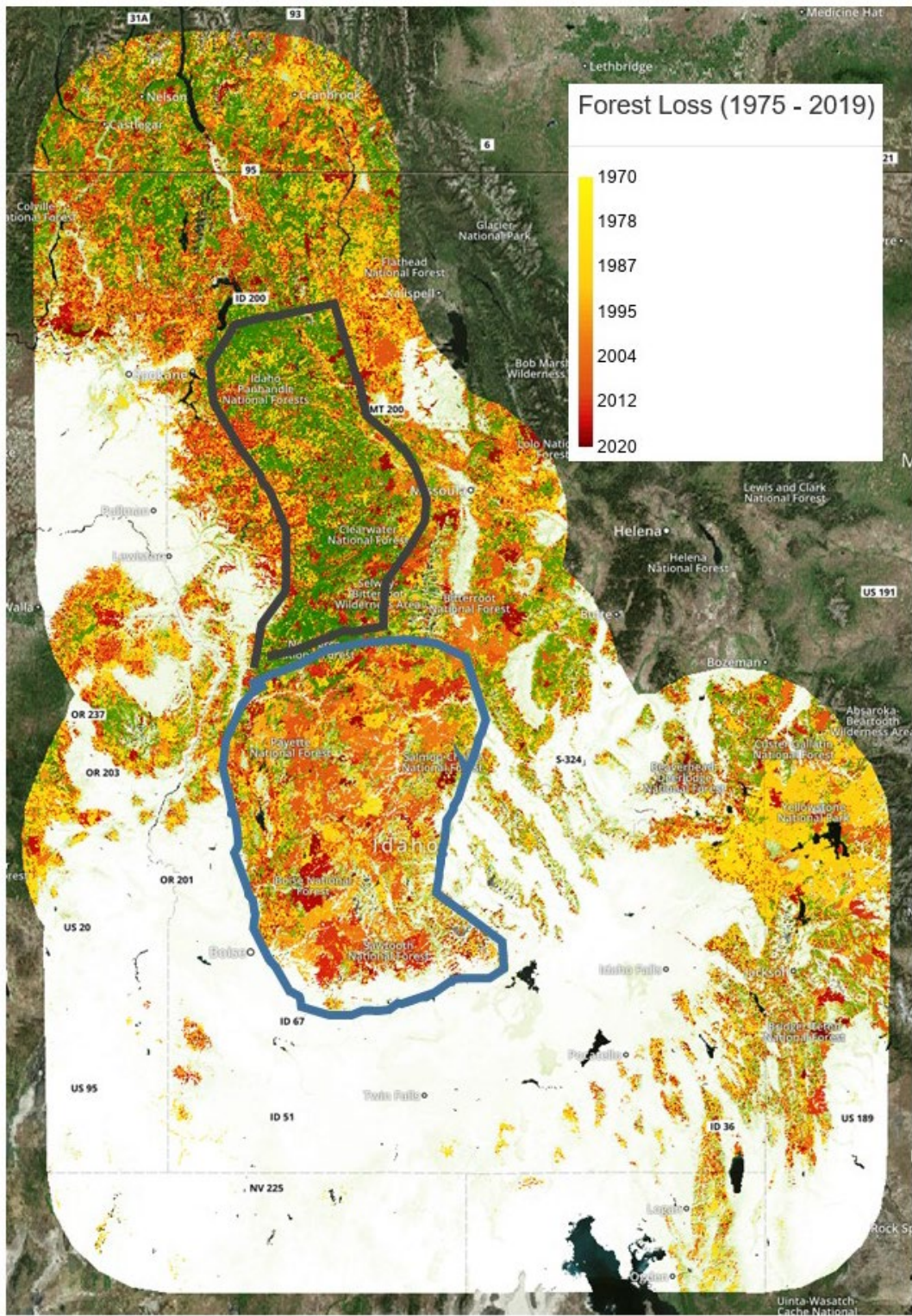


Figure 12. Age of last canopy disturbance in forested habitats in Idaho. There are distinct differences in fire disturbance at landscape scales as indicated by areas of where fire is a dominant factor determining forest structure and composition in the past 25 years (thick blue line) compared to other adjacent regions where canopy replacing disturbances occur at a much decreased frequency and extent.

## **Investigation 4 – Conduct 1 Bighorn Sheep study by 30 June, 2020**

### **Results**

*Disease Ecology* – We captured 108 bighorn sheep August 2019 – May 2020 (Table 3). We collected samples to test for exposure to and carriage of the respiratory pathogen *Mycoplasma ovipneumoniae* (Movi) and other bacteria, parasites and respiratory viruses. We used ultrasound and palpation to estimate body condition.

Table 3. Bighorn sheep captured in Hells Canyon, July 2019 – June 2020.

| Population            | Female | Male | Lamb | Total |
|-----------------------|--------|------|------|-------|
| Asotin                | 16     | 1    | 5    | 22    |
| Black Butte           | 2      | 1    | 0    | 3     |
| Tucannon              | 3      | 1    | 0    | 4     |
| Lostine <sup>1</sup>  | 26     | 1    | 1    | 28    |
| Lower Hells Canyon    | 9      | 0    | 3    | 12    |
| Muir                  | 3      | 3    | 1    | 7     |
| Redbird <sup>2</sup>  | 10     | 3    | 5    | 18    |
| Saddle Creek          | 6      | 1    | 2    | 9     |
| Upper Hells Canyon ID | 4      | 1    | 0    | 5     |
| Total                 | 79     | 12   | 17   | 108   |

<sup>1</sup> Four females and one male captured twice in the Lostine population for a total of 33 captures.

<sup>2</sup> Includes 3 females and 1 male captured at Telcher Creek on the Salmon River.

Movi infection was detected in a single Hells Canyon population: Lostine, Oregon.

Four of 25 adult females (16%), a yearling male, and a lamb were PCR positive for Movi, and serologic antibodies to Movi were detected in 81% (22/27) of sheep tested indicating widespread exposure (Table 4). Two adult females that tested positive for Movi twice had also been positive in previous years and met the criteria for a chronic carrier. One of these was euthanized and necropsied at the Washington Animal Disease and Diagnostic Laboratory and paranasal sinus tumors were among several abnormalities detected. No Movi was detected along the Snake River in Idaho or Oregon, or in any sheep tested in the Washington portion of Hells Canyon (Asotin, Black Butte, Tucannon).

We monitored 304 radio-collared bighorn sheep in 13 populations July 2019 – June 2020.

Survival of radio-collared sheep over this period ranged from 0.60 – 1 by population and sex, with an overall annual survival of 0.79 for females and 0.82 for males (Table 5). Summer lamb survival ranged from 0.60 – 0.100 and late winter/early spring lamb:ewe ratios ranged from 0.15 (Lostine) – 0.70 and averaged 0.37 in 12 Hells Canyon populations (Table 6).

Table 4. Summary of *Mycoplasma ovipneumoniae* (Movi) testing in the Lostine Oregon bighorn sheep population November 2019 – April 2020.

| Age class | n  | PCR positive | Seropositive |
|-----------|----|--------------|--------------|
| Adult     | 25 | 4 (16%)      | 20 (80%)     |
| Yearling  | 2  | 1 (50%)      | 1 (50%)      |
| Lamb      | 1  | 1 (100%)     | 1 (100%)     |
| Total     | 28 | 6 (20%)      | 22 (81%)     |

Table 5. Survival of radio-collared adult bighorn sheep in 13 Hells Canyon populations, 1 May 2019 to 30 April 2020.

|                         | Female |            |          | Male |            |          |
|-------------------------|--------|------------|----------|------|------------|----------|
|                         | n      | n survived | survival | n    | n survived | survival |
| Asotin                  | 21     | 16         | 0.81     | 9    | 8          | 0.89     |
| Big Canyon              | 7      | 5          | 0.86     | 2    | 2          | 1.00     |
| Black Butte             | 7      | 5          | 0.68     | 6    | 4          | 0.66     |
| Imnaha                  | 14     | 9          | 0.63     | 2    | 2          | 1.00     |
| Lostine                 | 36     | 34         | 0.94     | 20   | 20         | 1.00     |
| Lower Hells Canyon      | 25     | 20         | 0.79     | 6    | 5          | 0.85     |
| Mountain View           | 21     | 17         | 0.81     | 6    | 5          | 0.84     |
| Muir                    | 4      | 3          | 0.60     | 4    | 4          | 1.00     |
| Redbird                 | 45     | 37         | 0.83     | 12   | 11         | 0.99     |
| Saddle Creek            | 9      | 9          | 1.00     | 2    | 2          | 1.00     |
| Tucannon                | 6      | 5          | 0.82     | 3    | 3          | 1.00     |
| Upper Hells Canyon (ID) | 5      | 5          | 1.00     | 1    | 1          | 1.00     |
| Wenaha                  | 21     | 19         | 0.91     | 10   | 7          | 0.81     |
| Total                   | 221    | 184        | 0.79     | 83   | 74         | 0.82     |

Annual survival rates calculated as  $\left[1 - \left(\frac{n \text{ deaths}}{\# \text{ animal days}}\right)\right]^{365.25}$  to account for staggered entry (newly deployed collars).

We completed the final replicates of chronic Movi carrier crossover captive experiments at Washington State University (WSU) and South Dakota State University in 2018. Nearly all lambs survived in pens without carriers and nearly all lambs died when they were in a pen with a carrier. Pneumonia was only detected in pens with a carrier (Figure 12).

In 2019, we conducted an experiment at WSU placing 4 pregnant ewes in a pen with a carrier ewe that had not been bred. These were the same sheep involved in previous captive carrier experiments at WSU. We found that all 4 lambs in the pen with the carrier ewe showed clinical signs of pneumonia and were infected with Movi, but unlike previous years, only one (25%) died (Figure 13). Although this is a single data point, it suggests that transmission from the lamb of the carrier ewe to other lambs as completed in the previous studies vs. directly from the carrier ewe, as in this study, may increase lamb mortality, possibly due to an earlier age of contact and

first exposure to Movi and/or to a greater number of contacts and dose of infection. These may be factors that influence the effects of Movi transmission on lamb survival.

Table 6. Observed productivity of radio-collared ewes and survival of lambs born in 2019 in 12 Hells Canyon bighorn sheep populations, Idaho.

| Population         | <i>n</i><br>marked<br>ewes | <i>n</i> marked<br>ewes<br>w/lambs | Oct 1 lambs<br>(summer<br>survival) | Recruitment<br>(Lambs:100 ewes) <sup>1</sup> |
|--------------------|----------------------------|------------------------------------|-------------------------------------|--|
| Asotin             | 28                         | 24 (86%)                           | 19 (79%)                            | 33   |
| Big Canyon         | 7                          | 7 (100%)                           | 7 (100%)                            | 33   |
| Black Butte        | 11                         | 5 (45%)                            | 3 (60%)                             | 45   |
| Imnaha             | 18                         | 14 (78%)                           | 12 (86%)                            | 19   |
| Lostine            | 24                         | NA                                 | NA                                  | 15   |
| Lower Hells Canyon | 12                         | 11 (92%)                           | 7 (64%)                             | 33   |
| Mountain View      | 24                         | 23 (96%)                           | 20 (87%)                            | 49   |
| Muir               | 1                          | 1 (100%)                           | 1 (100%)                            | 20   |
| Myers              | 1                          | 1 (100%)                           | 1 (100%)                            | 70   |
| Redbird            | 49                         | 43 (88%)                           | 32 (74%)                            | 45   |
| Tucannon           | 10                         | 6 (60%)                            | 6 (100%)                            | 53   |
| Wenaha             | 26                         | NA                                 | NA                                  | 31   |
| Overall            | 211                        | 135/161<br>(84%)                   | 108/135<br>(80%)                    | 37   |

<sup>1</sup> Lamb/ewe ratio calculated from late winter/early spring population estimates

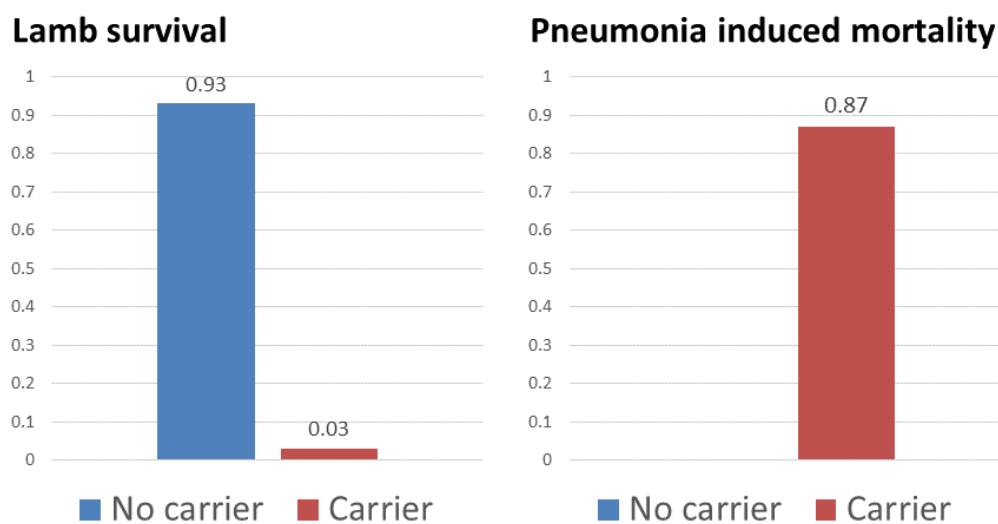


Figure 13. Lamb survival and pneumonia induced mortality of 31 lambs born in 13 pens with an Movi carrier ewe and 15 lambs born in 7 pens with no carrier ewe at Washington State University and South Dakota State University, 2015 – 2018.

*Population Estimation Methods* – We conducted ground-based mark-resight surveys in four bighorn sheep populations and were able to estimate abundance with confidence intervals of +/-

10 – 30%. The uncertainty associated with the point estimate scales with the average resight probability, the number of surveys conducted, and the proportion of the population that is marked (Table 7). We transferred analysis to a Program R interface for Program Mark (RMark) to allow development of a transparent user interface to simplify population estimation.

Table 7. Mark-resight survey results from 4 Hells Canyon bighorn sheep populations, 2019-2020.

| Population | % Adults & Yearlings Marked | Ewe Resight Probability | Ram Resight Probability | Mark-Resight estimate | 95% Confidence Interval | Min. Count |
|------------|-----------------------------|-------------------------|-------------------------|-----------------------|-------------------------|------------|
| Lostine    | 78%                         | 0.99                    | 0.30                    | 54                    | 48-65                   | 40         |
| Redbird    | 40%                         | 0.45                    | 0.45                    | 157                   | 132-191                 | 87         |
| Mtn View   | 34%                         | 0.93                    | 1.00                    | 88                    | 82-97                   | 84         |
| Wenaha     | 23%                         | 0.81                    | 0.60                    | 130                   | 100-184                 | 101        |

*Habitat, Nutrition, Movements, and Demographics* – During summer 2019 (July-August) we surveyed 47 habitat composition plots to quantify total biomass and nutritional quality of plant species available to bighorn sheep. We also sampled 8 phenology plots monthly in the East Fork of the Salmon and the Lost River Range to track the availability and succession of plant species. From these surveys we collected over 656 plant samples to be assayed for nutritional quality (e.g., crude protein, fiber, and digestible energy). During winter 2019-2020 we dried, ground, and organized over 1,400 plant samples in preparation for nutritional assays at the Idaho Wildlife Health Lab.

We also monitored a total of 52 ewes in the summer of 2019 to determine summer lamb survival in the East Fork of the Salmon (n=16), Lost River Range (n=33), and Owyhee (n=3). Lamb survival was highest in the East Fork of the Salmon (92%; Figure 13), followed by the Lost River Range (46%) and the Owyhee (33%). However, the Owyhee had a very small sample size, so the survival results likely do not reflect true average survival of lambs in 2019. During preliminary analyses, we found that ewes in the Lost River Range generally had the best body condition at capture (i.e., % ingesta-free body fat) and that lamb survival was positively associated with ewe body condition in February-March (Figures 14, 15 and 16).

During summer 2020, we completed biomass regression analyses and now have biomass predictions for all species, quadrats, and habitat plots in kg/hectare for each study site. In addition, we began using generalized additive models (GAMs) to predict spatiotemporal variation in the nutritional landscape (i.e., biomass of available forage) available to bighorn sheep at each of our study sites as a function of remotely sensed variables (e.g., greenness indices, topography, microclimatic variables, etc.).

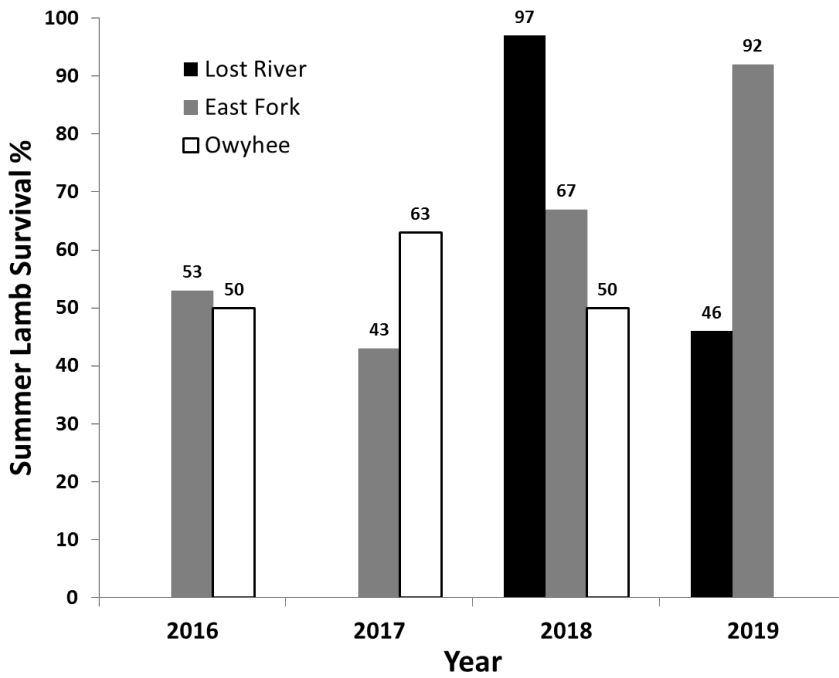


Figure 14. Estimates of summer lamb survival for bighorn sheep in the Lost River Range (black), East Fork of the Salmon River (grey), and Owyhee River (white) in Idaho from 2016-2019. Years where a site had less than 10 individuals collared are excluded from the graph.

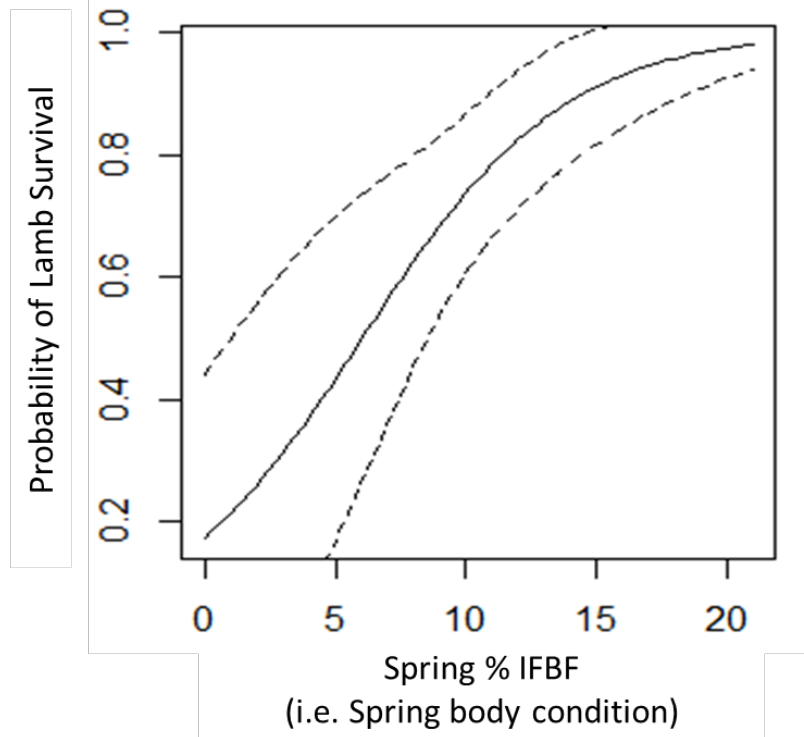


Figure 15. Probability of bighorn sheep lamb survival as a function of ewe condition (i.e., % ingesta-free body fat) in the East Fork of the Salmon, Lost River Range, and Owyhee River herds in Idaho. Dotted lines represent upper and lower 95% confidence intervals.

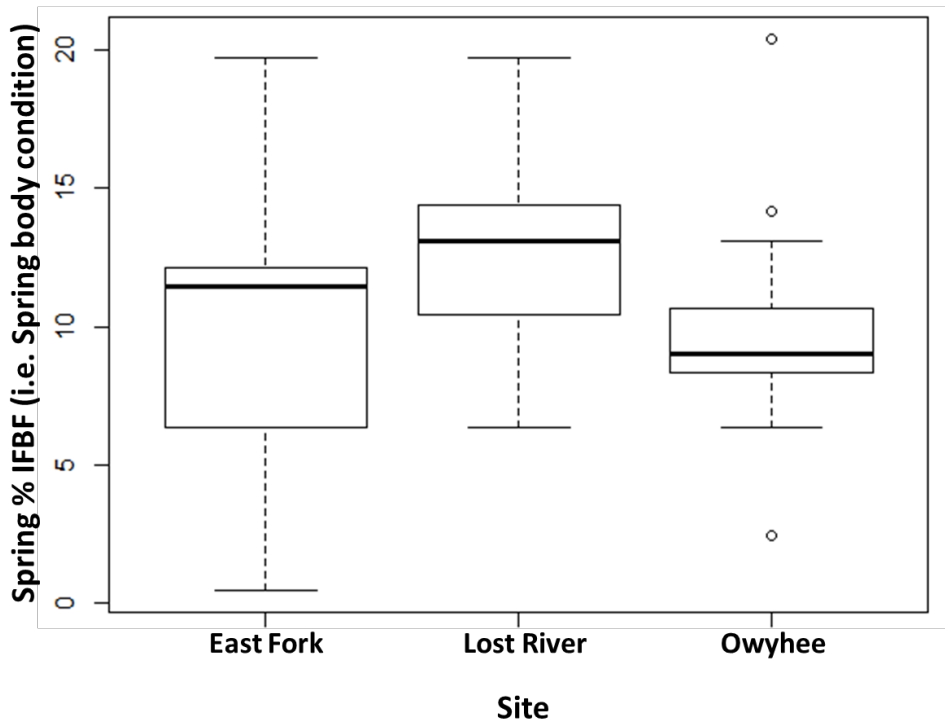


Figure 16. Boxplots comparing variation in ewe condition (i.e., % ingesta-free body fat) in February and March among Lost River Range, East Fork of the Salmon River, and Owyhee River, Idaho.

In the fall of 2019 we expanded our bighorn sheep nutrition research to include the Asotin Creek, Washington herd in the Hells Canyon metapopulation. Our primary aim in Asotin Creek is to uncover links between behavior (e.g., use of the nutritional landscape) and demography (e.g., lamb survival) of sheep occupying arid, low-elevation habitat.

We captured 16 ewes 15 October – 8 November 2019 to assess body condition and infection status and to deploy GPS collars to monitor movements, survival, and productivity. We estimated median ingesta-free body fat (IFBF) with ultrasound and palpation at 11% (range 9 – 17%). All ewes were negative on PCR for the pneumonia pathogen *Mycoplasma ovipneumoniae*. One ewe that survived a disease outbreak in 2011 – 2012 had antibodies to *M. ovipneumoniae*. No antibodies indicating exposure to *M. ovipneumoniae* were detected in the other ewes.

Three of the 16 study ewes (19%) died in April and May 2020. Both adults were pregnant (although one had miscarried prior to death), a yearling was not. Due in part to restrictions associated with COVID-19, we were only able to capture and collar 5 of the 8 live lambs confirmed to have been born to the 13 surviving study ewes (parturition dates 4/28 – 5/26). All lambs collared were male, and we monitored survival daily since capture (within 24 hours of birth). Survival of collared lambs to 60 days was 80% and survival of all lambs born to study ewes was 75% (6/8), although this estimate is likely biased due to small sample size and a ban on field work early in the season when some lambs may have been born but not survived. One collared lamb mortality occurred at 5 days of age, and was related to malnutrition and septicemia. Birthweight of this lamb (4.8 kg) was lower than the birth weights of the surviving collared lambs (range 5.2 – 5.5 kg).

Ewes observed with lambs, or that were known to be pregnant but died prior to parturition, were in slightly better body condition in the fall ( $n = 10$ , average IFBF 13%) than ewes that were never observed with lambs ( $n = 5$ , average fall IFBF 11%) and no relationship was detected between dam fall body condition and lamb birth weight (Figure 17). Small sample sizes preclude making any inferences from these preliminary data.

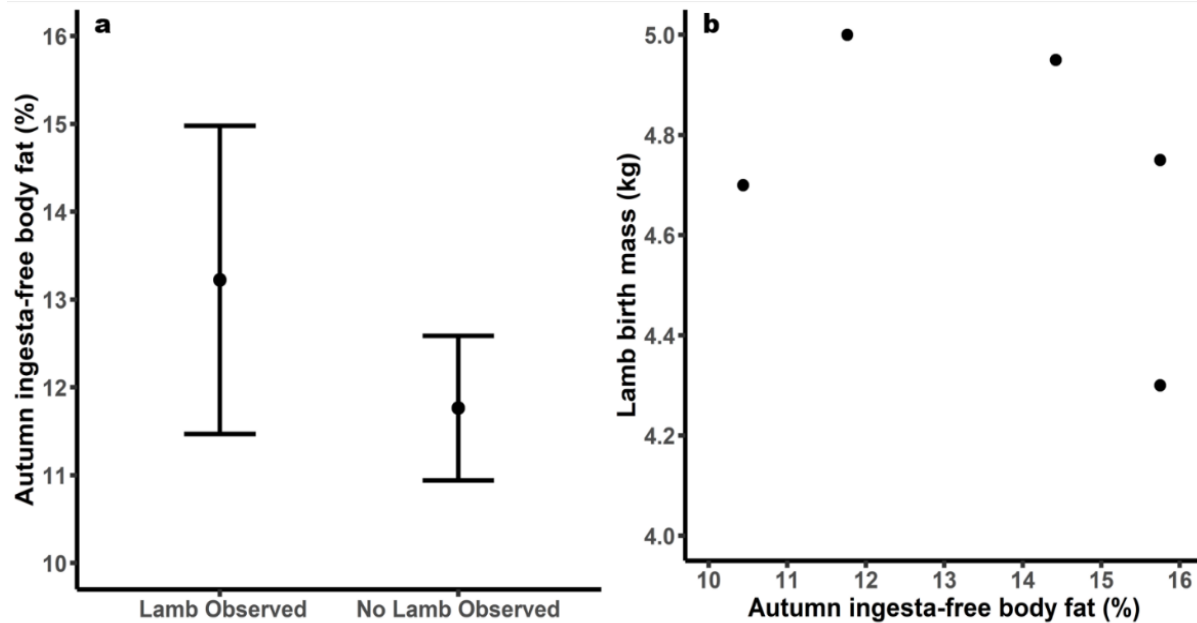


Figure 17. Relationship of fall ewe body condition to a) pregnancy (i.e., ewes known to have been pregnant [ $n = 10$ ] and those not observed with lambs or known to be pregnant [ $n = 5$ ]) and b) lamb birth weights ( $n = 5$ ), Asotin Creek 2019 – 2020.

We established 6, 100m vegetation phenology line intercept transects stratified by vegetation type, elevation, and aspect that we monitored on a monthly basis to track availability and succession of plant species across the study area. We also collected fecal pellets and vegetation data to assess diet composition and plant species availability. We plan to continue quantifying lamb survival and collecting plant phenology data in Asotin Creek during the summers of 2021–2023 to obtain sample sizes sufficient to facilitate reliable inference. Furthermore, we will quantify biomass and nutritional quality of plant species in Asotin Creek during the summers of 2021 and 2022. In 2021, we will be collaborating with the University of Wyoming to collect similar data for alpine bighorn sheep populations in northwestern Wyoming.

*Genetic Diversity, Ancestry, and Connectivity* - We continued to work on population genetics and ancestry analysis of reintroduced populations of Rocky Mountain bighorn sheep, comparison of historic and current population genetics in Idaho's native wild sheep populations, and evaluation of population genetics of California bighorn sheep with the University of Idaho Department of Fish and Wildlife. We also initiated a study of genomic diversity and evolution of *Mycoplasma ovipneumoniae* in domestic and wild sheep and goats at the University of Idaho Institute for Bioinformatics and Evolutionary Studies.

## Investigation 5 – Conduct 1 Moose study by 30 June, 2020

### Results

*Monitoring survival and cause-specific mortality* – During January-March, 2020 we used helicopter and ground darting operations to capture and GPS-collar 113 female moose across the state. About half of the collared moose were located in the same study areas as the ongoing predator-prey research (described under white-tailed deer, elk, black bear, mountain lion, and wolf projects) in GMUs 1, 6, and 10A (Table 8), while the remainder were spread across other moose populations in differing habitats across the State. This sampling design will allow us to both 1) fully integrate moose in to the predator-prey investigations of north Idaho and 2) begin to assess vital rates and causes of mortality for moose in all habitat types across the State.

Table 8. Game management unit (GMU) of capture locations for female moose collared during winter of 2020 ( $n = 113$ ), Idaho.

| GMU | Collared Moose | GMU | Collared Moose |
|-----|----------------|-----|----------------|
| 1   | 21             | 63  | 1              |
| 6   | 21             | 63A | 1              |
| 8   | 3              | 64  | 3              |
| 8A  | 7              | 65  | 2              |
| 10A | 9              | 66  | 2              |
| 50  | 4              | 66A | 3              |
| 51  | 2              | 67  | 4              |
| 54  | 4              | 69  | 1              |
| 58  | 1              | 70  | 1              |
| 59  | 1              | 71  | 2              |
| 59A | 1              | 74  | 1              |
| 60  | 1              | 75  | 2              |
| 60A | 7              | 76  | 6              |
| 62  | 2              |     |                |

We monitored collared moose for survival, determination of cause-specific mortality, and to conduct monthly calf-at-heel surveys to assess calf survival and female body condition throughout the year. There were a total of 8 non-capture related mortalities of collared moose through the monitoring period. Causes of death included winter tick infestation/emaciation (3 from GMUs 1, 6, and 67), wolf predation (1 in GMU 1), possible mountain lion predation (1 in GMU 62), bacterial infection (1 in GMU 1), vehicle collision (1 in GMU 68A), and unknown cause (1 in GMU 64). Personnel also responded to reported mortalities of un-collared moose to conduct necropsies and determine cause of death when possible. We investigated 10 un-collared moose mortalities during the reporting period and causes of mortality included Japanese yew intoxication (1 in GMU 1), winter tick infestation/emaciation (2 in GMU 1 and 8A), a variety of infections from various causes (4 in GMUs 6 [3] and 74 [1]), vehicle collisions (2 in GMUs 8A and 76), and unknown cause (1 in GMU 6).

We used a combination of infrared and high definition video from a fixed wing aerial survey and ground surveys to attempt to physically observe each collared female that was pregnant at capture (99 of 113 determined pregnant by blood at capture), and their neonatal calf, at least once

per month from May through September. GPS collar failures and other logistical problem precluded intensive enough monitoring to adequately evaluate parturition for 18 females. Of the remaining 81 collared females that were pregnant at capture and adequately monitored for parturition, 57 were confirmed with a calf and 24 were confirmed without a calf. It's possible the 24 without calves didn't carry their pregnancy to term or the calves were born and died prior to our survey efforts. If this pattern holds for future years of monitoring, we may need to add aspects of the research to better understand the causes for the decreased parturition rate or document the early neonatal mortality. We observed 57 females with 65 total neonatal calves sometime during the spring, 53 of which were still present with their dam during the July survey.

*Abundance modeling from trail camera data* – During spring-summer of 2020, we deployed 500 remote cameras in GMUs 6 and 10A (250 per GMU) to seasonally estimate density and abundance of all large mammals, including moose, using the methods of Moeller et al. (2018). We generated random points throughout the study areas and deployed 2 cameras within 1 km of the generated points. One of the cameras at each point was restricted to being placed within 30m of the point, while the other could be placed on the best road/trail within 1 km of the point. This paired camera design will allow us to investigate the effect of random and non-random camera placement on detection of the various species, estimate the density of all large mammals in the system (even those that occur in low density), and attempt to estimate neonatal ungulate survival with cameras. These camera grids will remain deployed year-round, with visits by field staff for picture retrieval and battery replacement, allowing us to also examine seasonal changes in spatial distribution/density and interactions between the species over time and space.

## **Investigation 6 – Conduct 1 Mountain Goat study by 30 June, 2020**

### **Results**

Our primary goal with this project was to design and evaluate noninvasive, ground-based field and analytical methods for estimating mountain goat abundance and occupancy. The project was completed in December 2019 and an overview of results follows. For all data analyses and complete results, see the University of Montana thesis entitled: “Methods for Estimating Mountain Goat Abundance and Occupancy” <https://scholarworks.umt.edu/etd/11512/>.

The 2019 field season ran from July 1, 2019 - August 23, 2019. A few minor changes were made to the 2018 data collection protocol that hugely improved efficiency and organization of the 2019 field season. These improvements, along with the addition of a third observer team, allowed the mountain goat monitoring crew to over triple the amount of data collected (in addition to added camera trapping efforts) during the 2019 season.

By surveying sites in 70 out of 574 potential cells across the study area, we monitored approximately 12% of the Snake River Range study area (Figure 18). During the 8 week season, we completed 3 – 4 repeat visits to each survey site. Mountain goats were detected at 7 unique sites throughout the season, 2 of which had repeat mountain goat detections, totaling 9 sites with at least 1 mountain goat detection throughout the survey season. We also placed cameras in 61 sites, which took 859,033 photos during the season. Of these 61 deployed cameras, 53 remained functional throughout the survey period.

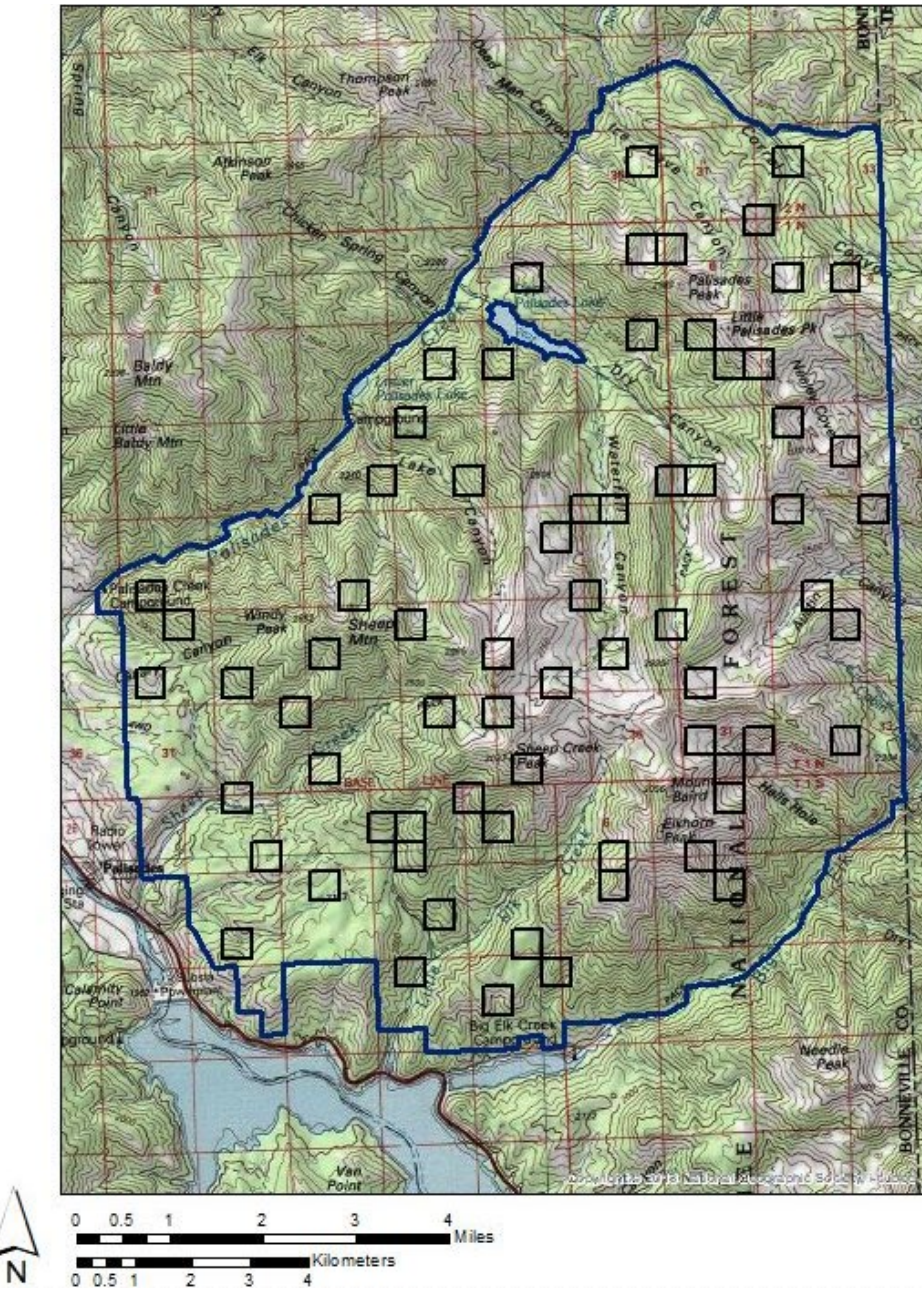


Figure 18. Mountain goat population estimation project study area, Snake River Range, Idaho

In an effort to design a method for monitoring mountain goats over a shorter duration, while still maintaining statistical rigor, we developed the Mountain Goat Blitz (MoGoBlitz). The MoGoBlitz's 12 participants surveyed 27 of the 70 survey sites between the August 2<sup>nd</sup> and August 7<sup>th</sup>. All MoGoBlitz personnel were IDFG employees who participated in day hikes or 2 – 3 day backpacking trips. Mountain goats were detected in 2 the 27 sites surveyed. There were not enough detections and surveys conducted for effective abundance estimates from these data. A larger effort would be needed to collect sufficient data for this approach to effectively estimate abundance.

On August 19, we conducted an aerial survey of the Idaho portion of the Snake River Range and documented 65 mountain goats. This was about half the number of goats counted during the

same aerial survey in 2018. The area flown included the project study area in addition to Baldy Mountain, Atkinson Peak, and Thompson Peak areas northwest of the study area.

Ground observation data were analyzed using 3 different n-mixture abundance models to test the effect of geographic closure assumptions on abundance estimates. The 3 models assumed geographic closure (i.e., animals don't leave or enter the area during the timeframe) at the season, sampling occasion, or daily levels. Of the three models, abundance results ranged from a mean estimate of 435 goats (95 % credible CRI = 113 – 721) with the season abundance model to 104 mountain goats (95 % CRI = 78 – 144) with the daily abundance model. Of the three abundance models tested, the daily abundance model appeared to best meet the sampling assumptions.

Data from remote cameras were analyzed to estimate mountain goat occupancy and evaluate variation in mountain goat use both spatially and temporally. Occupancy models estimated that 0.18 of sites were occupied by mountain goats in this study area. Based on results from occupancy models, mountain goat distribution varied across covariate values. Covariates included were elevation, forest cover, slope, and aspect.

Our results suggest that multiple observer surveys were more effective than cameras surveys for estimating abundance for the Palisades mountain goat population. A manuscript describing the method developed for effectively estimating mountain goat abundance from observer-based ground surveys will be submitted to the journal “Ecosphere” in September 2020.

## **Investigation 7 – Conduct 1 Gray Wolf study by 30 June, 2020**

### **Results**

*Estimating Wolf Abundance and Distribution* - Occupancy-specific cameras (cameras set to only take motion triggered photos, generally placed in locations for numerous years) accounted for 218 of the total cameras we deployed and abundance-specific cameras (set to take motion and time-triggered photos & placed in groups of 16 cameras within a focal cell) accounted for 573 of the cameras we deployed. Abundance cameras were placed in 3 strata. We used occupancy estimates from 2016-2018 to stratify statewide occupancy cells in to high, medium, or low strata. We then used generalized random tessellation sampling to select 37 occupancy grid cells across the state for abundance estimation. We selected occupancy grid cells so that 50% of effort went to the low occupancy stratum (total statewide area 14,633 km<sup>2</sup>), 30% to the medium occupancy stratum (12,824 km<sup>2</sup>), and 20% to high occupancy stratum (8,124 km<sup>2</sup>). Each selected occupancy grid cell was then split into 16 sub-cells and an abundance camera was placed in each sub-cell. Within the selected occupancy grid cells and abundance sub-cells, cameras were placed in locations consistent with previously developed occupancy sampling protocols that relied on predicting and sampling wolf rendezvous site habitat. Occupancy cameras were placed in the same locations as previous years.

A total of 8,073,364 time-triggered and 3,612,712 motion-triggered photos were taken by all cameras combined (11,686,098 total). Of these, 1,159,652 photos contained animals and 10,526,424 did not contain any animal (or human/vehicle). We continued to work with Microsoft Corp. on development of an artificial intelligence detector that gives us a likelihood that each picture contains an animal or not. The detector has proven very accurate in testing to date and allowed us to not look at about 9,531,968 photos that had a low likelihood of containing an animal.

The statewide camera grid captured a total of 10,424 pictures of wolves on 259 cameras, the vast majority of which were captured with motion detection (Figure 19).

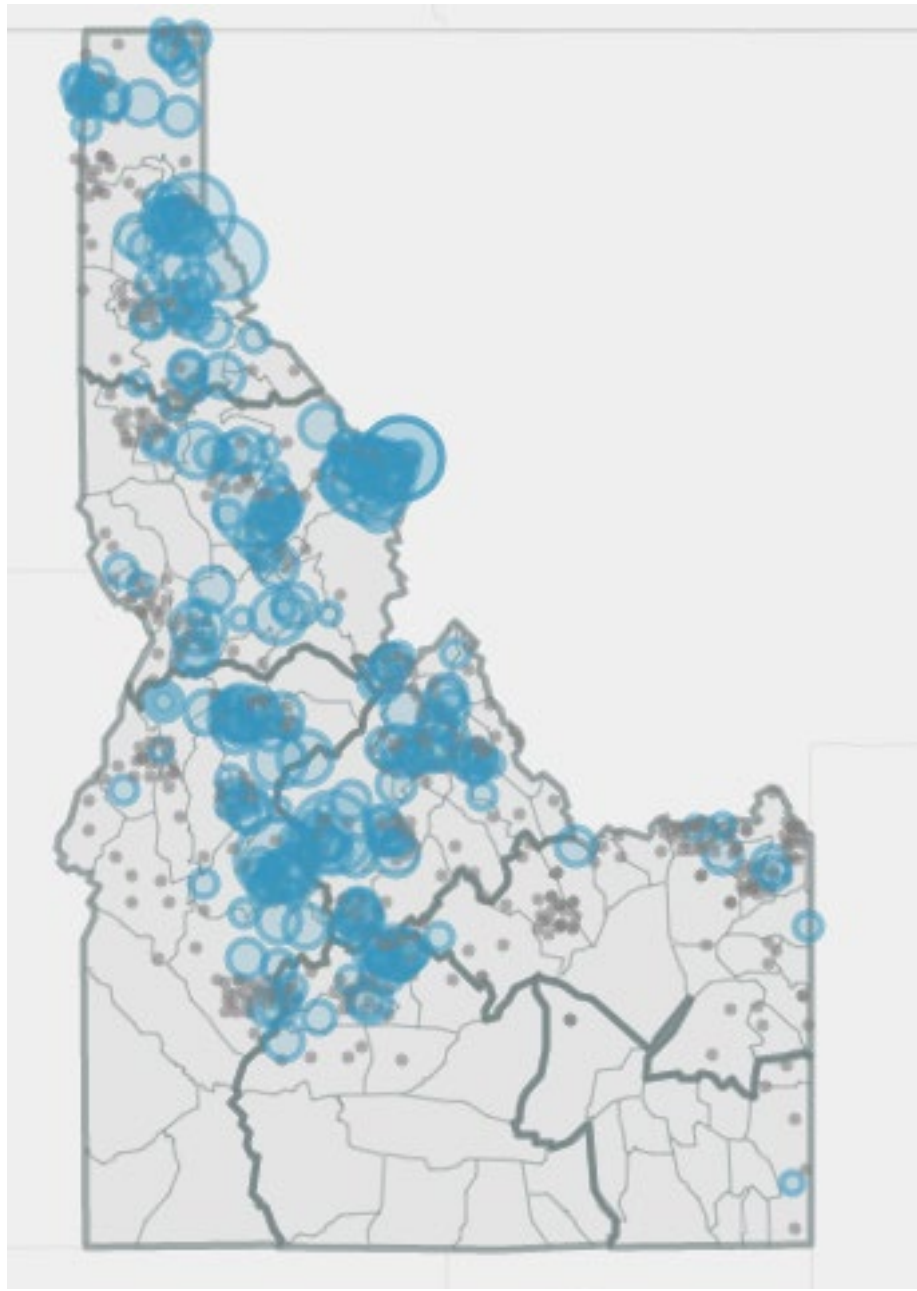


Figure 19. Relative number of wolf pictures captured from statewide camera grid, 2019 (blue circle means wolf pictures were taken, size of blue circle reflects relative number of pictures taken, gray circle means no pictures of wolves).

We used a space-to-event analysis to estimate the number of wolves by stratum (Moeller et al. 2018). We limited the analysis period to July 1, 2019-August 31, 2019 to provide a period of consistent wolf numbers and consistent camera deployment. To estimate abundance, we extrapolated the mean wolves per square meter to the area of predicted rendezvous site habitat,

after areas of water and human development were removed. The estimated wolf abundance was 1,541 (SE = 219, 95% CI: 1,111-1,971) across the statewide grid (Table 9).

Table 9. Abundance estimates ( $\hat{N}$ ), standard errors (SE) and 95% confidence intervals (LCL-UCL) for wolves in Idaho in 2019 across three strata from camera data. Area represents the entire area of each stratum, not predicted high use wolf rendezvous site habitat only.

| Stratum | Area (km <sup>2</sup> ) | $\hat{N}$ | SE  | LCL   | UCL   | Density (per 1000 km <sup>2</sup> ) |
|---------|-------------------------|-----------|-----|-------|-------|-------------------------------------|
| Low     | 36,381                  | 290       | 47  | 199   | 382   | 7.98                                |
| Medium  | 37,068                  | 294       | 60  | 176   | 412   | 7.94                                |
| High    | 37,068                  | 956       | 112 | 736   | 1,176 | 25.8                                |
| Total   | 110,517                 | 1,541     | 219 | 1,111 | 1,971 | 13.9                                |

The statewide camera grid also captured pictures of over 40 unique species (dozens more that were not identifiable to the species level due to their size [e.g., songbirds, rodents]; Table 10) that will provide a wealth of additional information on species distribution and relative abundance.

Table 10. Regional summary of cameras deployed, photos taken, and species detected during 2019 statewide wolf estimation efforts, Idaho.

| Region | Cameras | Photos    | Unique Species Detected |
|--------|---------|-----------|-------------------------|
| 1      | 129     | 1,721,086 | 34                      |
| 2      | 160     | 2,283,440 | 34                      |
| 3      | 136     | 2,309,824 | 37                      |
| 4      | 56      | 1,072,043 | 35                      |
| 5      | 6       | 41,804    | 19                      |
| 6      | 109     | 2,109,228 | 35                      |
| 7      | 153     | 2,276,220 | 39                      |

We also conducted ground-based rendezvous site surveys in GMUs 24, 32A and a portions of 23, 25, and 33 in an attempt to document wolf abundance and distribution in this low density, high conflict area. We visited 462 potential rendezvous site locations, based on predicted rendezvous site habitat characteristics, and conducted howl surveys and searches for wolf scat. We also visited 3 recent livestock depredations in the area identified as probable or definite wolf depredations in an attempt to collect wolf scat. We collected 216 total scats (150 potential adults, 66 potential pups) during the entire summer June-September. We were liberal on the scats we collected, erring on the side of collecting scats that had potential to be other species (mountain lion, coyote, bobcat, domestic dog), in an effort to not miss any wolf presence. We documented 1 active wolf rendezvous site, from which 112 of the scat samples were collected. The majority of the scats collected outside of the confirmed rendezvous site were not of wolf origin. We collected 5 additional scats from depredation sites. DNA analyses of these samples are ongoing.

*Harvest Effect on Predator/Prey Relationships* – We used helicopter darting and ground trapping efforts to capture and GPS collar 5 wolves for predator-prey research during the reporting period, 2 in GMU 10A (2 adult male) and 3 in GMU 6 (1 yearling female, 2 adult male). Survival and

location data from these, and future, collared wolves, along with pictures from remote camera work, will be used to better understand habitat selection and interactions between wolves, their prey, and other predators.

## **Investigation 8 – Conduct 1 Mountain Lion study by 30 June, 2020**

### **Results**

Working with management staff, we utilized houndsmen (both volunteer and professional) to tree, dart, and GPS collar mountain lions in the north Idaho predator-prey study areas (GMUs 1, 6, and 10A), GMU 32A, and in the Bear River area of southeast Idaho where we also had a camera grid deployed. We collared 1 adult female in GMU 1, 2 subadult males in GMU 6, 3 in GMU 10A (2 subadult males, 1 adult female), 2 adults in GMU32A, and 10 in GMUs 75/77 (6 subadults, and 4 adults). The locations from these lions are being used to better understand habitat selection to inform future camera-based estimation efforts and as marked individuals during current camera-based estimation method validation efforts.

We worked with management staff in the southeast region of Idaho to design and deploy a remote camera grid of 95 cameras to estimate mountain lion density in the Bear River area (GMUs 75 and 77). The grid was designed to cover the entirety of mule deer winter range in the area, assuming mountain lion distribution during the winter would emulate their primary prey in this system (Figure 20). We then generated a primary and alternate random point in each cell for camera placement. The alternate point was only used if the primary was inaccessible. Personnel deployed cameras as close the generated point coordinates as possible facing a road or trail. Cameras were deployed in November 2019 and retrieved in April 2020. Picture classification is almost complete and then we will generate density estimates and, if possible, compare to density estimates from mark-recapture models utilizing collared lions.

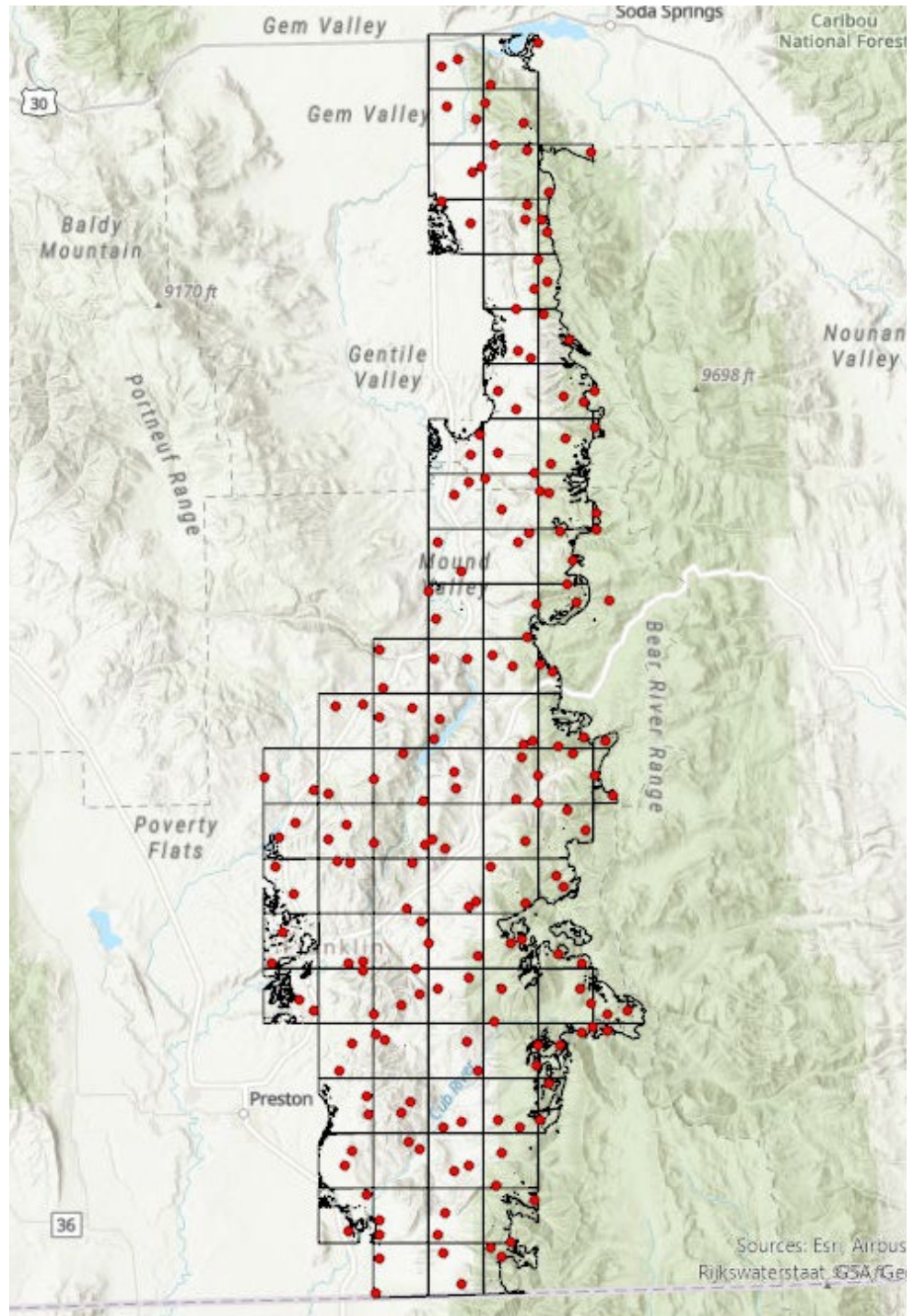


Figure 20. Map of camera grid, and primary and alternate random camera location points in each grid cell, designed to represent mule deer winter range extent for estimation of mountain lion density, Bear River, Idaho, 2019-2020.

## **Investigation 9 – Conduct 1 Black Bear study by 30 June, 2020**

### **Results**

We used ground trapping efforts to collar 28 black bears during the reporting period, bringing the total collared for the overall project to 32 (Table 11). We have a goal of 36 total collared bears (12 in 3 GMUs) and will attempt to reach full sample size during the 2021 spring-summer trapping season. We will use these collared bears to monitor survival, movements, habitat selection, and interactions with other species of prey and predators. Habitat selection and movement data, along with sighting of collared bears in remote camera pictures, will be used to improve camera-based estimation techniques.

Table 11. Black bears collared, slipped collars, and currently active collars for Idaho research.

| GMU   | Collared | Slipped | Active Collars |
|-------|----------|---------|----------------|
| 6     | 8        | 0       | 8              |
| 10A   | 12       | 1       | 11             |
| 32A   | 12*      | 2       | 10             |
| Total | 32       | 3       | 29             |

\* - 4 collared in 2019, 8 collared in 2020

During summer 2019 and 2020 we also continued to sample berry production in an effort to correlate mast production with bear population performance. In 2020, we used a fine-scale understory vegetation prediction model we developed from NAIP imagery and other environmental covariates to predict presence of berry producing shrubs that are desirable to black bears (e.g., huckleberry) to make sampling more efficient. Vegetation sampling and modeling will be the major focus of the project for the 2021 field season.

During spring-summer of 2020, we deployed 500 remote cameras in GMUs 6 and 10A (250 per GMU) to seasonally estimate density and abundance of all large mammals, including black bears, using the methods of Moeller et al. (2018). We generated random points throughout the study areas and deployed 2 cameras within 1 km of each generated point. One of the cameras was restricted to being placed within 30m of the point, while the other could be placed on the best road/trail within 1 km of the point. This paired camera design will allow us to investigate the effect of random and non-random camera placement on detection of the various species, estimate the density of all large mammals in the system (even those that occur in low density), and attempt to estimate neonatal ungulate survival with cameras. These camera grids will remain deployed year-round, with visits by field staff for picture retrieval and battery replacement, allowing us to also examine seasonal changes in spatial distribution/density and interactions between the species over time and space. We also placed 75 cameras in GMU 32A during the summer of 2020, using the methodology described above, where we selected the best road or trail for camera placement, specifically to estimate black bear density and distribution in this system.

## Investigation 10 – Conduct 1 Greater Sage-grouse study by 30 June, 2020

### Results

*Effect of Livestock Grazing* – This long-term, landscape-scale project has been ongoing for 7 years and now encompasses 6 study areas. We have monitored the survival, habitat selection, and reproductive effort and success of 760 female greater sage-grouse to date (Table 12). Female survival during the breeding season has varied from 60% to 85% during 2014-2018. We have monitored the success of 722 nests during the study to date (Figure 21; we are monitoring 153 nests in 2020 but survival estimates were not available during the reporting period and are not included in the figure).

Table 12. Adult and yearling female greater sage-grouse captured by year across 6 study sites in southern Idaho for the grazing project.

| Age      | 2014     | 2015     | 2016     | 2017     | 2018     | 2019      | 2020      |
|----------|----------|----------|----------|----------|----------|-----------|-----------|
| Adult    | 52 (57%) | 57 (53%) | 82 (68%) | 76 (58%) | 90 (73%) | 111 (59%) | 118 (74%) |
| Yearling | 40 (43%) | 51 (47%) | 38 (32%) | 55 (42%) | 33 (27%) | 77 (41%)  | 41 (26%)  |
| Total    | 92       | 108      | 120      | 131      | 123      | 188       | 159       |

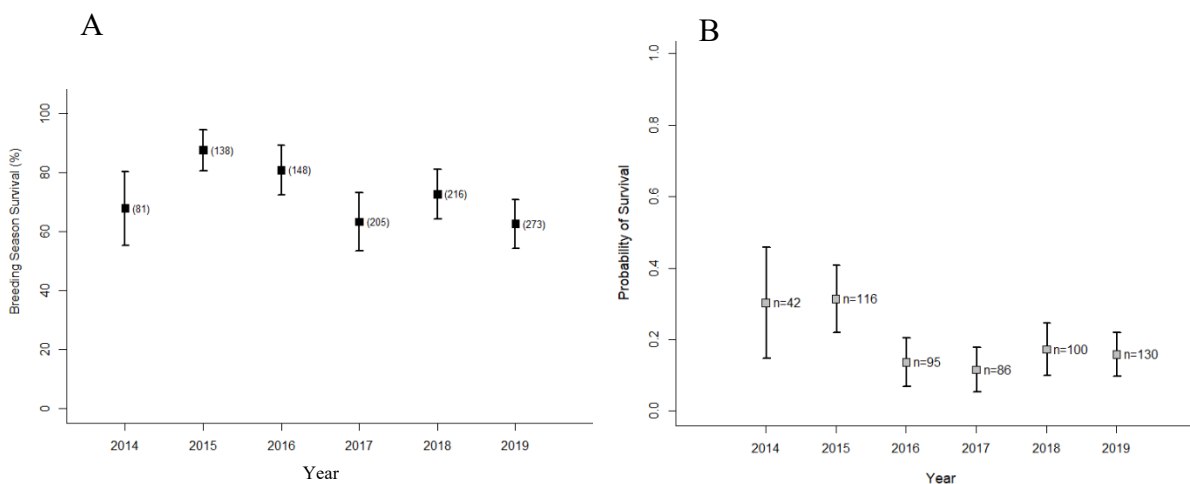


Figure 21. A) Survival estimates ( $\pm$  95% C.I.) of female sage-grouse during the breeding season monitoring period (Mar – Jul) and B) annual probability of nest survival ( $\pm$  95% C.I.) at 6 southern Idaho study areas, 2014-2019. n = the number of encounter histories that contributed to the estimate.

Grazing schedules for treatment pastures within each study area follow a before-after treatment plan (Figure 22). The 2 years of pre-treatment monitoring allows us to determine where sage-grouse nests are most likely to be located and allows us to measure survival and reproductive parameters at the site under the current management conditions. The study areas are divided into 4 pastures and 4 years of treatments are implemented in each pasture; with alternate years of spring grazing for 2 pastures, no grazing at all for 1 pasture, and alternating spring/fall grazing for 1 pasture. At the conclusion of the 2020 season, 2 study areas (Jim Sage and Browns Bench) will have 2 years of pretreatment and 5 years of treatment (one additional year), 2 study areas (Sheep Creek and Big Butte) will reach the end of 4 treatment years, and Pahsimeroi Valley will finish

the second year of the treatment period. The Idaho National Laboratory (INL) site was not continued in 2020 due to complications with gaining access due to COVID-19 pandemic and a fire that burned a majority of the study pasture in 2019.

| Treatment                | Year 1          | Year 2          | Implement Grazing Treatments | Year 3         | Year 4         | Year 5         | Year 6         |
|--------------------------|-----------------|-----------------|------------------------------|----------------|----------------|----------------|----------------|
| <b>Spring Odd Years</b>  | Current grazing | Current grazing |                              | Spring Grazing | No Grazing     | Spring Grazing | No Grazing     |
| <b>Spring Even Years</b> | Current grazing | Current grazing |                              | No Grazing     | Spring Grazing | No Grazing     | Spring Grazing |
| <b>No Grazing</b>        | Current grazing | Current grazing |                              | No Grazing     | No Grazing     | No Grazing     | No Grazing     |
| <b>Spring and Fall</b>   | Current grazing | Current grazing |                              | Spring Grazing | Fall Grazing   | Spring Grazing | Fall Grazing   |

Figure 22. Monitoring and treatment schedule used to evaluate effects of cattle grazing on sage-grouse demographic traits and habitat features within 4 treatment pastures at each southern Idaho project study area.

We have deployed and maintained over 45 km of temporary electric fence (solar powered) to aid in utilization and livestock distribution and to allow permittees to continue their regular grazing schedules on portions of pastures not used by nesting sage-grouse. We use visual estimates of forage utilization and measurements of vegetation heights along transects to quantify forage utilization in each study pasture at the end of each growing season (Figures 23, 24, and 25). We also sample vegetation at nest sites and random plots within our treatment and control pastures. Analyses of those data are ongoing.

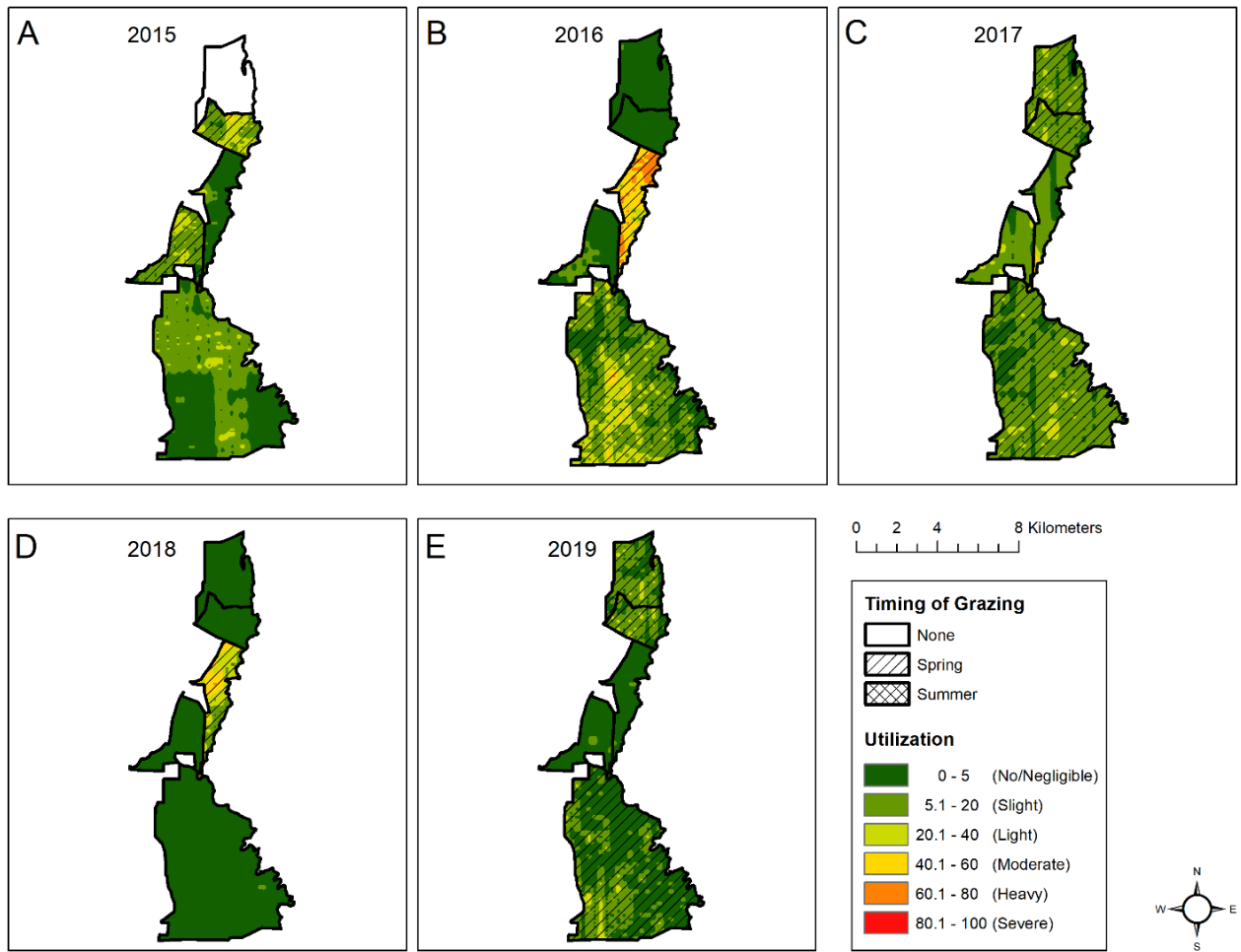


Figure 23. Map of estimated livestock utilization at Browns Bench study area, Idaho, 2015-2019

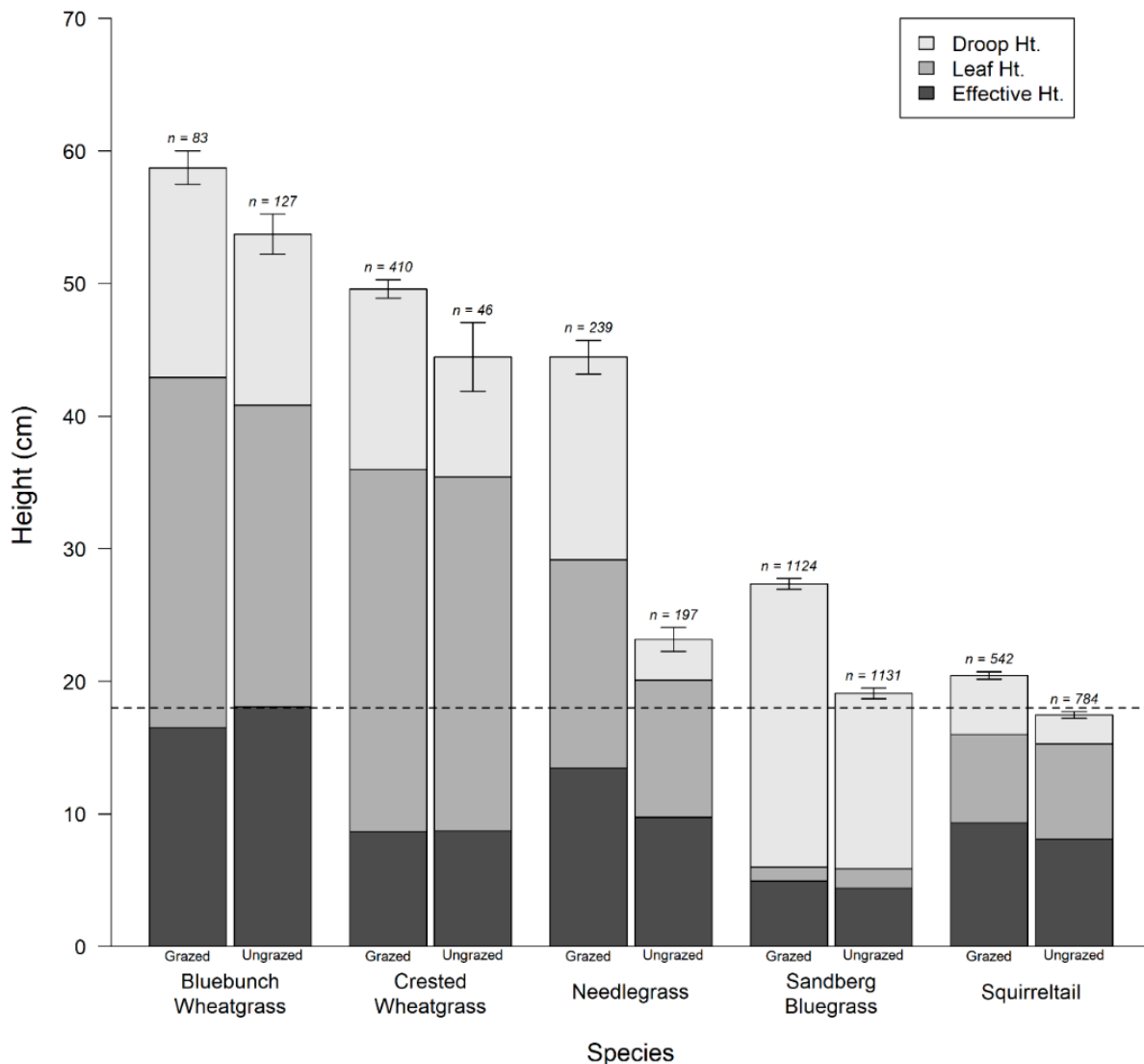


Figure 24. Mean values ( $\pm 1$  SE for droop height only) of 3 height measurements of the 5 most common species of perennial grasses collected at post-growing season (Jul-Aug) random plots at Browns Bench, Idaho, 2019. Droop Ht = maximum droop height (using highest part of plant), Leaf Ht = maximum droop height excluding the flowering stalk, and Effective Ht = effective height (modified visual obstruction for an individual plant). Sample sizes are denoted at the top of each bar. The dashed line represents 18 cm (7 in.), the grass height recommended in the sage-grouse habitat guidelines.

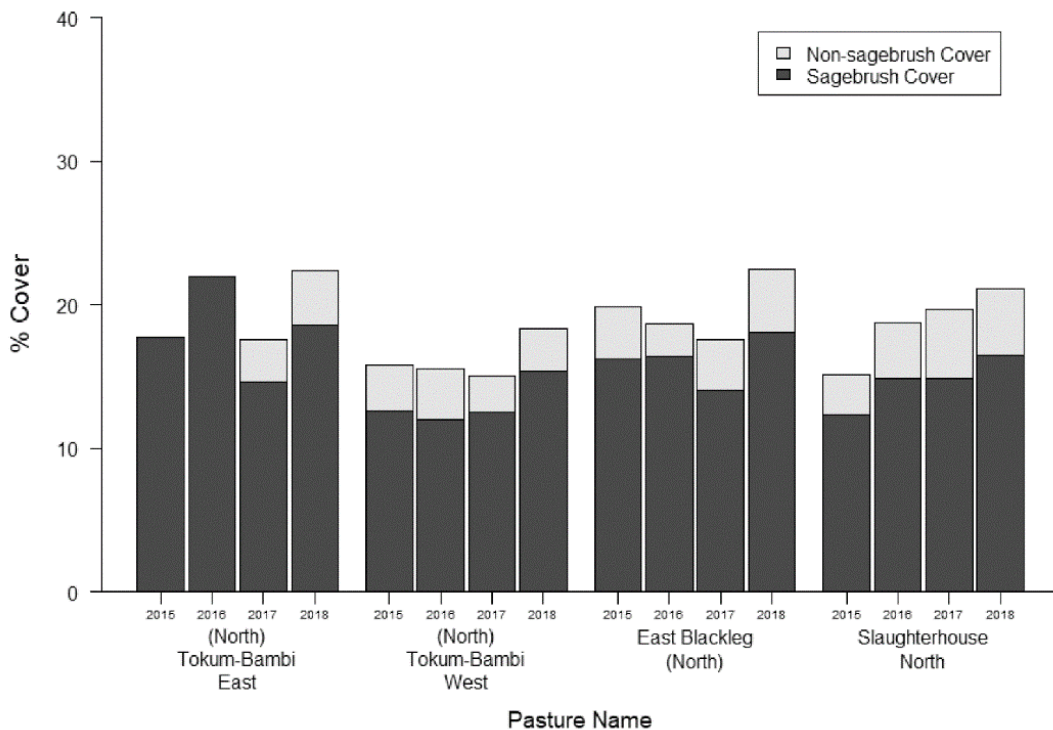


Figure 25. Shrub canopy cover of all brush species combined within each of 4 treatment pastures at Browns Bench, Idaho, 2015-2019.

We conducted arthropod sampling at 129 sampling locations across 4 study sites in 2019: 40 plots at Big Butte, 40 plots at Brown's Bench, 20 plots at Idaho National Lab, and 29 plots at Jim Sage (Table 13). We reduced sampling effort in 2019 (relative to 2018) due to funding constraints. Each of the 129 sampling locations had four pitfall traps and we emptied those pitfall traps once per week for 4 weeks, yielding a total of 1,960 pitfall arthropod samples collected in 2019. For each visit, we also conducted 2 sweep-net transects per plot. These efforts yielded 1,105 sweep-net samples. Additionally, we conducted ant mound surveys at each arthropod sampling plot across each of the 4 study sites where we sampled arthropods in 2019. We detected and measured the size of 266 ant mounds on these 127 transects.

Table 13. Summary of arthropod sampling efforts at 6 study sites across southern Idaho, 2015-2019

| Year | Start Date      | End Date        | Study Sites Collected <sup>a</sup> | Total Plots | Pitfall Samples | Sweep-Net Samples | Ant Mounds |
|------|-----------------|-----------------|------------------------------------|-------------|-----------------|-------------------|------------|
| 2015 | -- <sup>b</sup> | -- <sup>b</sup> | BB, BR, JS, SC                     | 59          | -- <sup>b</sup> | -- <sup>b</sup>   | 106        |
| 2016 | 5-May           | 26-Jun          | BB, BR, JS, SC                     | 120         | 3,556           | 1,958             | 354        |
| 2017 | 15-Jun          | 6-Jul           | BB, BR, JS, SC                     | 92          | 1,100           | -- <sup>c</sup>   | 92         |
| 2018 | 31-May          | 30-Jun          | BB, BR, JS, PV, SC                 | 178         | 2,540           | 1,728             | 309        |
| 2019 | 23-May          | 13-Jun          | BB, BR, INL, JS                    | 129         | 1,960           | 1,105             | 264        |

<sup>a</sup>BB = Big Butte, BR = Brown's Bench, INL – Idaho National Laboratory, JS = Jim Sage, PV = Pahsimeroi Valley, SC = Sheep Creek

<sup>b</sup>Part of David Gotsch's thesis research

<sup>c</sup>We did not have sufficient funding to collect sweep-net samples in 2017

<sup>d</sup>Data were collected at these study sites all 4 years in which we sampled arthropods

*Sage-grouse Ecology in High-elevation Sagebrush Habitats* – During 2015-2020, we monitored the success of 291 greater sage-grouse nests from PTT-marked females throughout the Upper Snake Region of eastern Idaho (Figure 26), 66 of those during the spring 2020 breeding season. Apparent nest success (# successful nests / total # nests documented) across all nests in the Upper Snake ranged from a low of 0.31 in 2019 to a high of 0.71 in 2016 (Figure 27).

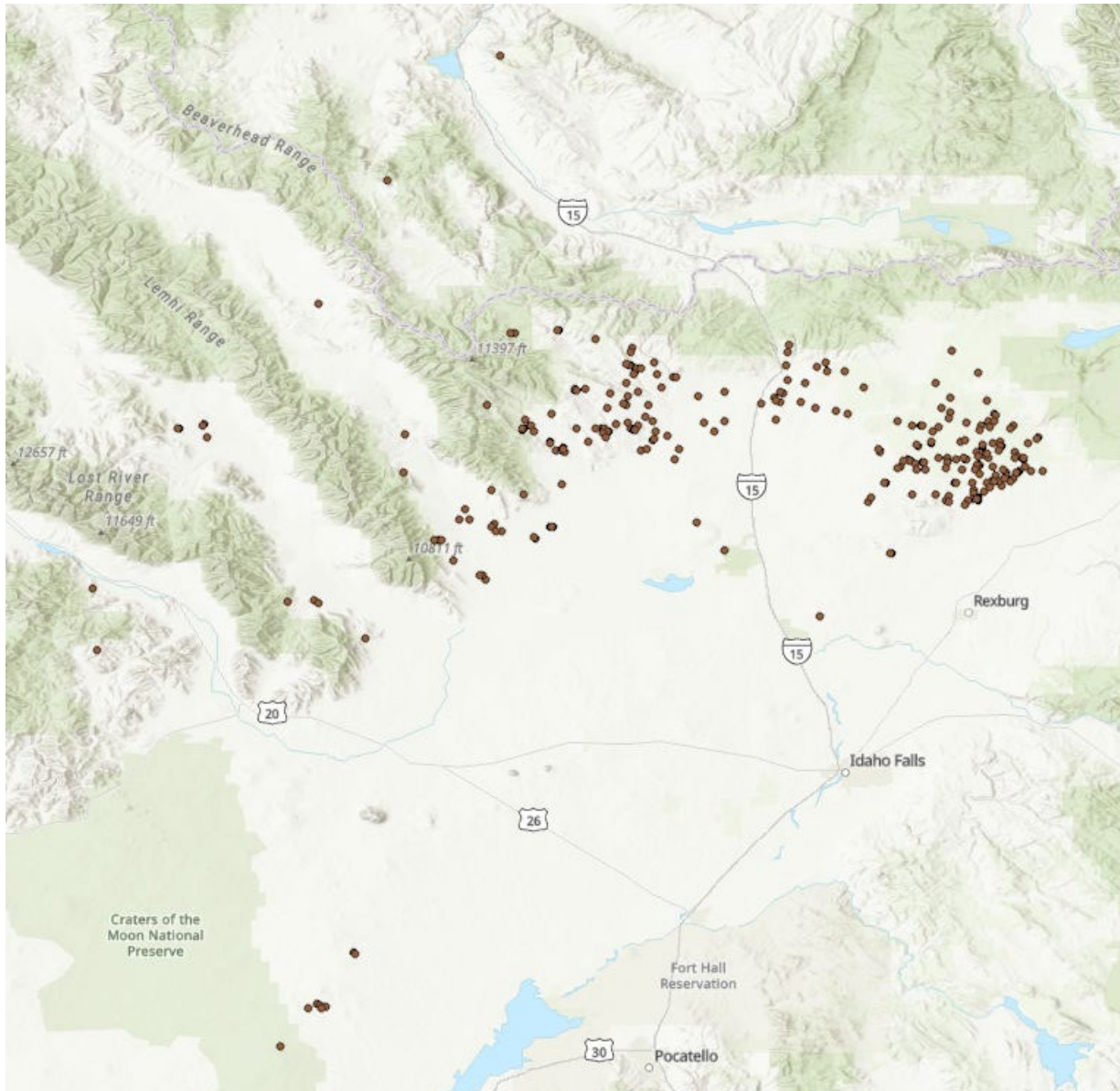


Figure 26. Sage-grouse nests of marked females monitored in the Upper Snake Region, Idaho, 2015-2020.

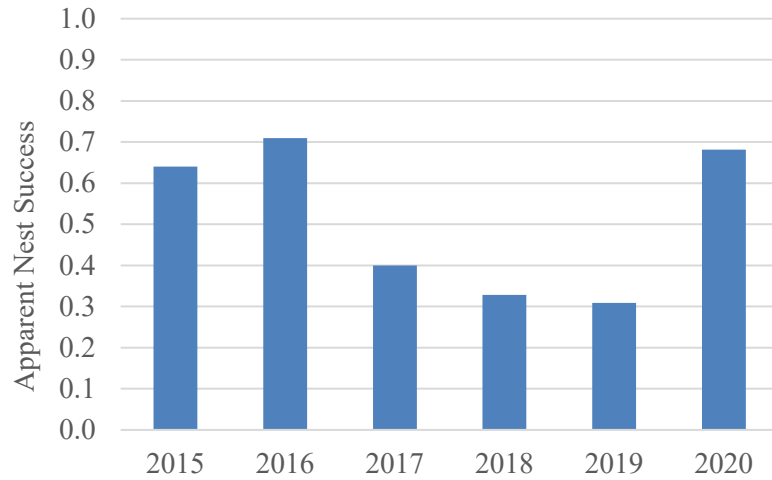


Figure 27. Apparent nest success from marked female sage-grouse monitored in the Upper Snake Region, Idaho, 2015-2020.

We used BLM's HAF-AIM vegetation sampling protocol to measure vegetation at nests and at 524 random plots throughout predicted sage-grouse habitat that occurred within 18 km of the leks marked females were captured from. The majority of vegetation transects were from the Sand Creek and Medicine Lodge areas of the Upper Snake Region. Preliminary nest site selection analyses incorporating 2020 data suggest Upper Snake Region sage-grouse tended to select nest sites with relatively high sagebrush and total brush canopy cover, lower perennial grass cover, in relatively forb rich areas (Figure 28). Final analyses will include similar examinations of the effects of vegetation, at various spatial scales, on nest and brood success. The ultimate goal of these analyses will be to inform habitat and sage-grouse population management in these unique systems.

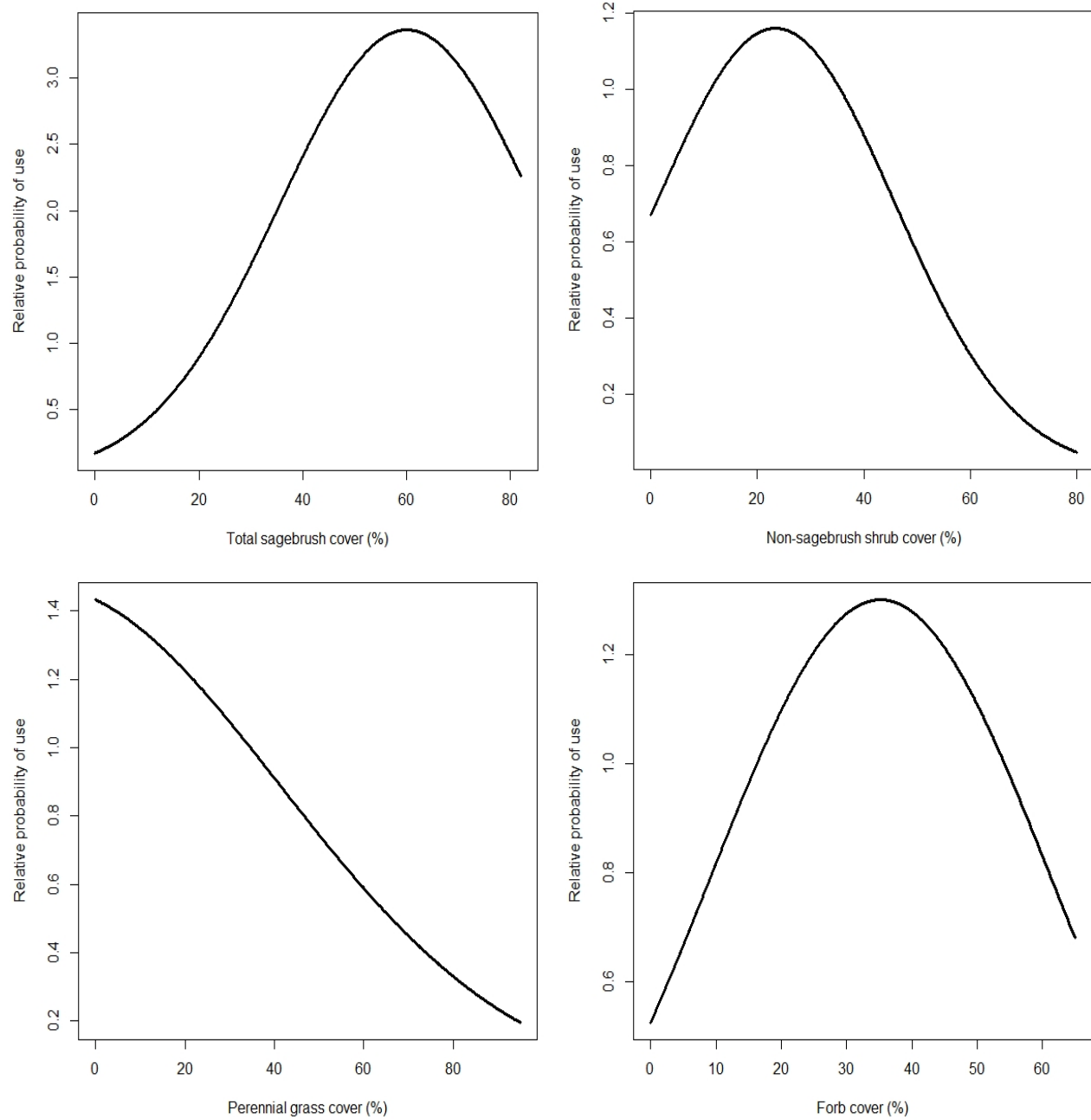


Figure 28. Partial effects plots of shrub, perennial grass, and forb cover from best preliminary model describing vegetation nest site selection by sage-grouse in the Upper Snake Region, Idaho, 2015-2020.

*Effects of Wildfire on Habitat Selection and Demographics* – We monitored the location, survival, and habitat characteristics of 100 nests at Sand Creek and 85 nests at Medicine Lodge/Crooked Creek during 2017-2020, 66 of which were monitored during the 2020 breeding season (37 Sand Creek, 27 Medicine Lodge). Monitored females selected several nest sites inside the burn perimeter prior to the Grassy Ridge fire (2015-2017) but no nests were inside the boundary during the two years post-fire (2019-2020; Figure 29).

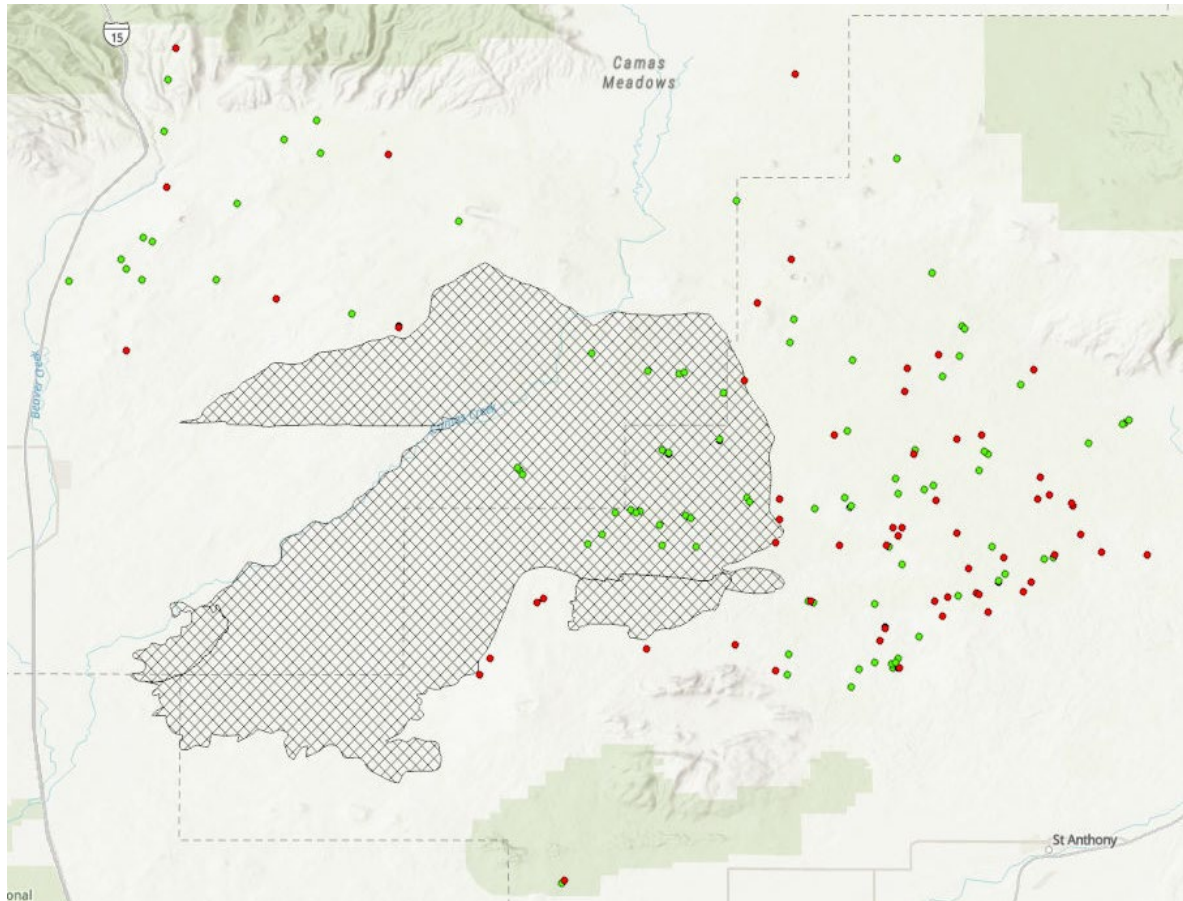


Figure 29. Locations of monitored sage-grouse nests, before (2015-2018 = green dots) and after (2019-2020 = red dots) the Grassy Ridge fire (cross-hatched area = burn boundary), on the Sand Creek desert, Idaho.

Ongoing analyses will take a detailed look at the factors that affected daily nest survival of these nests, quantify the apparent avoidance of the burn scar for nesting, examine the use of the burn scar and surrounding habitats by non-nesting adults and broods, examine how the burn and vegetation structure may have influenced survival of broods to 42 days post-hatch, and examine if there were any differences in vital rates, habitat selection, or movements between grouse inhabiting the unburned Medicine Lodge/Crooked Creek area and Sand Creek.

*Demographics and Lek Distribution in the Curlew* – During the current reporting period we completed analyses of data collected from monitored sage-grouse and aerial surveys in the Greater Curlew Valley Area (GCVA) of southeastern Idaho and wrote a draft report on the findings that is currently in revision prior to sharing with partners.

We conducted 3 mornings of aerial surveys of the GCVA on April 15-17, 2017. We surveyed 23 (40%) of the 58 known greater sage-grouse leks in the GCVA (Figure 30). None of these leks were active from the air but 2 were active when observed during later ground surveys. No new leks were found with aerial surveys.

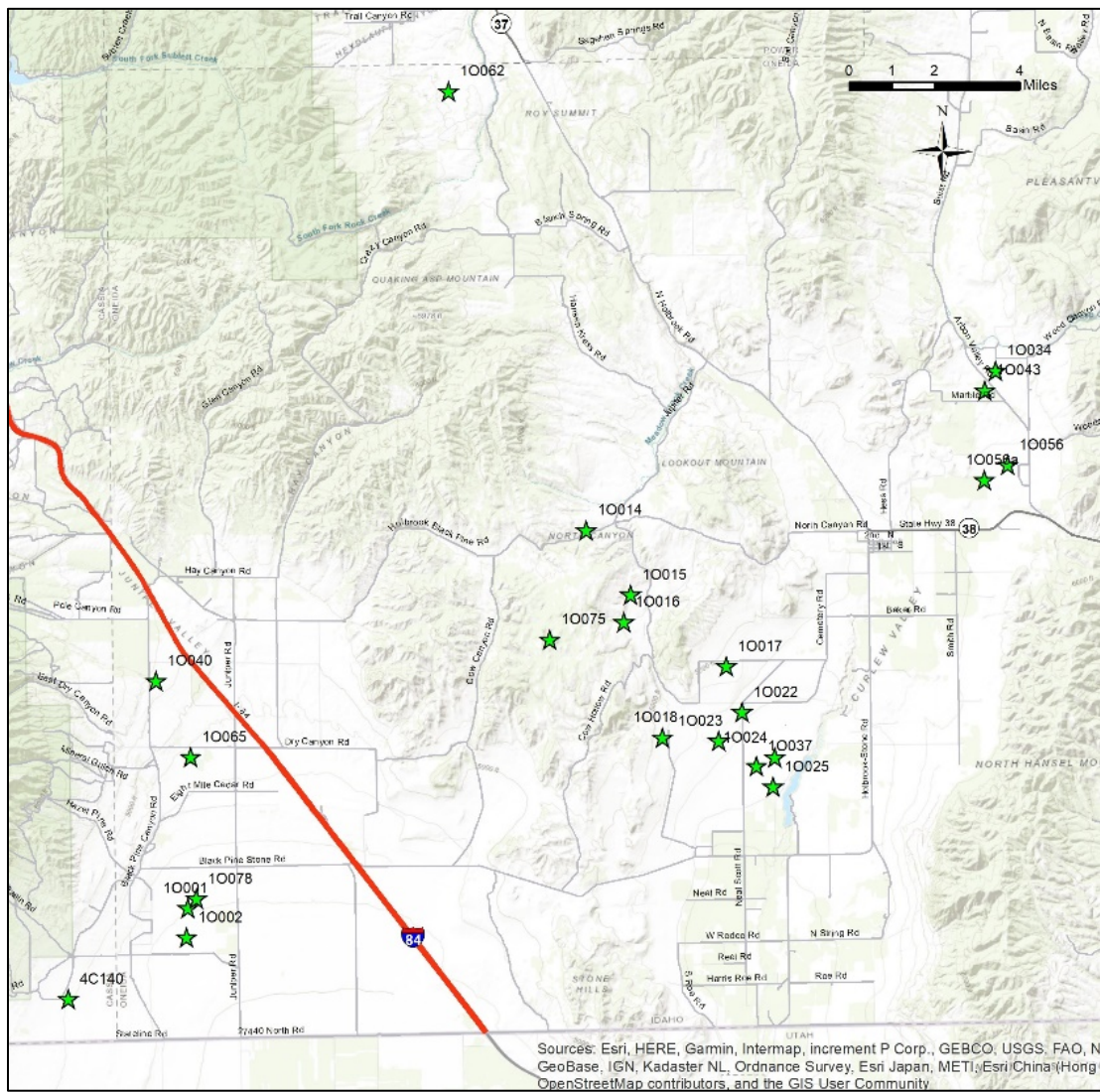


Figure 30. Previously-documented sage-grouse leks that we aerially surveyed on April 15-17, 2017 in the Greater Curlew Valley Area, Idaho.

Seven of 38 (18%) leks ground surveyed in 2017 had displaying males and averaged  $16.1 \pm 7.6$  males/active lek (mean  $\pm$  95% CI). In 2018, 8 of 37 (22%) surveyed leks were active and averaged  $9.9 \pm 4.0$  males/active lek. In 2019, 11 of 45 (24%) leks surveyed had males attending and averaged  $11.6 \pm 5.7$  males/active lek. For the 33 leks surveyed in both 2019 and 2017, 9 (27%) were active in 2019 and 7 (21%) in 2017. The number of males counted on active leks was similar between 2017 (113) and 2019 (119).

For a longer-term examination of lek trends, we also compared lek counts during 2019 to those collected from the same leks 20 years earlier (1999). Of 27 leks observed in both 1999 and 2019, 78% (21) were active in 1999 but only 19% (5) were active in 2019. There were also 61% fewer

males counted on these same leks in 2019 (88 males) than in 1999 (228 males). Collectively, the aerial and ground lek survey results and comparisons from this study align with other IDFG lek count data suggesting there are fewer sage-grouse leks and fewer males in each lek in the GCVA today than historically and there is little to no evidence that birds simply shifted to new lek locations in nearby habitats.

We captured and marked 58 sage-grouse (54 females, 4 male). The majority (34 females, 4 males) were fitted with PTT transmitters and 20 females were fitted with VHF radio-collars. We captured 29 females and 1 male in 2017 and 25 females and 3 males in 2018. We monitored all PTT-marked birds until death or transmitter failure and all VHF-marked birds through the nesting season each year. PTT-marked birds were used in all analyses, while VHF marked birds were only used in nest site selection and success analyses. Due to personnel limitations on the project, VHF marked birds were not monitored regularly enough, post-nesting, to be used in the annual survival and movement analyses.

Females in the GCVA typically visited only 1 lek per spring and showed strong fidelity to leks between years. A total of 53 females monitored in other areas of east Idaho (Salmon/Lemhi, Sand Creek, and Big Desert) during the same years visited an average of 2.2 leks per season (range = 1-6; IDFG, unpublished data) and only 3 of those females visited the same lek in two consecutive years. It's possible the relatively low lek density in GCVA ( $\text{GCVA} \approx 1.3 \text{ leks}/1,000 \text{ km}^2$ , other 3 eastern Idaho study areas combined  $\approx 8.4 \text{ leks}/1,000 \text{ km}^2$ ) leads to fewer lek options for GCVA females and thus increased fidelity. The average date of initial lek visitation for females in GCVA was 14 March.

The average nest initiation date for female sage-grouse in the GCVA was 4 May (range = 4 Apr - 24 May) and the average date of hatch was 2 June (range = 19 May - 20 Jun). Females spent an average of 28 days incubating a successful first nest and 25 days incubating a successful second nest (after a first nest was depredated). Depredated nests averaged 9.5 days of incubation (range = 3 – 25 days) before the depredation event. When nesting females left the nest, the average distance of the excursion was only 72 m (SD= 51 m). The average distance between a female's nest sites in consecutive years was 1,799 m (SD = 3,268 m, range = 94 - 8,440 m). However, this average was highly influenced by one individual bird that nested 8,440 m apart in consecutive years. If that outlier is removed, the average distance between consecutive nests is reduced to 470 m (SD = 345 m). Our findings of high site fidelity between years are similar to those of Fischer et al. (1993) and Peck et al. (2012).

We examined whether remotely-sensed measures of shrub or grass cover within sage-steppe habitats influenced sage-grouse nest site selection in the GCVA by comparing measurements at 52 nests to measurements at 494 random locations. There was a weak positive selection for shrub cover (Table 14), though the shrub cover model barely outperformed an intercept-only null model ( $\Delta\text{AIC}_c = 0.41$ ) and the slope term of the model only approached statistical significance ( $p = 0.11$ ). An effects plot of the shrub cover coefficient plotted across the range of potential shrub cover values suggests that areas with 92% total shrub cover (relative probability of selection = 0.16) were approximately twice as likely to be selected as areas with 22% shrub cover (relative probability of selection = 0.08; Figure 31). A model including grass cover performed worse than the null model, suggesting remotely-sensed grass cover was not a good predictor of nest site selection.

Apparent nest success was 47.8% in 2017 ( $n = 23$ ), 66.7% in 2018 ( $n = 27$ ), and 59.6% across 2017-2019 combined ( $n = 52$ , 2 additional successful nests monitored in 2019). A null model of nest success outperformed all models incorporating remotely-sensed measures of shrub or grass cover, suggesting neither of those variables was useful in explaining why sage-grouse nests failed in the GCVA. When examining the effect of field-measured vegetation structure around nests, univariate models suggested forb cover and sagebrush height had some ability to explain differences between nests that succeeded and those that failed. When those two univariate models were compared to an additive model containing both variables and the null model, there was significant model uncertainty and none of the models fit dramatically better than the null model (Table 15). The univariate models performed slightly better than the additive model and both suggested a strong positive relationship between each habitat variable and nest success (Figure 31), though the slope terms for both parameter estimates only approached statistical significance (Forb Cover  $p = 0.08$ , Sagebrush Height  $p = 0.07$ ).

Table 14. Model selection results and parameter estimates for resource selection function models describing sage-grouse nest site selection of remotely-sensed habitat variables in the Greater Curlew Valley Area, Idaho, 2017-2018.

| Model       | K | log likelihood | AIC <sub>c</sub> | $\Delta\text{AIC}_c$ | $\omega$ | Parameter Estimates |             |
|-------------|---|----------------|------------------|----------------------|----------|---------------------|-------------|
|             |   |                |                  |                      |          | Intercept           | Coefficient |
| Shrub Cover | 2 | -151.10        | 306.22           | 0.00                 | 0.46     | -2.747              | 0.010       |
| Null Model  | 1 | -152.31        | 306.63           | 0.41                 | 0.37     | -2.418              | N/A         |
| Grass Cover | 2 | -152.26        | 308.55           | 2.33                 | 0.14     | -2.522              | 0.002       |

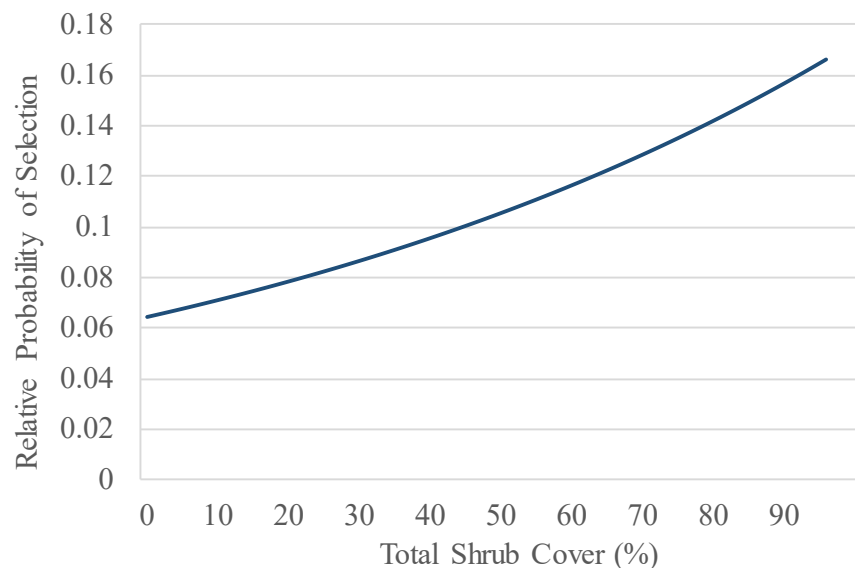


Figure 31. Plot of the modeled effect of remotely-sensed shrub canopy cover on the relative probability of an area being selected by a nesting sage-grouse (top model in Table 14), Greater Curlew Valley Area, Idaho, 2017-2018.

Table 15. Additive model selection results describing seasonal habitat selection of sage-grouse, Greater Curlew Valley Area, Idaho, 2017-2018.

| Model                         | K | log likelihood | AIC <sub>c</sub> | $\Delta AIC_c$ | $\omega$ | Parameter Estimates |            |                  |
|-------------------------------|---|----------------|------------------|----------------|----------|---------------------|------------|------------------|
|                               |   |                |                  |                |          | Intercept           | Forb Cover | Sagebrush Height |
| Forb Cover                    | 2 | -13.10         | 30.77            | 0.00           | 0.34     | -0.573              | 0.100      | NA               |
| Sagebrush Height              | 2 | -13.30         | 31.16            | 0.39           | 0.28     | -1.429              | NA         | 0.043            |
| Forb Cover + Sagebrush Height | 3 | -12.14         | 31.48            | 0.71           | 0.24     | -2.031              | 0.089      | 0.034            |
| Null Model                    | 1 | -15.28         | 32.73            | 1.96           | 0.13     | 0.693               | NA         | NA               |

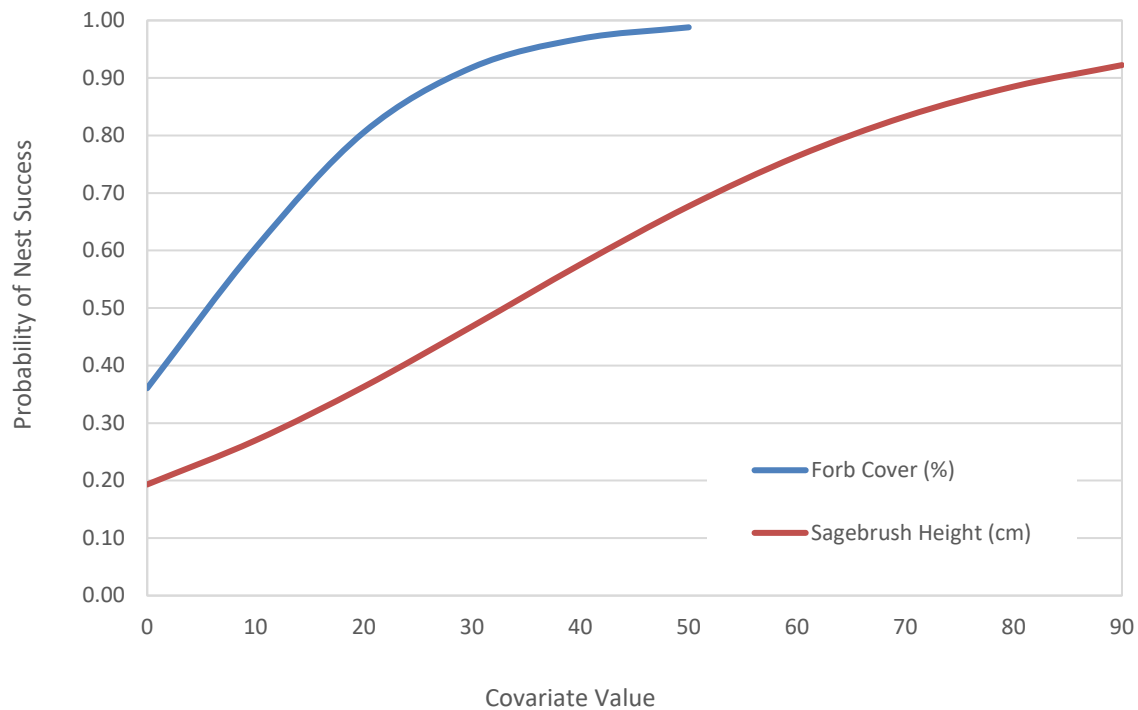


Figure 32. Plot of the modeled effects of field-measured forb canopy cover (%) and sagebrush height (cm) from the top two univariate models (Table 3) describing the probability of sage-grouse nest success, Greater Curlew Valley Area, Idaho, 2017-2018.

We conducted 30-day brood flushes on 27 hens, 18 of which had live broods consisting of 51 chicks (mean = 2.8 chicks, range = 1 – 6 chicks), resulting in an apparent brood success of 66.7% across both years of the study (Table 16). We also used eggshell fragment investigation to estimate that a total of 74 eggs hatched from monitored nests in 2018. That estimate, combined with the 28 chicks counted during 30-day brood flushes in 2018, results in an estimated 30-day chick survival rate of 38% in 2018.

Table 16. Summary of 30-day brood flush count data, Greater Curlew Valley Area, Idaho, 2017-2018.

|                        | 2017 | 2018 | Combined |
|------------------------|------|------|----------|
| Flush counts conducted | 12   | 15   | 27       |
| Live broods            | 9    | 9    | 18       |
| Total chicks counted   | 23   | 28   | 51       |
| Average chicks/brood   | 2.6  | 3.1  | 2.8      |

Sample sizes were insufficient to allow estimation of sex-specific survival estimates, so sexes were combined in the following survival analysis. Of the 45 birds marked with PTTs or VHF that we were able to monitor intensively enough to document annual survival, 2 were entirely removed from survival analyses because their mortality was likely caused by the capture event (i.e., notes on potential injury at capture and mortality soon after), 2 were censored during monitoring because their transmitters fell off prematurely, 28 died during monitoring, and 13 survived until 15 March of the following year (Table 17). We estimated that 12 birds were killed by avian predators, 5 were killed by mammalian predators, and the remaining causes of mortality were unknown. Survival was 32% in both years. Previous research in the GCVA reported annual survival rates that ranged from 30-59%, including the most recent, and highest, estimate from 2005-2006 of 59% (Connelly et al. 1994; Apa 1998; Idaho Fish and Game, unpublished data).

Table 17. Summary of monitoring and survival statistics from sage-grouse marked with PTTs in the Greater Curlew Valley Area, Idaho, 2017-2018.

| Year     | Monitored | Censor | Died | Lived | Survival (95% CI)* |
|----------|-----------|--------|------|-------|--------------------|
| 2017     | 22        | 0      | 15   | 7     | 0.32 (0.12 - 0.51) |
| 2018     | 21        | 2      | 13   | 6     | 0.32 (0.10 - 0.53) |
| Combined | 43        | 2      | 28   | 13    | 0.32 (0.17 - 0.46) |

\* - Kaplan-Meier annual survivorship based on weekly intervals initiating from the date of first capture each spring

To examine the effects of habitat type and structure on seasonal habitat selection, we compared habitat measurements at 6,794 used points to 154,217 random locations within mapped sage-grouse habitat. Initial model building steps suggested that a quadratic shape was best for shrub cover, a linear shape was best for grass cover, and that all variables considered (the two canopy cover variables and dummy variables for the bare ground, mesic grass, xeric grass, mesic shrub, xeric shrub, conifer, deciduous tree, agriculture, and development cover types) had some use in explaining habitat selection across all seasons. We then compared models with the mesic grass, xeric grass, mesic shrub, xeric shrub, agriculture and development land cover variables alone to a group of models incorporating interaction terms between those cover types and season, to examine whether sage-grouse were selecting those cover types differently throughout the year. We moved the covariates for whichever model performed better (i.e., interaction between land cover and season or no interaction term), for each land cover type, forward in the model building process. We then built additive resource selection function models of all combinations of covariates and seasonal interaction terms that were moved forward to the final model building process.

The top additive model suggested sage-grouse were selecting or avoiding xeric grass, xeric shrubs, and agriculture land cover types and that the selection of these types varied across seasons (Table 18). The addition of the developed land cover type and an interaction between developed and season to the top model did not improve the AIC<sub>c</sub> score, suggesting the developed covariate was an uninformative parameter and the more complex model was not truly competitive with the top model (Arnold 2010). No other additive models were competitive ( $\Delta\text{AIC}_c > 200.0$ ) with the top model, including all models containing shrub and grass cover.

Table 18. Additive model selection results (top 3 models only) describing seasonal habitat selection of sage-grouse, Greater Curlew Valley Area, Idaho, 2017-2018.

| Model  | K  | log likelihood | AIC <sub>c</sub> | $\Delta\text{AIC}_c$ | $\omega$ |
|--|----|----------------|------------------|----------------------|----------|
| Season + Xeric Grass + Xeric Shrub + Agriculture + Xeric Grass*Season + Xeric Shrub*Season + Agriculture*Season                                | 16 | -27125.6       | 54283.2          | 0.00                 | 0.53     |
| Season + Xeric Grass + Xeric Shrub + Agriculture + Developed + Xeric Grass*Season + Xeric Shrub*Season + Agriculture*Season + Developed*Season | 20 | -27121.7       | 54283.4          | 0.26                 | 0.47     |
| Season + Xeric Grass + Agriculture + Shrub Cover + Shrub Cover <sup>2</sup> + Xeric Grass*Season + Agriculture*Season                          | 14 | -27232.0       | 54492.1          | 208.91               | 0.00     |

To ease interpretation of the season and land cover interactions, we then split the used and random location dataset into four separate seasonal datasets and fit a version of the top model without season interactions (i.e., land cover covariates only) to each seasonal dataset. We split random points proportional to the number of use locations in each season. We then compared the modeled parameter estimates ( $\beta \pm 95\% \text{ C.I.}$ ) for each land cover type, across seasons, to examine selection for cover types (parameter estimate  $> 0$  and 95% C.I. does not include 0), avoidance of cover types (parameter estimate  $< 0$  and 95% C.I. does not include 0), and seasonal changes in these patterns (Figure 33).

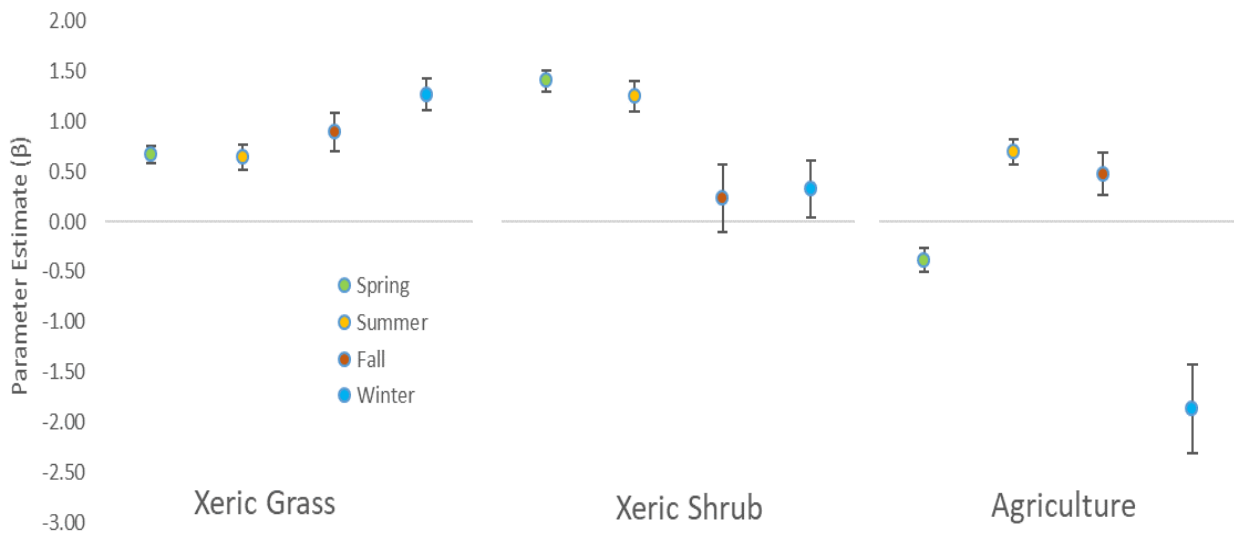


Figure 33. Parameter estimates ( $\pm 95\%$  C.I.) from resource selection function models—each containing xeric grass, xeric shrub, and agriculture land cover variables—from season-specific location datasets of sage-grouse, Greater Curlew Valley Area, Idaho, 2017-2018.

### **Investigation 11 – Conduct 1 Study of the Effects of Agriculture Landscape Change on Wildlife Populations by 30 June, 2020.**

#### **Results**

We flew 14 sUAS surveys of Columbian sharp-tailed grouse leks sites in southeastern Idaho. The selected leks were chosen to represent different population trajectories over 10 and 20 year histories. We collected multispectral image data at these sites and developed methods and procedures from which vegetation growth can be evaluated through proxies such as NDVI, as well as visual and near-infrared reflectance bands. Further, we're implementing structure from motion methods where we can develop 3-D reconstructions of the surveyed lek habitat, giving us more accurate metrics of habitat structure and function from which to evaluate CSTG lek selection sites.

At regional scales, we're collecting satellite imagery from LandSat systems (TM, ETM+, OLI, and Sentinel satellites) that we can classify into land-use categories. We're investigating how to use new high spatial and temporal NDVI datasets for the purposes of evaluating land-use tenure and stewardship (Figure 34; unpublished data, TerraPulse, <http://www.terrapulse.com>). This database will allow us to estimate the intensity of agricultural use beyond simple irrigated/non-irrigated classes. Dry land agricultural systems are especially hard to identify using traditional遥感 satellite imagery. By tracking NDVI through a season, we are able to estimate the number of agriculture harvests that occur on or near leks sites and in the surrounding brood-rearing landscape. Although there is an apparent ‘signal’ within the NDVI database (Figure 34), we are hoping to develop semi-automated phenological methods to characterize the intensity of agricultural at a spatial and temporal scale that coordinates with the scale of CSTG life history and population cycles.

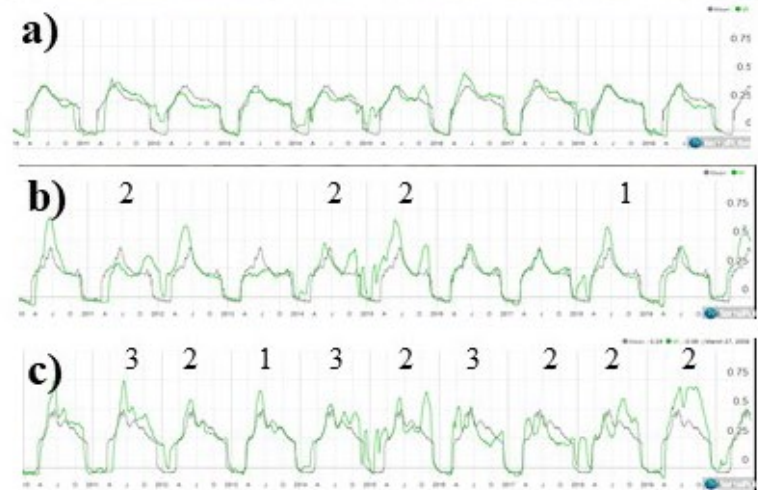


Figure 34. Area map and time series of measured normalized difference vegetation index (NDVI) values from three agriculture fields in Arbon Valley, Idaho. NDVI time series a) is from a field enrolled in the CRP/SAFE program with no active agriculture, so vegetation growth is seasonal; time series b) is from a field with irregular annual harvests (number above time series is how many harvests occurred that annum); and time series c) is from an irrigated field that is harvested on a more intense and regular cycle.

## Literature Cited

- Apa, A. D. 1998. Habitat use and movements of sympatric sage and Columbian sharp-tailed grouse in southeastern Idaho. Ph D. Dissertation, University of Idaho, Moscow. 199p
- Arnold, T. W. 2010. Uninformative parameters and model selection using Akaike's Information Criterion. *Journal of Wildlife Management* 74:1175–1178.
- Baraza, E., J. J. Villalba, and F. D. Provenza. 2005. Nutritional context influences preferences of lambs for foods with plant secondary metabolites. *Applied Animal Behaviour Science* 92:293-305.
- Barrett, M., J. Nolan, and L. Roy. 1982. Evaluation of hand held net-gun to capture large mammals. *Wildlife Society Bulletin* 10:108-114.
- Beasom, S., W. Evans, and L. Temple. 1980. The drive net for capturing western big game. *Journal of Wildlife Management* 44:478-480.
- Berg, J. E., M. Hebblewhite, C. C. St.Clair, and E.H. Merrill. 2019. Prevalence and mechanisms of partial migration in ungulates. *Frontiers in Ecology and Evolution* 7. <https://doi.org/10.3389/fevo.2019.00325>
- Boyce, M. S., P. R. Vernier, S. E. Nielsen, and F. K. A. Schmiegelow. 2002. Evaluating resource selection functions. *Ecological Modelling* 157:281-300.
- Bunnefeld, N., L. Borger, B. van Moorter, C. M. Rolandsen, H. Dettki, E. J. Solberg, and G. Ericsson. 2011. A model-driven approach to quantify migration patterns: individual, regional and yearly differences. *Journal of Animal Ecology* 80:466-476.
- Calenge, C., 2006. The package adehabitat for the r software: a tool for the analysis of space and habitat use by animals. *Ecological Modelling* 197: 516–519.
- Calenge, C., S. Dray, and M. Royer-Carenzi. 2009. The concept of animals' trajectories from a data analysis perspective. *Ecological Informatics* 4:34-41.
- Calenge, C. 2019. Analysis of animal movements in R: the adehabitatLT Package. 95 pgs.
- Clover, M. R. 1954. A portable deer trap and catch net. *California Fish and Game* 40:367-373.
- Connelly, J. W., K. P. Reese, W. L. Wakkinen, M. D. Roberson, and R. A. Fischer. 1994. Sage Grouse Ecology Study I: Sage grouse response to a controlled burn. Idaho Department of Fish and Game Job Completion Report, W-160-R-21.
- Dorgeloh, W. G. 2002. Calibrating a disc pasture meter to estimate above-ground standing biomass in Mixed Bushveld, South Africa. *African Journal of Ecology* 40:100-102.
- Fischer, R. A., A. D. Apa, W. L. Wakkinen, K. P. Reese, and J. W. Connelly. 1993. Nesting-area fidelity of Sage Grouse in Southeastern Idaho. *Condor* 95:1038-1041.
- Fleming, C. H., W. F. Fagan, T. Mueller, K. A. Olson, P. Leimgruber, and J. M. Calabrese. 2015. Rigorous home-range estimation with movement data: a new autocorrelated kernel-density estimator. *Ecology* 96:1182-1188.
- Fleming, C. H., W. F. Fagan, T. Mueller, K. A. Olson, P. Leimgruber, and J. M. Calabrese. 2016. Estimating where and how animals travel: an optimal framework for path reconstruction from autocorrelated tracking data. *Ecology* 97:576-582.
- Frair, J. L., E. H. Merrill, J. R. Allen, and M. S. Boyce. 2007. Know Thy Enemy: Experience Affects Elk Translocation Success in Risky Landscapes. *Journal of Wildlife Management* 71:541-554.
- Freeland, W. J., and D. H. Janzen. 1974. Strategies in Herbivory by Mammals: The Role of Plant Secondary Compounds. *The American Naturalist* 108:269-289.
- Hanley, T. A., C. T. Robbins, A. E. Hagerman, and C. McArthur. 1992. Predicting Digestible Protein and Digestible Dry Matter in Tannin-Containing Forages Consumed by Ruminants. *Ecology* 73:537-541.
- Hastie, T., T. Tibshirani, and J. Friedman, editors. 2001. *The elements of statistical learning: data mining, inference, and prediction*. Springer, New York.

- Horne, J. S., E. O. Garton, S. M. Krone, and J. S. Lewis. 2007. Analyzing animal movements using Brownian bridges. *Ecology* 88:2354-2363.
- Middleton, A. D., M. J. Kauffman, D. E. McWhirter, J. G. Cook, R. C. Cook, A. A. Nelson, M. D. Jimenez, and R. W. Klaver. 2013. Animal migration amid shifting patterns of phenology and predation: lessons from a Yellowstone elk herd. *Ecology* 94:1245–1256.
- Moeller, A. K. 2017. New Methods to Estimate Abundance from Unmarked Populations Using Remote Camera Trap Data. *Graduate Student Theses, Dissertations, & Professional Papers*. 10958.
- Moeller, A. K., P. M. Lukacs, and J. S. Horne. 2018. Three novel methods to estimate abundance of unmarked animals using remote cameras. *Ecosphere* 9:e02331.
- Peck, R. D., R. J. Baxter, R. T. Larsen, and J. T. Flinders. 2012. Nest-area fidelity of Greater Sage-Grouse in Strawberry Valley, Utah. *Western North American Naturalist*, 72:425-431.
- Sawyer, H. and M.J. Kauffman. 2011. Stopover ecology of a stopover ungulate. *Journal of Animal Ecology* 80:1078-1087.
- Villalba, J. J., F. D. Provenza, and J. P. Bryant. 2002. Consequences of the Interaction between Nutrients and Plant Secondary Metabolites on Herbivore Selectivity: Benefits or Detriments for Plants? *Oikos* 97:282-292.

**Name, title, phone number, and e-mail address of person compiling this report:**

Mark Hurley  
Wildlife Research and Data Manager  
[mark.hurley@idfg.idaho.gov](mailto:mark.hurley@idfg.idaho.gov)

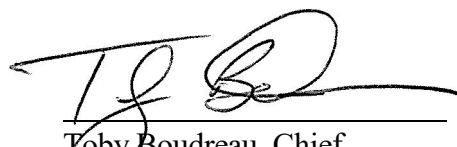
Shane Roberts  
Wildlife Research Coordinator  
[shane.roberts@idfg.idaho.gov](mailto:shane.roberts@idfg.idaho.gov)

Submitted by: IDAHO DEPARTMENT OF FISH AND GAME

David Smith  
Grants/Contracts Specialist  
[David.smith@idfg.idaho.gov](mailto:David.smith@idfg.idaho.gov)

Approved by:

  
\_\_\_\_\_  
Martha Wackenhut  
Federal Aid Coordinator

  
\_\_\_\_\_  
Toby Boudreau, Chief  
Bureau of Wildlife

## **FEDERAL AID IN WILDLIFE RESTORATION**

The Federal Aid in Wildlife Restoration Program consists of funds from a 10% to 11% manufacturer's excise tax collected from the sale of handguns, sporting rifles, shotguns, ammunition, and archery equipment. The Federal Aid program then allots the funds back to states through a formula based on each state's geographic area and the number of paid hunting license holders in the state. The Idaho Department of Fish and Game uses the funds to help restore, conserve, manage, and enhance wild birds and mammals for the public benefit.

These funds are also used to educate hunters to develop the skills, knowledge, and attitudes necessary to be responsible, ethical hunters. Seventy-five percent of the funds for this project are from Federal Aid. The other 25% comes from license-generated funds.

